CHALMERS

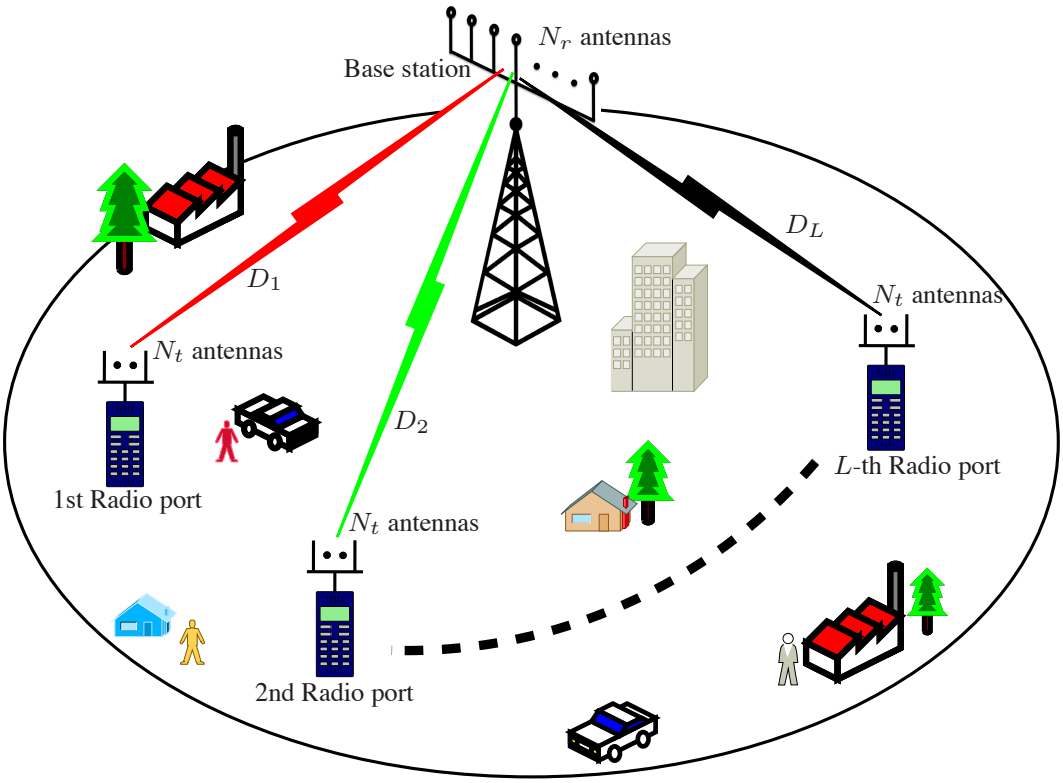

Inverse-Gaussian Distribution: A New Shadowing Model and Its Application to Communication Systems

Master of Science Thesis in the Communication Engineering Programme, Electrical Engineering

VETRISELVAM GOPAL

Department of Signals and Systems
Division of Signal Processing and Antennas
CHALMERS UNIVERSITY OF TECHNOLOGY
SE-412 96, Gothenburg, Sweden.

REPORT NO.: EX021/2012.

This page is intentionally left blank.

Inverse-Gaussian Distribution: A New Shadowing Model and Its Application to Communication Systems

Vetriselvam Gopal

Department of Signals and Systems

Chalmers University of Technology, Sweden

A thesis submitted for the degree of

Master of Science

May 2012

Inverse-Gaussian Distribution: A New Shadowing Model and Its Application to Communication Systems

VETRISELVAM GOPAL

REPORT NO.: EX021/2012

This thesis has been prepared using LaTeX.

Copyright © V. GOPAL, 2012.
All Rights Reserved.

Department of Signals and Systems
Division of Signal Processing and Antennas
CHALMERS UNIVERSITY OF TECHNOLOGY
SE-412 96 Gothenburg
Sweden
Telephone + 46 (0)31-772 1000
E-mail: vetri.gopal@gmail.com
gopalv@student.chalmers.se

Cover:
A schematic illustration of a distributed Multiple-Input Multiple-Output (MIMO) system with L multiple-antenna radio ports transmitting data to a multiple-antenna base station.

VETRISELVAM GOPAL
Gothenburg, Sweden, May 2012.

To my nephew Param
and
nieces Pirabhanju, Harini, Janani, Bharani, & Vaishu.

Acknowledgements

During the course of my master's studies at Chalmers, I have benefited tremendously from my interactions with many extraordinary individuals. Foremost, I want to gratefully acknowledge and express a sincere thank you to my supervisor, Professor Michail Matthaiou, for his invaluable support and guidance. His wisdom, technical knowledge, sharp focus, encouragement, and generosity was a constant source of motivation, and has resulted in outputs which I would not have previously thought possible. I am truly privileged to have had Professor Michail Matthaiou as a mentor. I also have to thank Professor Caijun Zhong for collaborating and co-authoring a paper with me.

I express gratitude to all my friends that helped make the past two years very enjoyable at Chalmers and Sweden. Besides of everything, I can never forget the overwhelming love and support from my mother Amirthavalli, elder brother Marimuthu, and rest of my family members, both direct and extended. They have always been there for me, and this work would simply not have been possible without them.

Vetriselvam Gopal
Gothenburg, May 2012.

Abstract

Real-time fading channels are affected by multipath fading as well as shadowing. In this thesis, we propose the Inverse-Gaussian distribution as a less complex alternative to the classical Log-normal model to describe shadowing effects in composite multipath fading/shadowing environments and to get closed-form solutions for the most important figures of merit. A main motivation for this selection has been the poor accuracy of the analytically friendlier Gamma distribution to approximate the Log-normal distribution, when the latter has a large variance or long tails. As such, we demonstrate that the Rayleigh/Inverse-Gaussian distribution can serve as a more efficient approximation to the prevalent Rayleigh/Log-normal distribution.

Our study starts with the performance evaluation of distributed multiple-input multiple-output (MIMO) systems in composite Rayleigh/Inverse-Gaussian fading channels. The potential of combining MIMO spatial multiplexing gains with macro-diversity gains is realized by distributed MIMO systems that promise to enhance the channel capacity and cell coverage. Capitalizing on some generic bounding techniques, we first derive new closed-form bounds on the ergodic capacity of optimal receivers. In order to gain useful insights into the impact of fading parameters on optimal receivers' performance, a detailed characterization in the asymptotically high and low signal-to-noise ratio regimes is also provided. In addition, we explore the "large-system" regime and provide asymptotic expressions when the number of antennas grows very large. A similar performance analysis is performed for the achievable sum rate of distributed MIMO systems employing linear zero-forcing and minimum mean-square error receivers.

Finally, we perform an effective rate analysis of multiple-input single-output systems over composite Nakagami-m/Inverse-Gaussian fading channels and in the presence of statistical queueing constraints. All the resulting closed-form expressions are validated via a set of Monte-Carlo simulations.

Index terms: Achievable sum rate, composite fading, effective rate, ergodic capacity, MIMO systems, Rayleigh/Inverse-Gaussian fading.

Abbreviations and Acronyms

AWGN	Additive White Gaussian Noise
a.k.a.	also known as
CSI	channel state information
D-MIMO	Distributed Multiple-Input Multiple-Output
IG	Inverse-Gaussian
i.i.d.	independent and identically distributed
MIMO	Multiple-Input Multiple-Output
MISO	Multiple-Input Single-Output
MMSE	Minimum Mean-Squared Error
p.d.f.	probability density function
QoS	Quality of Service
RIG	Rayleigh/Inverse-Gaussian
RV	random variable
SNR	signal-to-noise ratio
w.r.t.	with respect to
ZF	Zero-Forcing

Symbols and Notations

Symbols

β	fixed and finite ratio $\left(\frac{N_r}{LN_t} > 1\right)$
γ	average SNR
μ	Mean parameter of the IG distribution

λ	Scale parameter of the IG distribution
θ	Asymptotic decay-rate of the buffer occupancy
υ	Path loss exponent
φ	Gamma distributed RV
ξ	IG distributed RV (Large-scale fading coefficient)

Parameters

A	QoS constraint $(\theta TB/\ln 2)$
B	Bandwidth of the system
D_i	Distance between the receiver and i-th radio port
L	Number of radio ports
m	Nakagami-m fading factor
N_0	Noise power
N_r	Number of receive antennas
N_t	Number of transmit antennas per radio port
P	Total transmit power
T	Block-length

Numbers

$\mathbb{C}$	Set of complex numbers
$\mathbb{R}$	Set of real numbers
$\mathbb{N}$	Set of natural numbers

Matrix and Vector Representations

$\mathbf{0}$	all-zero vector
$\boldsymbol{\Xi}$	Diagonal matrix represents the large-scale fading effects
$\mathbf{A}^H$	Conjugate (hermitian) transpose of matrix $\mathbf{A}$
$\mathbf{A}^{-1}$	Inverse of matrix $\mathbf{A}$
$\mathbf{A}^\dagger$	Pseudo-inverse of matrix $\mathbf{A}$
$\mathbf{A}_i$	Matrix $\mathbf{A}$ with the i-th column removed
$[\mathbf{A}]_{ij}$	(i,j)-th minor of matrix $\mathbf{A}$
$\det(\mathbf{A})$	Determinant of matrix $\mathbf{A}$
$\mathrm{diag}\{\mathbf{a}\}$	Represents diagonal matrix with diagonal elements vector $\mathbf{a}$
$\mathbf{h}$	Channel fading vector representing the small-scale fading effects
$\mathbf{H}$	Channel fading matrix representing the small-scale fading effects
$\mathbf{I}_M$	$(M \times M)$ identity matrix
$\mathbf{n}$	Additive white Gaussian noise vector
$\mathrm{tr}(\mathbf{A})$	Trace of matrix $\mathbf{A}$
$\mathbf{x}$	Transmitted signal vector
$\mathbf{y}$	Received signal vector

Functions

$\Gamma(\cdot)$	Gamma function [1, Eq. (8.310.1)]
$\psi(\cdot)$	Euler's digamma function [1, Eq. (8.360.1)]
$\mathcal{CN}(\mathbf{a}, \mathbf{B})$	complex normally distributed vector with mean $\mathbf{a}$ and covariance matrix $\mathbf{B}$
$\mathcal{E}(\cdot)$	Expectation operation
$\mathtt{Ei}(x)$	Exponential integral function: $\mathtt{Ei}(x) = -\int_{-x}^{\infty} \frac{e^{-t}}{t} dt$ [1, Eq. (8.211.1)]

$\exp(\cdot)$	Exponential function
$\log_2(\cdot)$	Logarithmic function with base 2
$\ln(\cdot)$	Natural logarithmic function

Contents

Notations iv

Contents viii

List of Figures xi

1 Introduction 1

1.1 Multiple-Input Multiple-Output systems . . . 3
1.2 Distributed MIMO systems . . . 4
1.3 Goals of this thesis . . . 5
1.3.1 Channel modeling of D-MIMO systems . . . 5
1.3.2 Receivers selection for D-MIMO systems . . . 6
1.3.3 Effective capacity analysis . . . 6
1.4 Key contributions . . . 7
1.5 Structure of this thesis . . . 8

2 Basic Multipath Propagation Characteristics 9

2.1 Path loss . . . 9
2.2 Slow and fast fading . . . 10
2.3 Frequency-flat and frequency-selective fading . . . 11
2.4 Modeling of flat-fading channels . . . 11
2.5 Multipath fading . . . 12
2.5.1 Rayleigh model . . . 12
2.5.2 Nakagami-m model . . . 12
2.6 Shadowing . . . 13
2.6.1 Log-normal model . . . 13
2.6.2 Gamma model . . . 13
2.6.3 Inverse-Gaussian model . . . 14
2.7 Combined path loss and shadowing . . . 15

2.8 Composite multipath and shadowing 16

3 D-MIMO Systems in RIG Fading Channels **18**
3.1 MIMO system model 18
3.2 Ergodic capacity analysis of optimal receivers 19
3.2.1 Exact analysis 20
3.2.2 Low-SNR analysis 23
3.2.3 High-SNR analysis 26
3.3 Ergodic capacity analysis of optimal receivers in specific cases 28
3.3.1 Point-to-point MIMO systems 29
3.3.2 Lower bound – Distance parameter analysis 29
3.3.3 Lower bound – Large system analysis 30
3.3.4 Wideband slope $\mathcal{S}_0^{\text{opt}}$ characteristics 35
3.4 Achievable sum rate analysis of ZF receivers 36
3.4.1 Exact analysis 37
3.4.2 Lower bound – Distance parameter analysis 39
3.4.3 Lower bound – Large system analysis 40
3.4.4 Upper bound – High-SNR analysis 43
3.4.5 Low-SNR analysis 44
3.4.6 High-SNR analysis 46
3.5 Achievable sum rate analysis of MMSE receivers 47
3.5.1 A generic framework 48
3.5.2 Low-SNR analysis 49
3.5.3 High-SNR analysis 52

4 Effective Capacity Analysis of MISO Systems **55**
4.1 MISO system model 55
4.1.1 RIG fading channels 55
4.1.2 $\mathcal{G}$ fading channels 56
4.2 Low-SNR analysis 57
4.2.1 RIG fading channels 58
4.2.2 $\mathcal{G}$ fading channels 60
4.3 High-SNR analysis 64

5 Conclusions **67**
5.1 Summary of results 67
5.2 Future research areas 68

A Standard Results and Formulae **69**
A.1 Modified Bessel function of second kind 69
A.2 Properties of Inverse-Gaussian distributed RVs 69
A.3 Basic majorization theory results 70

B Original publications **72**

References **80**

List of Figures

1.1 Distributed MIMO system with L multiple-antenna radio ports transmitting data to a multiple-antenna base station. 4

2.1 Probability density function of the Inverse-Gaussian distribution for different λ values with $\mathcal{E}[\xi] = \mu = 1$ (courtesy of [33]). 15

2.2 Path loss, shadowing and multipath fading versus distance (with the slope of 10υ dB/decade) (courtesy of [2]). 16

3.1 Simulated ergodic capacity and analytical low-SNR approximation against the transmit E_b/N_0 ($N_t = 2$, $L = 3$, $\mu_i = \mu = 4$, $\lambda_i = \lambda = 3$, $D_i = D = 1500$m ($\forall i = 1, \ldots, L$), and $\upsilon = 4$). 26

3.2 Simulated ergodic capacity and low-SNR approximation against the transmit E_b/N_0 for different values of the large-scale fading mean parameter $\mu_i = \mu$ ($N_r = 12$, $N_t = 2$, $L = 3$, $\lambda_i = \lambda = 3$, $D_i = D = 1500$m ($\forall i = 1, \ldots, L$), and $\upsilon = 4$). . . . 27

3.3 Simulated ergodic capacity, analytical high-SNR approximation, analytical lower bound, and simulated upper bound against the average SNR ($N_t = 2$, $L = 3$, $\mu_i = [4, 2, 3]$, $\lambda_i = [3, 5, 7]$, $D_i = [1000\text{m}, 1500\text{m}, 2000\text{m}]$, where $i = 1, \ldots, L$, and $\upsilon = 4$). 28

3.4 Simulated ergodic capacity, analytical lower bound, analytical large-system lower bound, and its asymptote against the number of transmit antennas, N_t ($\gamma = 25$dB, $L = 1$, $\beta = 2$, $\mu_i = \mu = 1$, $\lambda_i = \lambda = 3$, $D_i = D = 1500$m ($\forall i = 1, \ldots, L$), and $\upsilon = 4$). 34

3.5 ZF receivers: Simulated sum rate, analytical upper and lower bounds against the average SNR ($N_t = 2$, $L = 3$, $\mu_i = \mu = 4$, $\lambda_i = \lambda = 3$, $D_i = D = 1500$m ($\forall i = 1, \ldots, L$), and $\upsilon = 4$). 38

3.6 ZF receivers: Simulated sum rate, analytical upper/lower bounds against the average SNR ($N_r = 12$, $N_t = 2$, $\mu_i = \mu = 4$, $\lambda_i = \lambda = 3$, $D_i = D = 1500$m ($\forall i = 1, \ldots, L$), and $\upsilon = 4$). 39

3.7 ZF receivers: Simulated sum rate, analytical upper/lower bounds against the average SNR for two different configurations ($N_r = 12$, $L = 3$, $N_t = 2$, $\mu_i = \mu = 4$, $\lambda_i = \lambda = 3$, ($\forall i = 1, \ldots, L$), $\upsilon = 4$ with (a) anti-symmetrical configuration: $D_1 = 1000$m, $D_2 = 1500$m, $D_3 = 2000$m and (b) symmetrical configuration: $D_1 = D_2 = D_3 = 1500$m). 41
3.8 ZF receivers: Simulated sum rate, exact and asymptotic lower bounds against the number of transmit antennas, N_t ($\gamma = 15$dB, $L = 2$, $\beta = 2$, $\mu_i = \mu = 1$, $\lambda_i = \lambda = 10$ ($\forall i = 1, \ldots, L$), $D_i = [1000\text{m}, 1500\text{m}]$, and $\upsilon = 4$). 43
3.9 MMSE receivers: Low-SNR simulated sum rate and analytical linear approximation against the transmit E_b/N_0 ($N_t = 3$, $L = 3$, $\mu_i = \mu = 4$, $\lambda_i = \lambda = 13$, $D_i = D = 1500$m ($\forall i = 1, \ldots, L$), and $\upsilon = 4$). 51
3.10 Low-SNR simulated sum rate (optimal, ZF, and MMSE) and analytical linear approximations against the transmit E_b/N_0 ($N_r = 12$, $N_t = 2$, $L = 3$, $\mu_i = \mu = 1$, $\lambda_i = \lambda = 10$ ($\forall i = 1, \ldots, L$), $D_i = [1000\text{m}, 1500\text{m}, 2000\text{m}]$, and $\upsilon = 4$). 52

4.1 Low-SNR effective rate and analytical linear approximation against the transmit E_b/N_0 ($N_t = 6$, $A = 4$, $\lambda = 10$, and $m = 1$). 63
4.2 Low-SNR effective rate and analytical linear approximation against the transmit E_b/N_0 ($N_t = 6$, $m = 1$, $\lambda = 10$, and $\mu = 0.5$). 64
4.3 Low-SNR effective rate and analytical linear approximation against the transmit E_b/N_0 ($N_t = 6$, $m = 1$, $\lambda = 10$, and $\mu = 0.5$). 65
4.4 Low-SNR effective rate and analytical linear approximation against the transmit E_b/N_0 ($N_t = 6$, $A = 4$, $\lambda = 10$, and $\mu = 0.5$). 66
4.5 High-SNR effective rate and analytical linear approximation against the SNR ($A = 4$, $m = 2$, $\lambda = 10$, and $\mu = 2$). 66

Chapter 1

Introduction

Wireless communications is one of the fastest growing segments of the communications industry. The exponential growth of cellular telephone usage and wireless access networks have led to great optimism about wireless technology in general [2]. Over the past several decades, demands for increasing the data rates within a fixed bandwidth and with no extra power consumption have gained much research interest. In addition to that, wireless networks are expected to provide high-quality services (such as data, voice, and video) between several users and multiple sources of information. Many new applications, including wireless sensor networks, smart homes and appliances, and remote telemedicine, are emerging from research ideas to concrete systems. However, many technical challenges remain in designing robust wireless systems to support these aforementioned emerging applications. On the other hand, the convergence between decentralized wired and wireless technologies will allow operators and end users to enjoy all the functionalities and network resources towards the direction of ubiquitous communications. This means that end users will be able to receive the same service through different wireless access networks regardless of the devices they utilize.

We have many different ways to segment this complex field into different *applications, systems*, or *coverage regions* [2], [3]. *Wireless applications* include internet access, web browsing, voice, paging and short messaging, file transfer, video tele-conferencing, entertainment, sensing, subscriber information services, and distributed control. *Systems* include cellular telephone systems, wireless local area networks, wide-area wireless data systems, satellite systems, and ad-hoc wireless networks. *Coverage regions* include inside-building, campus area, city, regional, and global. The best characterization of wireless based communications along these various segments has resulted in considerable fragmentation in the industry, as evidenced by the many different wireless standards, products, and services being offered. One reason for this fragmentation is that different wireless applications have

different requirements. For example, Voice systems have relatively low data rate requirements and can tolerate a fairly high probability of bit error, but the total delay must be less than around 30 msec or it becomes noticeable to the end user. On the other hand, data systems typically require much higher data rates and very small bit error rates but do not have a fixed delay requirement. Likewise, Real-time video systems have high data rate requirements coupled with the same delay constraints as voice systems, while paging and short messaging services have very low data rate requirements and no delay constraints. The associated bottlenecks and single points-of-failure are clearly undesirable for the overall system. In addition, the transmission and signal processing in the hand held portable device must consume minimal power, while the signal processing that required to support multimedia applications and networking functions should be power-intensive. Thus, wireless networks place as much of the processing burden as possible on fixed sites (typically base stations) with large power resources.

Design of wireless networks differs fundamentally from wired network design due to the nature of the wireless channel. This channel is an unpredictable and difficult communications medium. As a signal propagates through a wireless channel, it experiences random fluctuations in time if the transmitter, receiver, or surrounding objects are moving, due to changing reflections and attenuation. It is also susceptible to noise, interference, and other channel impediments, while these impediments change over time in unpredictable ways due to users' movement [4]. The wireless radio channel poses a severe challenge as a medium for reliable high-speed communications. Thus, the characteristics of the channel appear to change randomly with time, which makes it difficult to design reliable systems with guaranteed performance.

We can also characterize the variation in received signal power over distance due to *path loss*, *multipath fading*, and *shadowing*. This demanding task can normally be accomplished by conducting radio channel measurements followed by the extraction of the path's parameters and the development of accurate channel models. A wireless system also consists of multiple dimensions: *time, frequency, space,* and *users*. Opportunistic communication maximizes the spectral efficiency by measuring when and where the channel is good and only transmits in those degrees of freedom. In this context, channel fading is beneficial in the sense that the fluctuations of the channel across the degrees of freedom ensures that there will be some degrees of freedom in which the channel is very good [3]. The technological breakthroughs to enable higher frequency systems with the same cost

and performance would greatly reduce the spectrum shortage. However, path loss at these higher frequencies is larger, thereby limiting range, unless directional antennas are used.

1.1 Multiple-Input Multiple-Output systems

It has been known for a while that in a downlink (i.e., base station to mobile terminal communication) with multiple receive antennas at the base station, allows several users to simultaneously communicate with the transmitter. Multiple antennas in effect increase the number of degrees-of-freedom in the system and allow spatial separation of the signals from the different users. It has been shown that a similar effect occurs in a point-to-point channel with multiple transmit and receive antennas, i.e., even when the antennas of the multiple users are co-located. This holds, provided that the scattering environment is rich enough to allow the receive antennas to separate out the signal from the different transmit antennas, allowing spatial multiplexing of information [3]. The most promising technology that satisfies all these requirements is the so-called *Multiple-Input Multiple-Output (MIMO) systems*, which make use of multiple antenna elements at both the transmitter and receiver sides. Foschini [5] and Telatar [6] separately demonstrated in their seminal works, the performance improvement when multiple antenna elements are employed at both ends of a radio link. The price to pay is increased complexity of the hardware (number of RF amplifier front-ends, etc.), as well as the complexity and energy consumption of the signal processing at both ends. This is a typical example where channel fading is beneficial to communication.

The most attractive features of MIMO technology are the so-called *spatial multiplexing gain* and *spatial diversity* [7]. By transmitting parallel or orthogonal data streams over a MIMO channel, the capacity of MIMO channel can potentially increase linearly with the minimum number of transmit and receive antennas [3], [6]. Compared to conventional Single-Input Single-Output (SISO) systems, MIMO systems significantly increase the spectral efficiency when using spatial multiplexing. Diversity occurs when the antenna spacing is large enough such that independent signal propagation paths are created, resulting in a reduced variation of the received signal's power. Diversity also increases the system reliability by sending the same information through multiple independent paths so that the probability of successful transmission is higher and thus it enhances the error rate performance. However, there is an inherent trade-off between spatial multiplexing and spatial diversity, which means that increasing the diversity advantage comes at the expense of decreasing the spatial multiplexing gain, and vice versa [7]. In fact, the authors in [7]

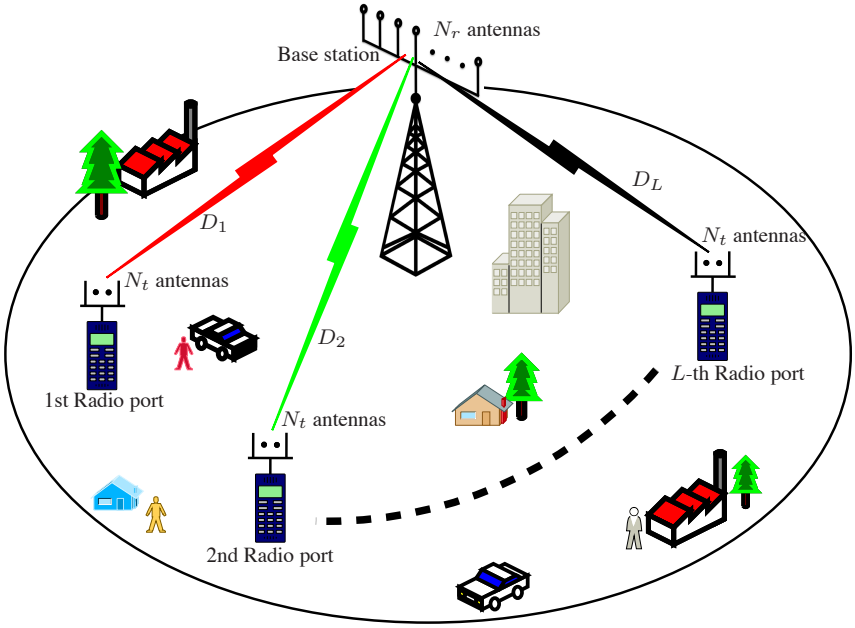

Figure 1.1: Distributed MIMO system with L multiple-antenna radio ports transmitting data to a multiple-antenna base station.

clearly showed that the diversity-multiplexing trade-off achievable by a system is a more fundamental measure of its performance than just its maximal diversity gain or its maximal multiplexing gain alone. In general, the optimal trade-off is determined by system requirements such as the desired data rate, efficiency, and reliability of transmission. Higher data rates can be achieved by employing multiplexing to full extent while high reliability benefits from diversity [8]. For this reason, the advantages of MIMO systems have been used in the most recent cellular standards, long-term evolution (LTE), to reach new performance heights [9].

1.2 Distributed MIMO systems

The potential of combining MIMO spatial multiplexing gains with macro-diversity[1] gains is realized by distributed MIMO (D-MIMO) systems, that promise to improve the capacity and cell coverage [10]. In D-MIMO systems, multiple antennas, placed at one end of the radio link, are deployed into multiple radio ports[2]. In such configurations, each radio

[1] In the wireless communications field, *macro-diversity* is a kind of space diversity scheme using several transmitter antennas and/or receiver antennas for transmitting the same signal. The distance between the transmitter and receiver is much larger than the wavelength, as opposed to *micro-diversity* where this distance is in the order of or smaller than the wavelength.

[2] The term "radio port" refers to every terminal or user transmitting data to a base station in an uplink scenario.

port experiences different large-scale fading effects and path loss (a.k.a. shadowing / slow fading), due to the different propagation paths. This is the key difference compared to conventional point-to-point MIMO configurations, which makes the performance analysis of D-MIMO systems a challenging mathematical problem. A schematic illustration of a D-MIMO system with L radio ports, with multiple-antennas transmitting data to a multiple-antenna base station is depicted in figure 1.1. In D-MIMO systems, the effects of large-scale fading are very critical. As such, there are very few analytical works (for e.g., [11], [12]) investigating the impact of composite fading channels (i.e., mixture of both small- and large-scale fading) on the performance of D-MIMO systems, mainly due to the difficulty in averaging the channel eigen-statistics over the shadowing distribution. Note also that the system under investigation can be considered as a typical MIMO MAC system or Multiuser MIMO system. The main reason for using the terminology distributed MIMO herein, is for the sake of consistency with previous related papers [11], [12].

1.3 Goals of this thesis

The main goals of this thesis work can be summarized as follows:

1.3.1 Channel modeling of D-MIMO systems

In this thesis, our main focus will be on the modeling of a new and an appropriate stochastic channel model that will capture exactly the composite fading fluctuations of D-MIMO channel. Also, we need to design new antenna array configurations based on channel models and antenna theory, to achieve higher ergodic capacity. On the other hand, we need to develop a simpler, tractable information-theoretic analysis, for a fundamental communication theory behind MIMO systems to utilize available analytical tools and random matrix theory principles.

In the literature, the Nakagami-m, Rayleigh distributions are often used to model the fast fading effects, whereas the Log-normal, Gamma distributions model the slow fading effects. In this context, the performance analysis of D-MIMO systems was explored for the case of Nakagami-m/Log-normal fading channels in [11] while in [12] it was investigated over Nakagami-m/Gamma fading (a.k.a. $\mathcal{K}$ fading) channels. The results using the gamma distribution as an alternative to the Log-normal distribution are essentially approximations and for the large variance case or in the tails of the Log-normal distribution, the gamma

distribution does not yield a good approximation [18]. Motivated by these intrinsic deficiencies, in this thesis, we propose the *Inverse-Gaussian* distribution as a more accurate approximation to the classical Log-normal model to describe large-scale fading effects.

1.3.2 Receivers selection for D-MIMO systems

One common approach to exploit the ergodic capacity of D-MIMO systems is to employ spatial multiplexing where independent information streams are transmitted from the antennas. These information streams are then separated at the receiver by means of appropriate signal processing techniques which achieve optimal performance. Despite the abundance of literature on D-MIMO channel capacity, the vast majority of existing works have focused primarily on systems employing nonlinear optimal receivers. These receivers minimize the error probability when all data vectors are equally likely by performing an exhaustive search (see e.g., [11–13]). The main disadvantages of such schemes are their high complexity and cost of implementation, especially for large number of antennas, which prohibits their deployment in practical communication systems.

To circumvent these issues, linear receivers such as zero-forcing (ZF) [14], [15] and minimum mean-squared error (MMSE) [16] receivers are often considered as low complexity alternatives. They provide sub-optimal performance but offer significant computational complexity reduction with tolerable performance degradation. Linear MMSE receiver is particularly important as it uses full degrees-of-freedom of the channel to optimally trades off strengthening the energy of the desired signal of interest and canceling unwanted interference, such that the signal-to-interference-and-noise ratio (SINR) is maximized [3]. Also, it operates close to optimal receivers' performance at both low- and high-SNRs. On the other hand, linear ZF receiver is relatively simpler compared to MMSE; yet, when independent decoding is used, it suffers from an inherent noise enhancement.

While prior relevant works have improved our knowledge on optimal, ZF and MMSE receivers' characterization, an analytical framework encompassing D-MIMO systems operating over *composite Rayleigh/Inverse-Gaussian fading* channels is not yet available, which motivated our research interest in this topic.

1.3.3 Effective capacity analysis

The delay constraints imposed by next generation wireless applications (e.g., interactive and multimedia streaming, interactive gaming, voice over IP (VoIP), mobile TV and com-

puting) require a suitable metric (for e.g., quality-of-service (QoS)) for assessing their impact on the overall system performance. In most of studies on MIMO/Multiple-Input Single-Output (MISO) channel capacity, the classical Shannon's ergodic capacity is employed as the main performance metric. However, this formulation does not capture the performance in the presence of QoS limitations in the form of constraints on queuing delays, although providing QoS assurances in many delay-sensitive wireless systems. Since the classical Shannon's ergodic capacity fails to do so, the so-called *effective capacity* was recently established as a rigorous alternative [17].

While prior relevant works have improved our knowledge on the effective capacity characterization of communication systems, a performance analysis of MISO systems operating over composite Rayleigh/Inverse-Gaussian and *Nakagami-m/Inverse-Gaussian fading* channels is not yet available, which motivated our research interest in this topic.

1.4 Key contributions

The original contributions of this thesis work are now summarized as follows:

- The main objective is to analytically investigate the performance of D-MIMO systems with optimal, linear ZF and MMSE receivers over Rayleigh/Inverse-Gaussian (RIG) fading channels. It is important to note that, to the best of the author's knowledge, the results in this thesis present the first-ever analytical investigation of D-MIMO systems over composite RIG fading channels.

- Capitalizing on some generic bounding techniques, we first derive new closed-form bounds on the ergodic capacity/sum rate of optimal, ZF and MMSE receivers. The proposed bounds apply for any finite number of antennas and remain relatively tight across the entire SNR range. These bounds are particularly tractable and allow for fast and efficient computation. With the help of these proposed bounds, we analytically explore the "large-system" regime by assuming that either the number of receive or transmit antennas grows large.

- In order to gain useful insights into the impact of fading parameters on optimal, ZF and MMSE receivers' performance, a detailed characterization in the asymptotically high and low SNR regimes is also provided. In these asymptotic cases, we investigate the notions of minimum normalized energy per information bit to reliably convey any positive rate and wideband slope, along with the high-SNR slope

and high-SNR power offset, respectively. We explicitly assess the performance offset between ZF, MMSE, and optimal receivers, we compare the derived results with previously reported results for the latter receivers. Our analytical results are quite informative and insightful; for example, they enable us to characterize the impact of large-scale fading parameters as well as path-loss on the sum rate.

- We pursue a detailed effective capacity analysis of Nakagami-m/Inverse-Gaussian MISO fading channels by deriving new, analytical expressions in the asymptotically high and low SNR regimes, for which tractable, closed-form effective capacity expressions are presented. These results enable us to draw useful conclusions about the impact of system parameters, such as delay constraints, fading parameters and number of antennas, on the effective rate of MISO fading channels.

1.5 Structure of this thesis

An outline of the remainder of this thesis is given as follows:

Chapter 2 introduces the basic principles of multipath propagation and subsequently presents the fundamental properties of path loss and different fading models. More specifically, in this chapter, we describe composite fading models, the Inverse-Gaussian distribution and their characteristics.

Chapter 3 studies the performance evaluation of D-MIMO systems in composite RIG fading channels. Capitalizing on some generic bounding techniques, we first derive new closed-form bounds on the ergodic capacity of optimal receivers. In order to gain useful insights into the impact of fading parameters on optimal receivers' performance, a detailed characterization in the asymptotically high and low SNR regimes is also provided. In addition, we explore the "large-system" regime and provide asymptotic expressions when the number of antennas grows large. A similar performance analysis is performed for the achievable sum rate of D-MIMO systems employing linear ZF and MMSE receivers.

Chapter 4 presents the closed-form expressions for the effective capacity of composite MISO channels, which enable efficient evaluation of the effective capacity of the systems with arbitrary numbers of antennas, for high and low SNRs.

Chapter 5 forms a summary of the most important conclusions drawn from this thesis and proposes several research paths for future work.

Chapter 2

Basic Multipath Propagation Characteristics

In a wireless channel, the interaction of the transmitted signal with the physical environment as it travels towards the receiver creates multiple propagated wavefronts. This phenomenon is commonly referred to as *multipath propagation*. Multipath propagation occurs due to three basic mechanisms, namely *reflection, diffraction*, and *scattering*. The multipath propagation can also be characterized by means of *path loss* and *fading*. The superposition of all impinging waves at the receiver side gives rise to fluctuations in the amplitude and phase of the received signal, commonly referred as *fading*, which is also distance dependent. We further classify fading in two categories namely *slow fading* (or *shadowing* or *large-scale fading* when path loss is included) and *fast fading* (or *multipath fading* or *small-scale fading*). In this chapter, we characterize the variations in received signal power over distance due to path loss, multipath fading, and shadowing. A brief description of these manifestations is provided in the following sections as follows:

2.1 Path loss

Path loss is caused by dissipation of the power radiated by the transmitter as well as the effects of the propagation channel. Path loss can be defined as the ratio between the received and transmitted powers. Accurate path loss models can be obtained from complex analytical models or empirical measurements. A number of path loss models have been developed over the years to predict path loss in wireless environments such as macro-cells, micro-cells, and inside buildings (refer to [2, Ch. 2], [19], and [20]).

A simplified model for path loss as a function of distance is given by [2]

$$\frac{P_r}{P_t} = K\left(\frac{D}{D_0}\right)^{-\upsilon} \tag{2.1}$$

where P_t, P_r are the average transmit and receive powers, respectively, K is a unit-less constant which depends on the antenna characteristics and the average channel attenuation, D_0 is a reference distance for the antenna far-field, and υ is the *path loss exponent* with typical values ranging from 2 to 6. Path loss models generally assume that path loss is the same at a given transmit-receive distance, D. The values for K, D_0, and υ can be obtained to approximate either an analytical or empirical model.

2.2 Slow and fast fading

Slow fading (a.k.a. large-scale fading) is due to path loss of the signal as a function of distance and shadowing by large objects such as buildings and hills. This occurs as a mobile user moves through a distance of the order of the cell size. On the other hand, fast fading (a.k.a. small-scale/multipath fading), occurs due to the constructive and destructive interaction of the multiple signal paths between the transmitter and receiver. This occurs at the spatial scale of the order of the carrier wavelength, and is frequency dependent.

A clear distinction between slow and fast fading is very important for the mathematical modeling of fading channels and for the performance evaluation of communication systems operating over such class of channels. This distinction is related to the so-called *coherence time* T_c of the channel, which measures the period of time over which the fading process is correlated (or equivalently, the period of time after which the correlation function of two impulses of the channel response taken at the same frequency but different time instants drops below a certain predetermined threshold). The coherence time is also related to the channel *Doppler spread* B_D by [2], [21]

$$T_c \approx \frac{1}{B_D}. \tag{2.2}$$

The fading is said to be *slow fading* if the *symbol duration* T_s is smaller than the channel's coherence time T_c (i.e., $T_s << T_c$); otherwise it is considered to be *fast fading*.

In slow fading a particular level of fade will affect many successive symbols, which leads to burst of errors, whereas in fast fading the fading differs from symbol to symbol. In the latter case and when the receiver decisions are based on an observation over two or

more symbol durations (e.g., differentially coherent or coded communications), it becomes necessary to consider the variation of the fading channel from one symbol duration to the next. This can be done through prevalent correlation model that depends essentially on the particular propagation environment and the communication systems under consideration.

2.3 Frequency-flat and frequency-selective fading

Frequency selectivity is an another important characteristic of fading channels. If all the spectral components of the transmitted signal are affected in a similar manner, the fading is said to be *frequency-flat*. This is the case for *narrowband systems*, in which the transmitted *signal bandwidth* B_s is much smaller than the channel's *coherence bandwidth* B_c (i.e., $B_s << B_c$). This bandwidth measures the frequency range over which the fading process is correlated and is defined as the frequency band over which the correlation function of two samples of the channel response, taken at the same time but different frequencies, falls below a predifined value. In addition to that, the coherence bandwidth is related to the *maximum delay spread* $\sigma_{\tau_{max}}$ by

$$B_c \approx \frac{1}{\sigma_{\tau_{max}}}. \tag{2.3}$$

On the other hand, if all the spectral components of the transmitted signal are affected by different amplitude gains and phase shifts, the fading is said to be *frequency-selective*. This applies to *wideband systems* in which the transmitted bandwidth is much bigger than the channel's coherence bandwidth.

2.4 Modeling of flat-fading channels

When fading affects narrowband systems, the received carrier amplitude is modulated by the fading amplitude/envelope φ, where φ is a random variable (RV) with mean-square value $\Omega = \overline{\varphi^2}$ and probability density function (p.d.f.) $p_\varphi(\varphi)$, which is dependent on the radio propagation environment. After passing through the fading channel, the signal is perturbed at the receiver by additive white Gaussian noise (AWGN), which is typically assumed to be statistically independent of the fading amplitude φ, and which is characterized by a one-sided power spectral density N_0 Watts/Hertz. Equivalently, the received instantaneous signal power is expressed as φ^2. Thus, we define the instantaneous signal-to-noise ratio (SNR) per symbol by $\gamma_{in} = \varphi^2 E_s/N_0$ and the average SNR per symbol by $\gamma = \Omega E_s/N_0$, where E_s is the energy per symbol. In this thesis, our performance evaluation over fading channels will be a function of the average SNR per symbol γ.

2.5 Multipath fading

As we mentioned earlier, multipath fading occurs due to the constructive and destructive combinations of randomly delayed, reflected, scattered, and diffracted transmitted signal components. This type of fading is relatively 'fast' and is therefore responsible for the short-term signal variations. Depending on the nature of the radio propagation environment, there are different models describing the multipath fading envelope's statistical behavior. It is thus of interest, to outline the commonly used statistical models, their corresponding p.d.f.s and their relation to physical channels.

2.5.1 Rayleigh model

The *Rayleigh distribution* is commonly used to model multipath fading environment if no line-of-sight (LOS) path exists between the transmitter and receiver antennas. In this case, the channel fading envelope φ is distributed according to

$$p_{\varphi}(\varphi) = \frac{2\varphi}{\Omega} \exp\left(-\frac{\varphi^2}{\Omega}\right), \qquad \varphi, \Omega > 0. \tag{2.4}$$

The Rayleigh distribution gives the best fit to the propagation of reflected and refracted paths through the troposphere and ionosphere, and to ship-to-ship radio links [21]. For any two Gaussian random variables X and Y, both with mean zero and equal variance σ^2, it can be shown that $Z = \sqrt{X^2 + Y^2}$ is Rayleigh-distributed [22].

2.5.2 Nakagami-m model

The *Nakagami-m distribution* is a more general multipath fading distribution, which is given by [23]

$$p_{\varphi}(\varphi) = \frac{2m^m \varphi^{2m-1}}{\Omega^m \Gamma(m)} \exp\left(-\frac{m\varphi^2}{\Omega}\right), \qquad \varphi, \Omega > 0 \tag{2.5}$$

where m is the Nakagami-m fading factor, which ranges from 0.5 to ∞. The Nakagami-m distribution includes the one-sided Gaussian distribution ($m = 0.5$) and the Rayleigh distribution ($m = 1$) as special cases. In the limit as $m \to +\infty$, the Nakagami-m fading channel converges to a nonfading AWGN channel (i.e., there is no fading). The Nakagami-m distribution gives the best fit to land-mobile and indoor-mobile multipath propagation, as well as ionospheric radio links [21], [23]. Note that some empirical measurements support values of the m parameter less than one, in which case the Nakagami-m fading causes more severe performance degradation than Rayleigh fading [2].

2.6 Shadowing

A signal transmitted over a wireless channel will experience random, 'slow' variations of the mean signal level at a given distance due to blockage from obstacles (such as trees, buildings, etc.), reflecting surfaces, and scattering objects in the signal path. Since the location, size, and dielectric properties of the blocking objects as well as the changes in reflecting surfaces and scattering objects that cause the random attenuation are generally unknown, statistical models must be used to characterize this attenuation. Communication systems' performance will depend only on this *shadowing* if the radio receiver is able to average out the fast multipath fading or if an efficient "micro" diversity system is used to eliminate the effects of multipath fading. Shadowing also decorrelates the transmitted signal over decorrelation distance. It is thus of interest, to outline the commonly used statistical models, their corresponding p.d.f.s and their relation to physical channels.

2.6.1 Log-normal model

The *Log-normal distribution* is the prevalent model in the characterization of the shadowing effects in various radar, optical and land-mobile systems [2], [21]. This model has been confirmed empirically to accurately model the variation in received power in both outdoor and indoor radio propagation environments (see e.g., [19], [20]), in which case the path SNR per symbol γ has a p.d.f. [24]

$$p_\xi(\xi) = \frac{\eta}{\xi\sqrt{2\pi\sigma^2}} \exp\left(-\frac{(\eta \ln \xi - \mu)^2}{2\sigma^2}\right), \qquad \xi \geq 0 \tag{2.6}$$

where $\eta = 10/\ln 10 = 4.3429$, and μ (dB) and σ (dB) are the mean and the standard deviation of the variable's natural logarithm, respectively.

2.6.2 Gamma model

Although the classical Log-normal distribution appears to be a simple expression to represent shadowing effects, it is often inconvenient when it is used in the performance evaluation of several communication systems due its logarithmic nature. The *Gamma distribution* has been recently proposed as an approximation to the Log-normal distribution (e.g., [25], [26]) and it was demonstrated as a substitute to the Log-normal distribution to describe the shadowing phenomena in terrestrial and satellite channels (e.g., [27], [28]). The p.d.f. of the Gamma distribution is given by

$$p_\xi(\xi) = \frac{1}{\Gamma(k)}\left(\frac{\xi^{k-1}}{\theta^k}\right)\exp\left(-\frac{\xi}{\theta}\right), \qquad \xi, \theta, k > 0 \tag{2.7}$$

where $k, \theta = \mathcal{E}[\xi]/k$, are the *shape* and *scale* parameters of the Gamma distribution, respectively.

One of the most useful properties of the Gamma distribution is the reproductive property. This means that the sum of n independent and identically distributed (i.i.d.) Gamma random variables (RVs) with common scale parameter θ and shape parameters $\{k_i\}_{i=1}^{n}$ is also Gamma distributed with parameters $\left(\sum_{i=1}^{n} k_i, \theta\right)$ [29], [30]. We also invoke that a squared Rayleigh RV follows the Gamma distribution with scale parameter 1.

2.6.3 Inverse-Gaussian model

For the large variance case or in the tails of the Log-normal distribution, the Gamma distribution does not yield a good approximation [18]. The *Inverse-Gaussian (IG) distribution* has been demonstrated as a more accurate approximation to the the Log-normal distribution when heavy-tailed behavior is expected [31–33]. The IG distribution was initially proposed by Tweedie in 1945 during a statistical investigation of data relating to electrophoretic measurements [34], [35]. The name "Inverse-Gaussian" comes from the inverse relationship between the cumulant generating functions of these distributions and those of standard normal (i.e., Gaussian) distributions [36], [37]. The same class of distributions was derived by Wald [38] as an asymptotic form of distribution of average sample number in sequential analysis. Sometimes, the name "Wald distribution" is also used for members of this class. The IG distribution is generally used to model any non-negative positively skewed data.

This IG distribution was originally introduced in [18], [39] as an accurate substitute to the Log-normal distribution for describing shadowing effects in RF wireless communications. In the context of optical systems, it has been employed for modeling the statistical behavior of avalanche photo diodes receivers [40] and it has been used to describe turbulence-induced fading in free-space optical systems [41]. In addition to that the authors of [41], [42] employed *Kolmogorov–Smirnov* goodness of fit statistical tests in order to measure the difference between the two models (i.e., IG and Log-normal) and they proposed the IG distribution, as a less complex alternative to the Log-normal distribution. On the other hand, Karmeshu and Agrawal used the *Kullback–Leibler* measure and found that the IG approximates the Log-normal distribution more accurate than the Gamma distribution [18]. The p.d.f. of the IG distribution is given by [33], [36], [37]

$$p_{\xi}(\xi) = \sqrt{\frac{\lambda}{2\pi}} \xi^{-\frac{3}{2}} \exp\left(-\frac{\lambda(\xi-\mu)^2}{2\mu^2\xi}\right), \qquad \xi, \mu, \lambda > 0 \tag{2.8}$$

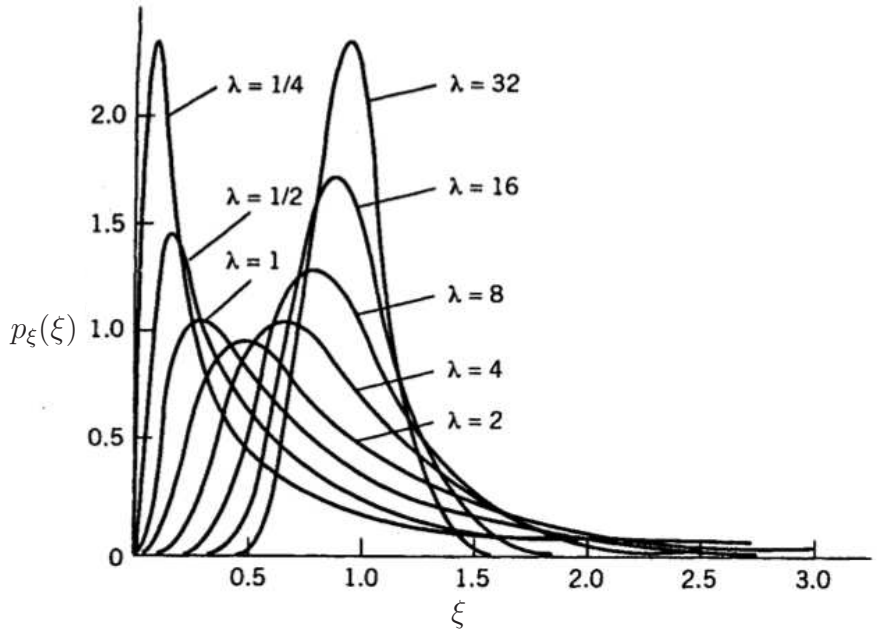

Figure 2.1: Probability density function of the Inverse-Gaussian distribution for different λ values with $\mathcal{E}[\xi] = \mu = 1$ (courtesy of [33]).

where μ, λ are the *mean* and the *scale* parameters of the IG distribution, respectively. The p.d.f. of the IG distribution for different λ values is plotted in Fig. 2.1. As $\lambda \to \infty$, the IG distribution becomes more like a Gaussian distribution. The IG distribution also represents the first hitting time distribution for a Brownian motion with drift and this interpretation has been extensively used in situations where one is actually concerned with waiting times [43], [44].

The advantage of using the Gamma and the IG distribution as an alternative to the Log-normal distribution is that it can allow tractable algebraic manipulation in the performance analysis of communication systems.

2.7 Combined path loss and shadowing

Models for path loss and shadowing can be superimposed to capture power falloff versus distance along with the random attenuation about this path loss due to shadowing. In this combined model, average path loss (dB) is characterized by the path loss model and shadow fading, with a mean of 0 dB, creates variations about this path loss. The figure 2.2 shows the combination of the simplified path loss model (2.1) and the Log-normal shadowing random process defined by (2.6). For this combined model, the ratio of received to transmitted

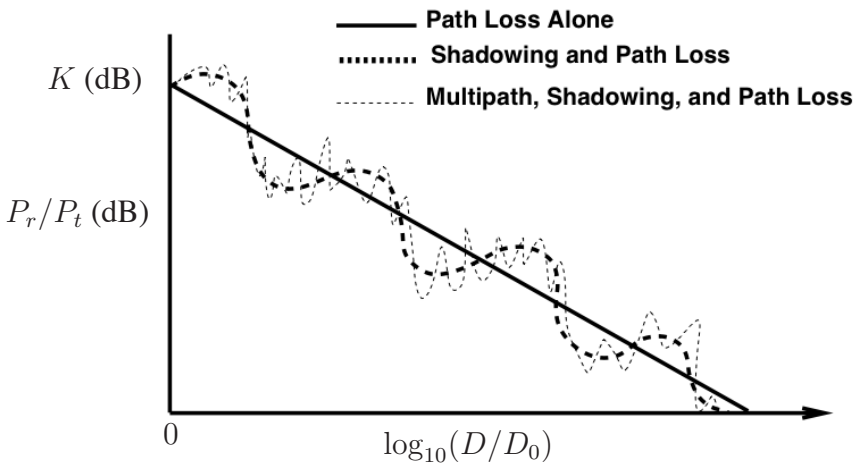

Figure 2.2: Path loss, shadowing and multipath fading versus distance (with the slope of 10υ dB/decade) (courtesy of [2]).

power in dB is given by

$$\frac{P_r}{P_t}(\text{dB}) = 10\log_{10} K - \upsilon 10\log_{10}\left(\frac{D}{D_0}\right) - \psi_{dB} \tag{2.9}$$

where ψ_{dB} is a Gaussian distributed RV with zero-mean and variance $\sigma^2_{\psi_{dB}}$. In (2.9) and as shown in Fig. 2.2, the path loss decreases linearly with $\log_{10}(D/D_0)$ with a slope of 10υ dB/decade.

2.8 Composite multipath and shadowing

Mixtures of multipath fading and shadowing are frequently encountered in different realistic scenarios in wireless communication systems. A composite multipath/shadowed fading environment consists of multipath fading superimposed by shadowing effects. In this environment, the receiver does not average out the envelope fading due to multipath but rather reacts to the instantaneous composite multipath/shadowed signal [45, Sec. 2.4.2]. This is often the scenario in congested downtown areas with slow moving pedestrians and vehicles or stationary users [46–48]. This type of composite fading is also observed in land–mobile satellite systems subject to urban shadowing [49], [50]. There are many approaches and various combinations suggested in the literature for obtaining the composite distribution. The interested readers are referred to [50, Table I] for a brief survey of those composite distributions in the context of narrowband land–mobile satellite modeling.

A composite distribution arises therefore as a suitable statistical characterization of the SNR in such class of channels. Composite multipath/shadowing fading channels are gen-

erally modeled as a mixture of Nakagami-m or Rayleigh multipath fading and Log-normal shadowing. The composite Gamma/Log-normal p.d.f. was introduced by Ho and Stüber [48] and arises in Nakagami-m shadowed environments, whereas Suzuki [46] proposed a composite Rayleigh/Log-normal p.d.f. to model the multipath/shadowing distribution for the fading amplitude that characterizes the mobile channel. Since the Log-normal distribution is used to describe the shadowing phenomenon for both the Suzuki and the Rayleigh/Log-normal models, the resulting composite p.d.f. is unfortunately not in closed-form, thereby making the performance evaluation of communication links cumbersome.

Using the Gamma or IG distribution as an alternative to the Log-normal distribution leads to other simpler composite closed-form distributions. For example, the composite distribution that approximates the Rayleigh/Log-normal one quite well is the so-called $\mathcal{K}$ distribution [51], which is a mixture of both the Rayleigh and Gamma distributions. The $\mathcal{K}$ distribution has been suggested for modeling diverse scattering phenomena such as tropospheric propagation of radio waves, various types of radar clutter, and optical scintillation from the atmosphere [52], [53].

In this thesis, we first propose the IG distribution as an alternative distribution to the Log-normal distribution for the performance evaluation of distributed MIMO and MISO systems. We then consider the more general Rayleigh/IG (RIG) and Nakagami-m/IG (a.k.a. $\mathcal{G}$ distribution) composite distribution models in the performance analysis. The $\mathcal{G}$ distribution was first proposed in [54] in the context of Synthetic Aperture Radar image modeling, whereas in [55], it was first applied to the performance evaluation of communications systems, and in [56], in the context of relaying systems.

Chapter 3

D-MIMO Systems in RIG Fading Channels

In this chapter, we present a detailed performance analysis of three receivers, namely optimal, ZF, and MMSE. First, we introduce a distributed MIMO (D-MIMO) system operating over RIG fading channels. Secondly, we present analytical expressions for the ergodic capacity of optimal receivers and derive new upper/lower capacity bounds, along with low- and high-SNR analytical expressions. Next, we analyze these analytical expressions for various types of special cases, especially in the "large-system" regime. Finally, we perform a similar analysis for the achievable sum rate of linear ZF and MMSE receivers.

3.1 MIMO system model

Consider a typical MIMO system with N_r receive antennas and L radio ports each connected to N_t transmit antennas with the assumption $N_r \geq LN_t$. The input-output model for this D-MIMO system is

$$\mathbf{y} = \sqrt{\gamma}\mathbf{H}\boldsymbol{\Xi}^{1/2}\mathbf{x} + \mathbf{n} \tag{3.1}$$

where $\mathbf{x} \in \mathbb{C}^{LN_t \times 1}$ and $\mathbf{y} \in \mathbb{C}^{N_r \times 1}$ are the transmitted and received signal vectors, respectively, while $\mathbf{n} \sim \mathcal{CN}(\mathbf{0}, \mathbf{I}_{N_r})$ is the complex additive white Gaussian noise (AWGN) and $\gamma = P/N_0$ is the average SNR, where P is the total transmit power and N_0 is the noise power. The large-scale fading effects are represented by the diagonal matrix $\boldsymbol{\Xi} \in \mathbb{R}^{LN_t \times LN_t}$ whose structure is $\boldsymbol{\Xi} = \mathrm{diag}\{\mathbf{I}_{N_t}\xi_i/D_i^{\upsilon}\}$ for $i = 1, \ldots, L$. Note that all N_t antennas in the i-th radio port experience the same large-scale fading[1]. The distance between the receiver and the i-th radio port is denoted by D_i, while υ is the path-loss exponent. The

[1]This assumption is valid because total antenna separation distance between N_t antennas (in the i-th radio port) is much lesser compared to distance from the receiver. Moreover, all radio ports are uniformly distributed in a cell and they are separated with larger distances between them. As such, each radio port

large-scale fading coefficients, ξ_i, are modeled as independent IG random variables (RVs), $\xi_i \sim \mathrm{IG}(\mu_i, \lambda_i)$, or

$$p(\xi_i) = \sqrt{\frac{\lambda_i}{2\pi}} \xi_i^{-\frac{3}{2}} \exp\left(-\frac{\lambda_i(\xi_i - \mu_i)^2}{2\mu_i^2 \xi_i}\right), \qquad \xi_i, \mu_i, \lambda_i > 0 \tag{3.2}$$

where μ_i, λ_i are the mean and the scale parameters of the IG distribution, respectively [33].

The entries of the channel matrix $\mathbf{H} \in \mathbb{C}^{N_r \times LN_t}$ are assumed to be independent and identically distributed (i.i.d.) Rayleigh RVs, i.e., $h_{st} \sim \mathcal{CN}(0,1)$, where $s = 1, \ldots, N_r$ and $t = 1, \ldots, LN_t$. We invoke that a squared Rayleigh RV follows the Gamma distribution with scale parameter 1. We now recall that the sum of n i.i.d. Gamma RVs with common scale parameter θ and shape parameters $\{k_i\}_{i=1}^n$ is also Gamma distributed with parameters $\left(\sum_{i=1}^n k_i, \theta\right)$ [30]. As such, the sum of N_r i.i.d. Gamma RVs with scale parameter 1 is distributed as $\varphi_i \sim \mathrm{Gamma}(N_r, 1)$, or

$$p(\varphi_i) = \frac{\varphi_i^{N_r - 1}}{\Gamma(N_r)} \exp(-\varphi_i), \quad \varphi_i \geq 0. \tag{3.3}$$

3.2 Ergodic capacity analysis of optimal receivers

In this section, we perform an ergodic capacity analysis of D-MIMO systems with optimal receivers in RIG fading channels. We assume that the receiver has perfect channel state information (CSI) while the transmitter has nor statistical neither instantaneous CSI and as such performs uniform power allocation across all the data streams. Then, the MIMO mutual information reads as [6]

$$\mathcal{I} \triangleq \log_2\left(\det\left(\mathbf{I}_{N_r} + \frac{\gamma}{LN_t}\mathbf{H}\boldsymbol{\Xi}\mathbf{H}^H\right)\right) \quad (\text{bits/s/Hz}) \tag{3.4}$$

while the MIMO ergodic capacity is given by

$$\mathcal{C}_{\text{erg}} \triangleq \mathcal{E}[\mathcal{I}] = \mathcal{E}\left[\log_2\left(\det\left(\mathbf{I}_{N_r} + \frac{\gamma}{LN_t}\mathbf{H}\boldsymbol{\Xi}\mathbf{H}^H\right)\right)\right] \tag{3.5}$$

where the expectation is taken over all channel realizations of $\mathbf{H}$, $\boldsymbol{\Xi}$ and the channel is assumed to be ergodic. We use the following matrix determinant property $\det(\mathbf{I}_n + \mathbf{A}_{n\times m}\mathbf{B}_{m\times n}) \triangleq \det(\mathbf{I}_m + \mathbf{B}_{m\times n}\mathbf{A}_{n\times m})$, to rearrange (3.5) and obtain the following alternative expression

$$\mathcal{C}_{\text{erg}} = \mathcal{E}\left[\log_2\left(\det\left(\mathbf{I}_{LN_t} + \frac{\gamma}{LN_t}\boldsymbol{\Xi}\mathbf{H}^H\mathbf{H}\right)\right)\right]. \tag{3.6}$$

experiences different large-scale fading and all N_t antennas in the i-th radio port experience the same large-scale fading [21].

3.2.1 Exact analysis

We now derive new ergodic capacity upper and lower bounds for optimal receivers. Capitalizing on the results of [11], we first derive an upper capacity bound as follows:

Proposition 3.1. *For D-MIMO systems with optimal receivers in RIG fading channels, the ergodic capacity in (3.5) is upper bounded by* $\mathcal{C}_{\text{UB}}$*, with*

$$\mathcal{C}_{\text{UB}} = \frac{\gamma}{2\sqrt{\pi}\ln 2\, L\, \Gamma(N_r)} \sum_{i=1}^{L} \frac{1}{D_i^v} \exp\left(\frac{\lambda_i}{\mu_i}\right) \sum_{j=1}^{N} w_j V_i(x_j) \tag{3.7}$$

where $V_i(t) = t^{-\frac{1}{2}} \exp\left(-\frac{\lambda_i^2}{4\mu_i^2 t}\right) G_{3,2}^{1,3}\left(\frac{\gamma_i \mu_i t}{LN_t \lambda_i D_i^v}\Big|_{0,-1}^{-N_r,0,0}\right)$*,* $\{x_j\}_{j=1}^{N}$ *are the zeros of the* N*-th order Laguerre polynomial,* $\{w_j\}_{j=1}^{N}$ *are the weight factors tabulated in [57, Table 25.9], and* $G_{p,q}^{m,n} = \left[x\Big|_{a_1,\ldots,a_p}^{b_1,\ldots,b_q}\right]$ *denotes the Meijer's-G function [1, Eq. (9.301)].*

Proof. Using [11, Eq. (64)], we can rewrite the ergodic capacity in (3.5) as

$$\mathcal{C}_{\text{erg}} \leq \mathcal{C}_{\text{UB}} = \frac{N_t}{\ln 2} \sum_{i=1}^{L} \underbrace{\mathcal{E}\left[\ln\left(1 + \frac{\gamma}{LN_t}\frac{\xi_i \varphi_i}{D_i^v}\right)\right]}_{I_1}. \tag{3.8}$$

Now, the expectation term is evaluated as follows:

$$I_1 = \int_0^\infty \int_0^\infty \ln\left(1 + \frac{\gamma}{LN_t}\frac{\xi_i\varphi_i}{D_i^v}\right)\, p(\varphi_i)\, p(\xi_i)\, d\varphi_i\, d\xi_i \tag{3.9}$$

$$= \int_0^\infty \int_0^\infty G_{1,2}^{2,2}\left(\frac{\gamma_i \xi_i \varphi_i}{LN_t D_i^v}\Big|_{1,0}^{1,1}\right)\, p(\varphi_i)\, d\varphi_i\, p(\xi_i)\, d\xi_i \tag{3.10}$$

where in (3.10), we have expressed $\ln(1+ax)$ in terms of a Meijer's-G function [58, Eq. (8.4.6.5)]. Substituting (3.3) into (3.10) and using [1, Eq. (7.813.1)], we can easily evaluate the first integral as

$$I_1 = \frac{1}{\Gamma(N_r)} \int_0^\infty G_{3,2}^{1,3}\left(\frac{\gamma_i \xi_i}{LN_t D_i^v}\Big|_{1,0}^{1-N_r,1,1}\right)\, p(\xi_i)\, d\xi_i. \tag{3.11}$$

Substituting (3.2) into (3.11) and making a change of variables namely, $t_i = (2\xi_i \mu_i^2/\lambda_i)$, gives

$$I_1 = \sqrt{\frac{\lambda_i}{2\pi}} \frac{\exp\left(\frac{\lambda_i}{\mu_i}\right)}{\Gamma(N_r)} \int_0^\infty \xi_i^{-\frac{1}{2}-1}\, \exp\left(-\frac{\lambda_i}{2\mu_i^2}\xi_i - \frac{\lambda_i/2}{\xi_i}\right) G_{3,2}^{1,3}\left(\frac{\gamma_i \xi_i}{LN_t D_i^v}\Big|_{1,0}^{1-N_r,1,1}\right) d\xi_i \tag{3.12}$$

$$= \frac{\lambda_i \exp\left(\frac{\lambda_i}{\mu_i}\right)}{2\sqrt{\pi}\mu_i \Gamma(N_r)} \int_0^\infty t_i^{-\frac{1}{2}-1}\, \exp(-t_i) V_i'(t_i) dt_i \tag{3.13}$$

where $V_i'(t_i) = \exp\left(-\frac{\lambda_i^2}{4\mu_i^2 t_i}\right) G_{3,2}^{1,3}\left(\frac{\gamma_i \mu_i t_i}{LN_t \lambda_i D_i^{\upsilon}}\middle|_{1,0}^{1-N_r,1,1}\right)$. We can simplify (3.13) using one of the properties of Meijer's-G function [1, Eq. (9.31.5)] as follows:

$$I_1 = \frac{\gamma \exp\left(\frac{\lambda_i}{\mu_i}\right)}{2\sqrt{\pi} LN_t D_i^{\upsilon} \Gamma(N_r)} \int_0^{\infty} \exp(-t_i)\, V_i(t_i)\, dt_i \tag{3.14}$$

where $V_i(t_i)$ is defined in (3.7). To the best of the author's knowledge, the above integration cannot be expressed in closed-form. Yet, it can be efficiently evaluated by Gauss-Laguerre quadratic integration [57, Eq. (25.4.45)] and it is given as follows:

$$I_1 = \frac{\gamma \exp\left(\frac{\lambda_i}{\mu_i}\right)}{2\sqrt{\pi} LN_t D_i^{\upsilon} \Gamma(N_r)} \sum_{j=1}^{N} w_j V_i(x_j). \tag{3.15}$$

To conclude the proof, we substitute (3.15) into (3.8) and simplify it. □

In the above proof, Gauss-Laguerre quadratic integration has been used to approximate the integral expression. While (3.7) can be used to compute the upper bound for D-MIMO systems in RIG fading channels, the computation of Gauss-Laguerre quadratic integration can still be time consuming at low SNRs (e.g., $\gamma < -15$ dB). More importantly, the above upper bound, though in analytical form, provides limited physical insights. Thus, it is of interest to consider the high-SNR regime for further analyzing the upper bound.

Corollary 3.1. *At high-SNRs (i.e., $\gamma \to \infty$), the ergodic capacity upper bound $\mathcal{C}_{\mathrm{UB}}$ simplifies to*

$$\begin{aligned}\mathcal{C}_{\mathrm{UB}}^{\infty} = {} & LN_t \log_2\left(\frac{\gamma}{LN_t}\right) + \frac{LN_t}{\ln 2}\psi(N_r) \\ & + N_t \sum_{i=1}^{L}\left(\log_2(\mu_i) - \upsilon \log_2(D_i) + \frac{1}{\ln 2}\exp\left(\frac{2\lambda_i}{\mu_i}\right) \mathtt{Ei}\left(\frac{-2\lambda_i}{\mu_i}\right)\right).\end{aligned} \tag{3.16}$$

Proof. By taking γ large in (3.8), we trivially get

$$\mathcal{C}_{\mathrm{UB}}^{\infty} = \frac{N_t}{\ln 2}\sum_{i=1}^{L} \mathcal{E}\left[\ln\left(\frac{\gamma}{LN_t}\frac{\xi_i \varphi_i}{D_i^{\upsilon}}\right)\right] \tag{3.17}$$

$$= \frac{N_t}{\ln 2}\sum_{i=1}^{L}\left(\mathcal{E}\left[\ln\left(\frac{\gamma}{LN_t D_i^{\upsilon}}\right)\right] + \mathcal{E}\Big[\ln(\varphi_i)\Big] + \mathcal{E}\Big[\ln(\xi_i)\Big]\right) \tag{3.18}$$

$$\begin{aligned} = {} & LN_t \log_2\left(\frac{\gamma}{LN_t}\right) - N_t \sum_{i=1}^{L} \upsilon \log_2(D_i) + \frac{N_t}{\ln 2}\sum_{i=1}^{L}\mathcal{E}\Big[\ln(\varphi_i)\Big] \\ & + \frac{N_t}{\ln 2}\sum_{i=1}^{L}\mathcal{E}\Big[\ln(\xi_i)\Big].\end{aligned} \tag{3.19}$$

Using [1, Eq. (4.352.1)], we can obtain the first log-moment of Gamma distributed RV as

$$\mathcal{E}[\ln(\varphi_i)] = \psi(N_r). \tag{3.20}$$

Thus, we can obtain (3.16) by combining (3.20), (A.7) with (3.19) and simplifying it. □

Clearly, the high-SNR upper bound in (3.16) decouples the effects of small- and large-scale fading on the ergodic capacity. Now, we give a new ergodic capacity lower bound via the following proposition.

Proposition 3.2. *For D-MIMO systems with optimal receivers in RIG fading channels, the ergodic capacity in (3.5) is lower bounded by* $\mathcal{C}_{\mathrm{LB}}$*, with*

$$\mathcal{C}_{\mathrm{LB}} = LN_t \log_2\left(1 + \frac{\gamma}{LN_t}\exp\left(\frac{1}{L}\sum_{i=1}^{L}\left(\ln\mu_i - \upsilon\ln D_i + \exp\left(\frac{2\lambda_i}{\mu_i}\right)\mathtt{Ei}\left(\frac{-2\lambda_i}{\mu_i}\right)\right) + \frac{1}{LN_t}\sum_{k=0}^{LN_t-1}\psi(N_r-k)\right)\right). \tag{3.21}$$

Proof. The proof relies on the application of Minkowski's inequality to (3.5), as proposed in [59, Th. 1]. Exploiting the fact that $\ln(1+\alpha\exp(x))$ is convex in x for $\alpha > 0$, and thereafter applying Jensen's inequality, we can obtain the following lower bound

$$\mathcal{C}_{\mathrm{erg}} \geq \mathcal{C}_{\mathrm{LB}} = LN_t\log_2\left(1+\frac{\gamma}{LN_t}\exp\left(\frac{1}{LN_t}\underbrace{\mathcal{E}\left[\ln\left(\det\left(\boldsymbol{\Xi}\mathbf{H}^H\mathbf{H}\right)\right)\right]}_{I_2}\right)\right). \tag{3.22}$$

Recalling the identity of square matrices $\det(\mathbf{AB}) = \det(\mathbf{A})\det(\mathbf{B})$, we can express the above expectation term as follows:

$$I_2 = \mathcal{E}\left[\ln(\det(\boldsymbol{\Xi}))\right] + \mathcal{E}\left[\ln\left(\det\left(\mathbf{H}^H\mathbf{H}\right)\right)\right]. \tag{3.23}$$

Since $\boldsymbol{\Xi}$ is diagonal, the first term in (3.23) can be given as

$$\mathcal{E}\left[\ln(\det(\boldsymbol{\Xi}))\right] = \mathcal{E}\left[\ln\left(\prod_{i=1}^{LN_t}\xi_i D_i^{-\upsilon}\right)\right] \tag{3.24}$$

$$= -N_t\sum_{i=1}^{L}\ln {D_i}^{\upsilon} + N_t\sum_{i=1}^{L}\mathcal{E}\left[\ln\xi_i\right] \tag{3.25}$$

$$\overset{(A.7)}{=} -N_t\upsilon\sum_{i=1}^{L}\ln D_i + N_t\sum_{i=1}^{L}\left(\ln\mu_i + \exp\left(\frac{2\lambda_i}{\mu_i}\right)\mathtt{Ei}\left(\frac{-2\lambda_i}{\mu_i}\right)\right). \tag{3.26}$$

Since $\mathbf{H}$ is Rayleigh distributed, the term $\mathbf{H}^H\mathbf{H}$ follows a central Wishart distribution (zero-mean) [60]. Using [60, Eq. (A.8.1)], the last term in (3.23) is expressed as

$$\mathcal{E}\Big[\ln\left(\det\left(\mathbf{H}^H\mathbf{H}\right)\right)\Big] = \sum_{k=0}^{LN_t-1}\psi(N_r-k). \tag{3.27}$$

Substituting (3.26) and (3.27) into (3.23) and combining with (3.22) gives

$$\begin{aligned}\mathcal{C}_{\mathrm{LB}} = LN_t\log_2\Bigg(1+\frac{\gamma}{LN_t}\exp\Bigg(\frac{1}{LN_t}\Bigg(-N_t\upsilon\sum_{i=1}^{L}\ln(D_i)\\ + N_t\sum_{i=1}^{L}\left(\ln(\mu_i)+\exp\left(\frac{2\lambda_i}{\mu_i}\right)\mathtt{Ei}\left(\frac{-2\lambda_i}{\mu_i}\right)\right)+\sum_{k=0}^{LN_t-1}\psi(N_r-k)\Bigg)\Bigg)\Bigg).\end{aligned} \tag{3.28}$$

Thus, we can conclude the proof after the basic simplifications of (3.28). □

Note that, in the high-SNR regime, the lower bound becomes by definition exact and equal to the ergodic capacity [59].

3.2.2 Low-SNR analysis

In this subsection, we examine the ergodic capacity in the power-limited (or low-SNR) regime. In general, the low-SNR performance of any MIMO channels can be investigated by taking a first-order expansion of (3.4) around $\gamma = 0^+$. The authors of [61], [62], however, demonstrated that this approach can mislead the analysis in the low-SNR regime. For this reason, the low-SNR performance of MIMO systems is typically analyzed via the normalized receive energy per bit (E_b^r/N_0) rather than via the per-symbol SNR. This capacity representation is given in [61] as

$$\mathcal{C}_{\mathrm{erg}}\left(\frac{E_b}{N_0}\right) \approx \mathcal{S}_0\log_2\left(\frac{\frac{E_b}{N_0}}{\frac{E_b}{N_0}_{\mathtt{min}}}\right) \tag{3.29}$$

$$\frac{E_b}{N_0}_{\mathtt{min}} = \frac{1}{\dot{\mathcal{C}}_{\mathrm{erg}}(0)} \quad \text{and} \quad \mathcal{S}_0 = -2\ln 2\frac{\left(\dot{\mathcal{C}}_{\mathrm{erg}}(0)\right)^2}{\ddot{\mathcal{C}}_{\mathrm{erg}}(0)} \tag{3.30}$$

where $E_b/N_{0_{\mathtt{min}}}$ and $\mathcal{S}_0$ are the *minimum normalized energy per information bit required to convey any positive rate reliably* and the *wideband slope*, respectively, while $\dot{\mathcal{C}}_{\mathrm{erg}}(0)$ and $\ddot{\mathcal{C}}_{\mathrm{erg}}(0)$ denote the first- and second-order derivatives of the ergodic capacity in (3.5) w.r.t. the SNR, respectively [61].

Proposition 3.3. *For D-MIMO systems with optimal receivers in RIG fading channels, the minimum energy per information bit and the wideband slope are*

$$\frac{E_b}{N_0}^{\mathtt{opt}}_{\mathtt{min}} = \frac{L \ln 2}{N_r} \left(\sum_{i=1}^{L} \mu_i D_i^{-\upsilon} \right)^{-1} \tag{3.31}$$

$$\mathcal{S}_0^{\mathtt{opt}} = \frac{2}{\frac{1}{N_r} + \frac{1}{N_t} \left(\frac{\sum_{i=1}^{L} \left(\mu_i^2 + \frac{\mu_i^3}{\lambda_i} \right) D_i^{-2\upsilon}}{\left(\sum_{i=1}^{L} \mu_i D_i^{-\upsilon} \right)^2} \right)}. \tag{3.32}$$

Proof. First, we recall that

$$\frac{d}{dx} \ln \left(\det \left(\mathbf{I} + x\mathbf{A} \right) \right) \big|_{x=0} = \mathrm{tr}(\mathbf{A}). \tag{3.33}$$

Now, we set $\gamma \to 0$ in (3.8) and evaluate $\dot{\mathcal{C}}_{\mathrm{erg}}$ as

$$\dot{\mathcal{C}}_{\mathrm{erg}}(0) = \mathcal{E}[\mathrm{tr}(\mathbf{Z}^H \mathbf{Z})] = \frac{N_t}{L N_t \ln 2} \sum_{i=1}^{L} \int_0^\infty \int_0^\infty \frac{\xi_i \varphi_i}{D_i^{\upsilon}} \, p(\varphi_i) \, p(\xi_i) \, d\varphi_i \, d\xi_i \tag{3.34}$$

$$= \frac{1}{L \ln 2} \sum_{i=1}^{L} \frac{1}{D_i^{\upsilon}} \int_0^\infty \varphi_i \, p(\varphi_i) \, d\varphi_i \int_0^\infty \xi_i \, p(\xi_i) \, d\xi_i \tag{3.35}$$

where $\mathbf{Z} = \mathbf{H}\boldsymbol{\Xi}^{1/2}$ and $\xi_i \varphi_i / D_i^{\upsilon}$ are the real, non-negative diagonal elements of $\mathbf{Z}^H \mathbf{Z}$. Now, we substitute (3.2) and (3.3) into (3.35). The first integral in (3.35) is the mean (first moment) of Gamma RV in (3.3), whereas the second integral is the mean of an IG RV in (3.2). Using [1, Eq. (3.381.4)], we can easily find the mean of Gamma RV as $\mathcal{E}[\varphi_i] = N_r$. Combining $\mathcal{E}[\varphi_i]$ and (A.4) with (3.35) gives

$$\dot{\mathcal{C}}_{\mathrm{erg}}(0) = \frac{N_r}{L \ln 2} \sum_{i=1}^{L} \mu_i D_i^{-\upsilon}. \tag{3.36}$$

The inverse of (3.36) directly yields (3.31). For the wideband slope $\mathcal{S}_0^{\mathtt{opt}}$, we invoke a classical result from random matrix theory on correlated Rayleigh MIMO channels [62, Eq. (19)]

$$\mathcal{S}_0^{\mathtt{opt}} = \frac{2 L N_t N_r}{L N_t \, \zeta(\boldsymbol{\Theta}_R) + N_r \, \zeta(\boldsymbol{\Theta}_T)} \tag{3.37}$$

where $\zeta(\boldsymbol{\Theta})$ is the dispersion of random matrix $\boldsymbol{\Theta}$, which is defined as [62, Eq. (8)]

$$\zeta(\boldsymbol{\Theta}_T) = \frac{L N_t \, \mathcal{E}[\mathrm{tr}(\boldsymbol{\Theta}_T^2)]}{\mathcal{E}^2[\mathrm{tr}(\boldsymbol{\Theta}_T)]}. \tag{3.38}$$

Assuming no correlation at the receiver, we can evaluate $\mathcal{S}_0^{\mathtt{opt}}$ by substituting $\mathbf{\Theta}_R = \mathbf{I}_{N_r}$ and $\mathbf{\Theta}_T = \mathbf{\Xi}$ in (3.37). Combining (A.8) and (A.9) with (3.38) and substituting into (3.37) gives

$$\mathcal{S}_0^{\mathtt{opt}} = \frac{2N_tN_r\left(\sum_{i=1}^{L}\mu_i D_i^{-\upsilon}\right)^2}{N_t\left(\sum_{i=1}^{L}\mu_i D_i^{-\upsilon}\right)^2 + N_r\left(\sum_{i=1}^{L}\left(\mu_i^2+\frac{\mu_i^3}{\lambda_i}\right)D_i^{-2\upsilon}\right)}. \tag{3.39}$$

Thus, the proof is concluded by simplifying (3.39). □

Note that $E_b/N_{0_{\mathtt{min}}}^{\mathtt{opt}}$ in (3.31) is independent of N_t, which agrees with the results of [61] and [62], while a higher N_r improves the low-SNR capacity in (3.29) by reducing $E_b/N_{0_{\mathtt{min}}}^{\mathtt{opt}}$. On the other hand, the presence of the large-scale fading mean parameter μ_i increases $E_b/N_{0_{\mathtt{min}}}^{\mathtt{opt}}$, especially in severe fading conditions (i.e., small values of μ_i). Note that the wideband slope in (3.32) is by definition always greater than one.

For i.i.d Rayleigh fading conditions ($L = 1, \mathbf{\Xi} = \mathbf{I}_{N_t}$), the two low-SNR metrics simplify to

$$\frac{E_b}{N_{0\,\mathtt{min}}}^{\mathtt{opt}} = \frac{\ln 2}{N_r} \quad \text{and} \quad \mathcal{S}_0^{\mathtt{opt}} = \frac{2N_tN_r}{N_t+N_r} \tag{3.40}$$

which coincide with [61, Eq. (206)] and [62, Eq. (17)], [62, Eq. (19)], respectively.

We can now validate all the above theoretical expressions via a set of Monte-Carlo simulations. We generate 10,000 random realizations of the small- and large-scale fading matrices, $\mathbf{H}$ and $\mathbf{\Xi}$ (using [63]), respectively. In Fig. 3.1, the simulated ergodic capacity of (3.5) is compared with the analytical low-SNR approximation in (3.29) against transmit energy per bit E_b/N_0 (i.e., γ/N_r). In this case, the large-scale fading parameters are kept constant in each L radio port (i.e., $\mu_i = \mu$, $\lambda_i = \lambda$, and $D_i = D$, $\forall i = 1, \ldots, L$) and validated for the different number of receive antennas. Clearly, we can observe that the low-SNR ergodic capacity increases in terms of the wideband slope when the number of receive antennas, N_r grows large.

In Fig. 3.2, the simulated ergodic capacity of (3.5) is compared with the analytical low-SNR approximation in (3.29). Here, we change only the large-scale fading mean parameter μ_i and keep all other fading parameters constant. We can clearly observe that the low-SNR capacity increases, whereas the wideband slope decreases when μ_i gets larger. On the other hand, the analytical approximation becomes tighter for small values of μ_i.

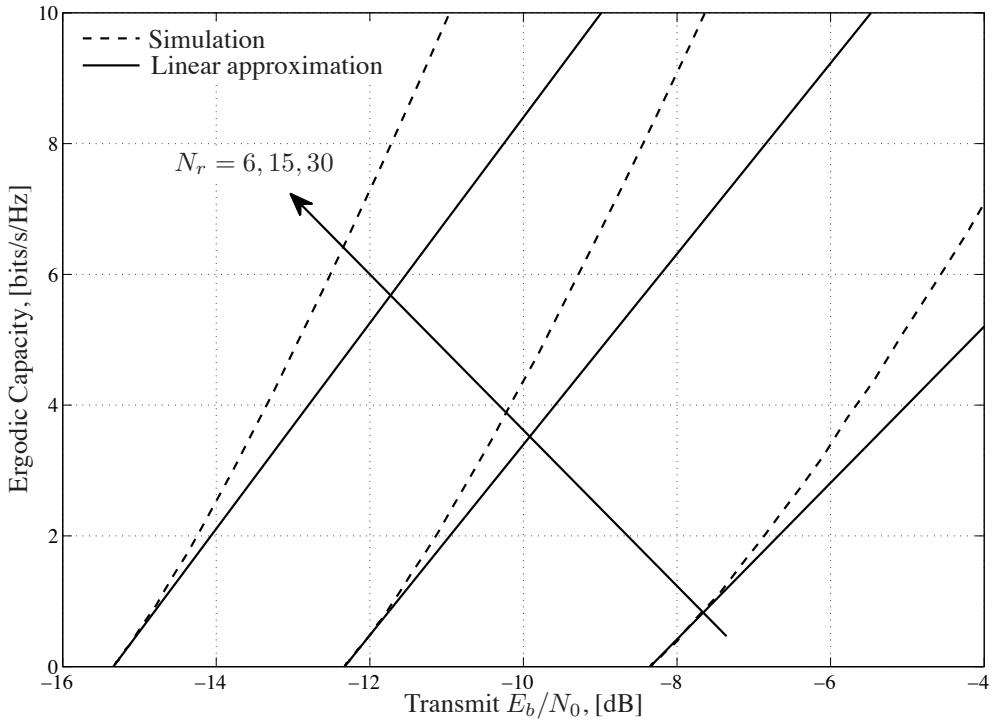

Figure 3.1: Simulated ergodic capacity and analytical low-SNR approximation against the transmit E_b/N_0 ($N_t = 2, L = 3, \mu_i = \mu = 4, \lambda_i = \lambda = 3, D_i = D = 1500$m ($\forall i = 1, \ldots, L$), and $v = 4$).

3.2.3 High-SNR analysis

We now examine the ergodic capacity in the high-SNR (i.e., $\gamma \to \infty$) regime. To get better insights into the high-SNR capacity performance, we can invoke the following affine capacity expansion, which was originally applied in the context of multiple access systems with random spreading [64] and thereafter in the analysis of MIMO systems [65]:

$$\mathcal{C}_{\text{erg}} = \mathcal{S}_\infty \left(\log_2(\gamma) - \mathcal{L}_\infty\right) + o(1) \tag{3.41}$$

where $\mathcal{S}_\infty$ is the so-called *high-SNR slope* in bits/s/Hz per 3-dB units, given by

$$\mathcal{S}_\infty = \lim_{\gamma \to \infty} \frac{\mathcal{C}_{\text{erg}}}{\log_2(\gamma)} \tag{3.42}$$

while $\mathcal{L}_\infty$ is the zero-th order term or *high-SNR power offset*, in 3-dB units, given by

$$\mathcal{L}_\infty = \lim_{\gamma \to \infty} \left(\log_2(\gamma) - \frac{\mathcal{C}_{\text{erg}}}{\mathcal{S}_\infty}\right). \tag{3.43}$$

Proposition 3.4. *For D-MIMO systems with optimal receivers in RIG fading channels, the*

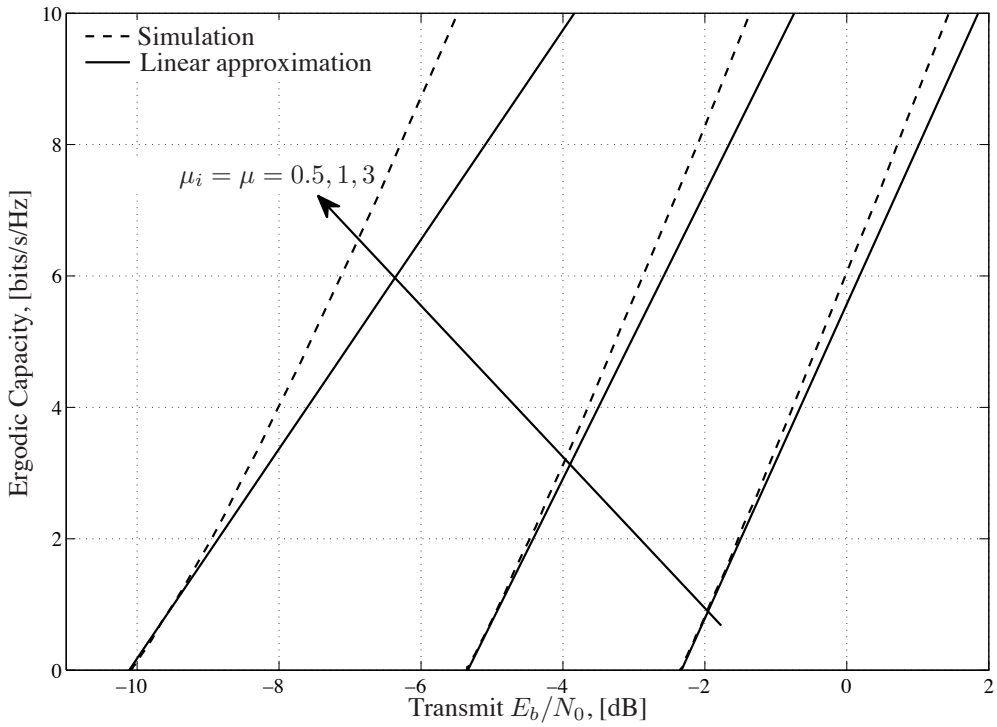

Figure 3.2: Simulated ergodic capacity and low-SNR approximation against the transmit E_b/N_0 for different values of the large-scale fading mean parameter $\mu_i = \mu$ ($N_r = 12$, $N_t = 2$, $L = 3$, $\lambda_i = \lambda = 3$, $D_i = D = 1500$m ($\forall i = 1, \ldots, L$), and $\upsilon = 4$).

high-SNR slope and offset parameters are respectively given by

$$\mathcal{S}_\infty^{\mathtt{opt}} = LN_t \tag{3.44}$$

$$\mathcal{L}_\infty^{\mathtt{opt}} = \log_2(LN_t) - \frac{1}{L}\sum_{i=1}^{L}\Bigg(\log_2(\mu_i) - \upsilon\log_2(D_i) + \frac{1}{\ln 2}\exp\left(\frac{2\lambda_i}{\mu_i}\right)\mathtt{Ei}\left(\frac{-2\lambda_i}{\mu_i}\right)\Bigg) - \frac{1}{LN_t\ln 2}\sum_{k=0}^{LN_t-1}\psi(N_r-k). \tag{3.45}$$

Proof. For MIMO systems with optimal receivers, the slope and the offset are obtained by [16, Eq. (16), (17)]

$$\mathcal{S}_\infty^{\mathtt{opt}} = \min(N_r, LN_t) \tag{3.46}$$

$$\mathcal{L}_\infty^{\mathtt{opt}} = \log_2(LN_t) - \frac{1}{LN_t\ln 2}\mathcal{E}\Big[\ln\left(\det\left(\mathbf{\Xi}\mathbf{H}^H\mathbf{H}\right)\right)\Big]. \tag{3.47}$$

Combining (3.23) with (3.47) gives (3.45) after simplifications. □

From the high-SNR power offset in (3.45), we can infer that the small- and large-scale fading terms are decoupled in the high-SNR regime. Furthermore, the higher Tx-Rx distances, D_i, effectively reduce the ergodic capacity due to the increased path-loss attenuation. Note that the high-SNR slope in (3.44) verifies that the high-SNR ergodic capacity

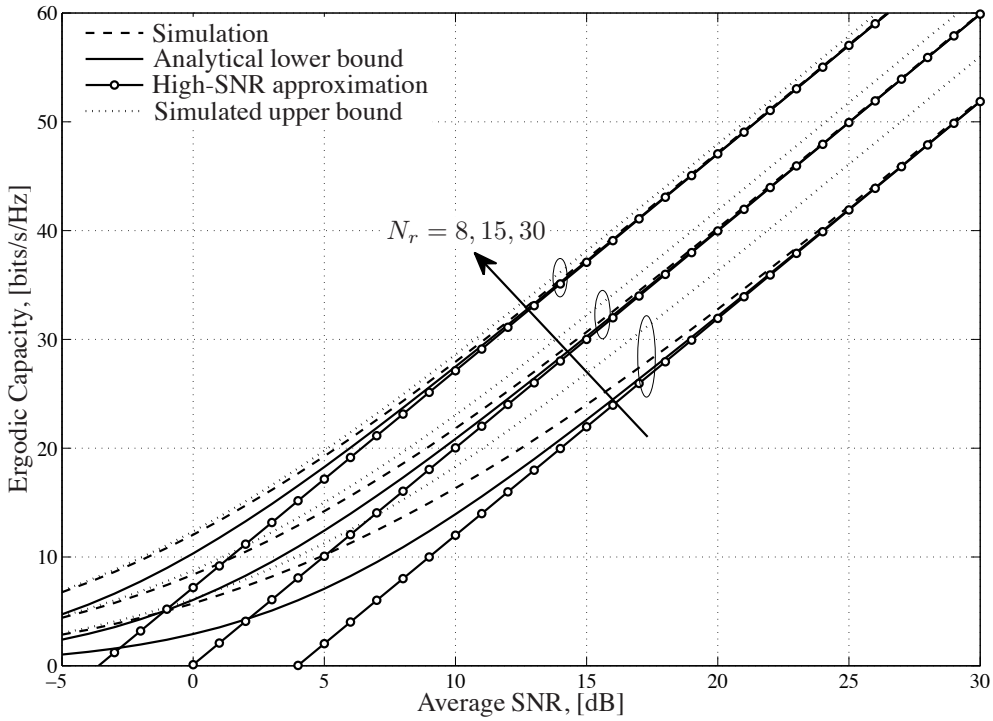

Figure 3.3: Simulated ergodic capacity, analytical high-SNR approximation, analytical lower bound, and simulated upper bound against the average SNR ($N_t = 2$, $L = 3$, $\mu_i = [4, 2, 3]$, $\lambda_i = [3, 5, 7]$, $D_i = [1000\text{m}, 1500\text{m}, 2000\text{m}]$, where $i = 1, \ldots, L$, and $\upsilon = 4$).

increases linearly with the minimum number of antennas, which is in line with [6], [59], [60], and [66].

In Fig. 3.3, the simulated ergodic capacity of (3.5) is compared with the analytical high-SNR approximation (3.41), the analytical lower bound (3.21), and the simulated upper bound (3.8). Both the upper and lower bounds become tighter when the number of receive antennas, N_r, increases. Also, we can easily observe that the high-SNR approximations become exact even at moderate SNR values. In the low-SNR regime, both the lower/upper bounds converge asymptotically to the empirical values of the ergodic capacity. These observations are in line with the results of [12], [59], and [67].

3.3 Ergodic capacity analysis of optimal receivers in specific cases

In this section, we analyze the high-SNR, low-SNR and the upper/lower bound analytical expressions of optimal receivers for specific cases. From these results, we can work out the D-MIMO characteristics and understand the impact of the fading parameters.

3.3.1 Point-to-point MIMO systems

When the communication system has a single radio port at the transmit side (i.e., $L = 1$), all the above ergodic capacity analytical expressions simplify to

$$\frac{E_b}{N_0}^{\texttt{opt}}_{\texttt{min}} = \frac{D^v \ln 2}{\mu N_r} \tag{3.48}$$

$$\mathcal{S}_0^{\texttt{opt}} = \frac{2}{\frac{1}{N_r} + \frac{1}{N_t}\left(1 + \frac{\mu}{\lambda}\right)} = \frac{2\, N_t\, N_r}{N_t + N_r + N_r \frac{\mu}{\lambda}} \tag{3.49}$$

$$\mathcal{C}_{\text{LB}} = N_t \log_2 \left(1 + \left(\frac{\gamma\mu}{N_t\, D^v}\right) \exp\left(\exp\left(\frac{2\lambda}{\mu}\right) \texttt{Ei}\left(-\frac{2\lambda}{\mu}\right) + \frac{1}{N_t}\sum_{k=0}^{N_t-1} \psi(N_r - k)\right)\right). \tag{3.50}$$

At high-SNRs, we can approximate (3.50) by

$$\mathcal{C}_{\text{LB}}^{\infty} = N_t \left(\log_2\left(\frac{\gamma\mu}{N_t\, D^v}\right) + \frac{1}{\ln 2} \exp\left(\frac{2\lambda}{\mu}\right) \texttt{Ei}\left(-\frac{2\lambda}{\mu}\right)\right) + \frac{1}{\ln 2}\sum_{k=0}^{N_t-1} \psi(N_r - k). \tag{3.51}$$

3.3.2 Lower bound – Distance parameter analysis

In this subsection, we analyze the impact of the distance parameter (D_i) on the ergodic capacity lower bound in (3.21). We assume that all L radio ports experience the same large-scale fading effects and they are placed at different distances w.r.t. the base station. As such, we have $\mu_i = \mu, \lambda_i = \lambda$ and D_i varies for all L radio ports, where $i = 1, \ldots, L$. We now rearrange the ergodic capacity lower bound (3.21) as

$$\mathcal{C}_{\text{LB}} = LN_t \log_2 \left(1 + \frac{\gamma\mu}{LN_t} \exp\left(\exp\left(\frac{2\lambda}{\mu}\right) \texttt{Ei}\left(\frac{-2\lambda}{\mu}\right) + \frac{1}{LN_t}\sum_{k=0}^{LN_t-1} \psi(N_r - k)\right) \exp\left(\sum_{i=1}^{L} \frac{-v}{L} \ln D_i\right)\right). \tag{3.52}$$

We can now apply the following manipulations

$$\exp\left(\sum_{i=1}^{L} \frac{-v}{L} \ln D_i\right) = \exp\left(\sum_{i=1}^{L} \ln D_i^{-\frac{v}{L}}\right) = \prod_{i=1}^{L} \exp\left(\ln D_i^{-\frac{v}{L}}\right) = \prod_{i=1}^{L} D_i^{-\frac{v}{L}}. \tag{3.53}$$

Using (3.53), we can rewrite (3.52) as

$$\mathcal{C}_{\text{LB}} = LN_t \log_2 \left(1 + b \exp\left(\sum_{i=1}^{L} \ln D_i^{-\frac{v}{L}}\right)\right) \tag{3.54}$$

$$= LN_t \log_2 \left(1 + b \left(\prod_{i=1}^{L} D_i^{-\frac{v}{L}}\right)\right) \tag{3.55}$$

where $b \triangleq \frac{\gamma\mu}{LN_t} \exp\left(\exp\left(\frac{2\lambda}{\mu}\right) \texttt{Ei}\left(\frac{-2\lambda}{\mu}\right) + \frac{1}{LN_t}\sum_{k=0}^{LN_t-1} \psi(N_r-k)\right)$. Now, let us take the second derivative of (3.55) w.r.t. D_i. We first recall that

$$\frac{d}{dx}\left(\prod_{i=1}^{k} f_i(x)\right) = \left(\prod_{i=1}^{k} f_i(x)\right)\left(\sum_{i=1}^{k} \frac{f_i'(x)}{f_i(x)}\right). \tag{3.56}$$

The first derivative of (3.55) w.r.t D_i is given by

$$\frac{d\mathcal{C}_{\mathrm{LB}}}{dD_i} = -\frac{vN_t\, b}{\ln 2}\left(\frac{\left(\prod_{i=1}^{L} D_i^{-\frac{v}{L}}\right)\left(\sum_{i=1}^{L} D_i^{-1}\right)}{\left(1+b\left(\prod_{i=1}^{L} D_i^{-\frac{v}{L}}\right)\right)}\right) \tag{3.57}$$

and the second derivative of (3.55) w.r.t D_i is given by

$$\begin{aligned}\frac{d^2\mathcal{C}_{\mathrm{LB}}}{dD_i^2} &= \frac{v^2N_t\, b}{L\ln 2}\left(\prod_{i=1}^{L} D_i^{-\frac{v}{L}}\right) \\ &\times\left(\frac{\left(\sum_{i=1}^{L} D_i^{-1}\right)^2 + \frac{L}{v}\left(\sum_{i=1}^{L} D_i^{-2}\right) + \frac{bL}{v}\left(\sum_{i=1}^{L} D_i^{-2}\right)\left(\prod_{i=1}^{L} D_i^{-\frac{v}{L}}\right)}{\left(1+b\left(\prod_{i=1}^{L} D_i^{-\frac{v}{L}}\right)\right)^2}\right).\end{aligned} \tag{3.58}$$

The result of the second derivative (3.58) is always positive for $D_i > 0$ and $b > 0$. Hence, we can conclude that $\mathcal{C}_{\mathrm{LB}}$ is convex with respect to D_i. Alternatively, this convexity can be verified by exploiting the fact that $\log_2(1+\alpha\exp(x))$ is convex in x for $\alpha > 0$ and invoke a result from Lemma A.3.5.

In order to better assess the impact of distances, we analyze the lower bound in (3.54) using some basic results from *majorization theory*[2]. Combining the above convexity result with Lemmas A.3.3 and A.3.4, we can infer the following useful fact: Radio ports should be placed at unequal distances to the base station (i.e., *non-symmetric deployment*) when they experience the same level of large-scale fading; this implies that a *symmetric deployment* of radio ports (i.e., equal distances to the base station) cannot in practice maximize the capacity.

3.3.3 Lower bound – Large system analysis

In the context of MIMO communication systems, when the number of receive or transmit antennas grows to infinity, it is commonly referred as *Large-MIMO systems* (a.k.a. massive MIMO, or large-scale multiple-antennas systems). Large-MIMO system is a recent research topic both in antenna systems, electronics, communication theory, and embedded

[2]For the basics of majorization theory, interested readers are referred to Appendix A.3 and [69].

systems. The ultimate vision is that arrays will consist of small active antenna elements, and each antenna will be using extremely low power (in the order of mW). More importantly, the design is extremely robust in that the failure of one or a few of the antennas would not affect the system appreciably and malfunctioning individual antennas may be hot-swapped. Large arrays may also be used for improved positioning and location-based services both indoors and outdoors (see [68] and references therein).

In this section, we analyze the lower bound analytical expression in the "large-system regime". In our first approach, we take N_r large and thereafter simplify the lower bound analytical expression. However, it is important to note that when $N_r \to \infty$ while N_t, L, and γ are kept fixed, the receiver captures more power with no bound. In the context of large-MIMO systems, a more interesting scenario is when the available transmit power is normalized by the large number of antennas at the receiver. With the aid of this normalization, we assure that the total received power does not diverge as $N_r \to \infty$. As such, we assume that the transmit power, P, is scaled down N_r times such that the effective transmit SNR can be defined as $\gamma_u \triangleq \gamma/N_r$, where γ is kept fixed and finite. We then have the following insightful result:

Corollary 3.2. *When the number of receive antennas grows large (i.e., $N_r \to \infty$) and N_t, L are kept fixed, while the effective SNR is given by $\gamma_u \triangleq \gamma/N_r$, the ergodic capacity lower bound $\mathcal{C}_{\mathrm{LB}}$ becomes*

$$\begin{aligned}\mathcal{C}_{\mathrm{LB}} \overset{N_r\to\infty}{=} & LN_t \log_2\left(1+\frac{\gamma_u N_r}{LN_t}\exp\left(\frac{1}{L}\sum_{i=1}^{L}\left(\ln\mu_i - \upsilon\ln D_i\right.\right.\right. \\ & \left.\left.\left. + \exp\left(\frac{2\lambda_i}{\mu_i}\right)\mathtt{Ei}\left(\frac{-2\lambda_i}{\mu_i}\right)\right)\right)\right) \qquad (3.59)\end{aligned}$$

$$\begin{aligned}= \; & LN_t \log_2\left(1+\frac{\gamma}{LN_t}\exp\left(\frac{1}{L}\sum_{i=1}^{L}\left(\ln\mu_i - \upsilon\ln D_i\right.\right.\right. \\ & \left.\left.\left. + \exp\left(\frac{2\lambda_i}{\mu_i}\right)\mathtt{Ei}\left(\frac{-2\lambda_i}{\mu_i}\right)\right)\right)\right). \qquad (3.60)\end{aligned}$$

At high-SNRs, we can approximate the above expression as

$$\begin{aligned}\mathcal{C}_{\mathrm{LB}}^{\infty} \overset{N_r\to\infty}{=} & LN_t\log_2\left(\frac{\gamma}{LN_t}\right) + N_t\sum_{i=1}^{L}\left(\log_2\mu_i - \upsilon\log_2 D_i\right. \\ & \left. + \frac{1}{\ln 2}\exp\left(\frac{2\lambda_i}{\mu_i}\right)\mathtt{Ei}\left(\frac{-2\lambda_i}{\mu_i}\right)\right). \qquad (3.61)\end{aligned}$$

Proof. First, we recall that [57, Eq. (6.3.18)]

$$\psi(x) \approx \ln x, \text{ if } x \to \infty. \tag{3.62}$$

Substituting (3.62) into (3.21) gives (3.59) after appropriate simplifications. At high-SNRs, first we approximate the ergodic capacity lower bound in (3.21) and then by using (3.62), we can easily obtain (3.61) after simplifications. □

From the large-system result in (3.60) and (3.61), we can clearly conclude that the small-scale fading effects are asymptotically averaged out and only the large-scale fading effects remains, when the number of receive antennas grows large, which is in line with the results of [68]. More importantly, even by scaling down the transmit power with the number of receive antennas, we can still average out the effects of fading and, at the same time, serve L radio ports (e.g., users). On the other hand, a linear increase with the number of transmit antennas per radio port and a logarithmic increase with the SNR can still be acquired.

In the next approach, we analyze an important case when both LN_t and N_r grow large. More specifically, when $LN_t \to \infty$ we need to separately analyze two cases based on $N_t \to \infty$ (keep L fixed) and $L \to \infty$ (keep N_t fixed). Also, we assume that $\beta = \frac{N_r}{LN_t} > 1$, and based on this fixed and finite ratio, we examine the ergodic capacity lower bound in the following two cases.

(i) L : Fixed *and* $N_r \to \infty, N_t \to \infty$*:*

Corollary 3.3. *When the number of receive and transmit antennas grow large (i.e., $N_r \to \infty, N_t \to \infty$), while L is kept fixed, the normalized ergodic capacity lower bound w.r.t. the number of transmit antennas, N_t, is given by*

$$\frac{\mathcal{C}_{\text{LB}}}{N_t} \overset{N_t, N_r \to \infty}{=} L \log_2 \left(1 + \frac{\gamma \beta^{\beta}}{\exp(1)(\beta - 1)^{(\beta-1)}} \times \exp\left(\frac{1}{L} \sum_{i=1}^{L} \ln \mu_i - \upsilon \ln D_i + \exp\left(\frac{2\lambda_i}{\mu_i}\right) \texttt{Ei}\left(\frac{-2\lambda_i}{\mu_i}\right) \right) \right). \tag{3.63}$$

Proof. Using (3.62), we first express the last sum term in (3.21) as follows:

$$\frac{1}{LN_t}\sum_{k=0}^{LN_t-1}\psi(N_r-k) \approx \ln N_r + \frac{1}{LN_t}\sum_{k=0}^{LN_t-1}\ln\left(1-\frac{k}{N_r}\right) \tag{3.64}$$

$$\approx \ln N_r + \frac{1}{LN_t}\int_0^{LN_t}\ln\left(1-\frac{k}{N_r}\right)dk \tag{3.65}$$

$$= \ln N_r + (\beta-1)\ln\left(\frac{\beta}{\beta-1}\right) - 1 \tag{3.66}$$

where in (3.65), we expressed the sum term in (3.64) in terms of an integral function and then, we used the following integral identity [70] to obtain (3.66)

$$\int_0^M \ln\left(1-\frac{x}{N}\right)dx = (N-M)\ln\left(\frac{N}{N-M}\right) - M, \quad \text{if } N > M. \tag{3.67}$$

Substituting (3.66) into (3.21) gives (3.63) after simplifications. □

From (3.63), we can infer that the capacity increases linearly with the number of transmit antennas for any $\beta > 1$.

In Fig. 3.4, the simulated ergodic capacity of (3.5) is compared with the analytical lower bound (3.21), and analytical large-system lower bound (3.63), against the number of transmit antennas, N_t, for $L = 1$. We can easily observe that the ergodic capacity curve converges very fast to the deterministic asymptote, even for the small number of transmit antennas (i.e., around $N_t = 8$); the exact lower bound and large-system lower bound remain sufficiently tight across the entire N_t range regardless of the number of radio ports, L. Note also that the exact lower bound follows the simulated ergodic capacity curve sufficiently tight regardless of the number of transmit antennas. An important observation from this analysis is that, in the large-system regime, for fixed L, increasing N_t does not have a beneficial impact on the ergodic capacity, since it slightly increases the number of interfering data streams (i.e., the decrease in normalized ergodic capacity is marginal ~ 0.05 bits/s/Hz).

(ii) N_t : Fixed *and* $L \to \infty, N_r \to \infty$*:* In this case, we assume that all radio ports are uniformly distributed in a circle of radius R_0, centered by the base station and experience the same large-scale fading effects. As such, we can set $\mu_i = \mu, \lambda_i = \lambda$ fixed values and D_i varying for all L ports, where $i = 1, \ldots, L$.

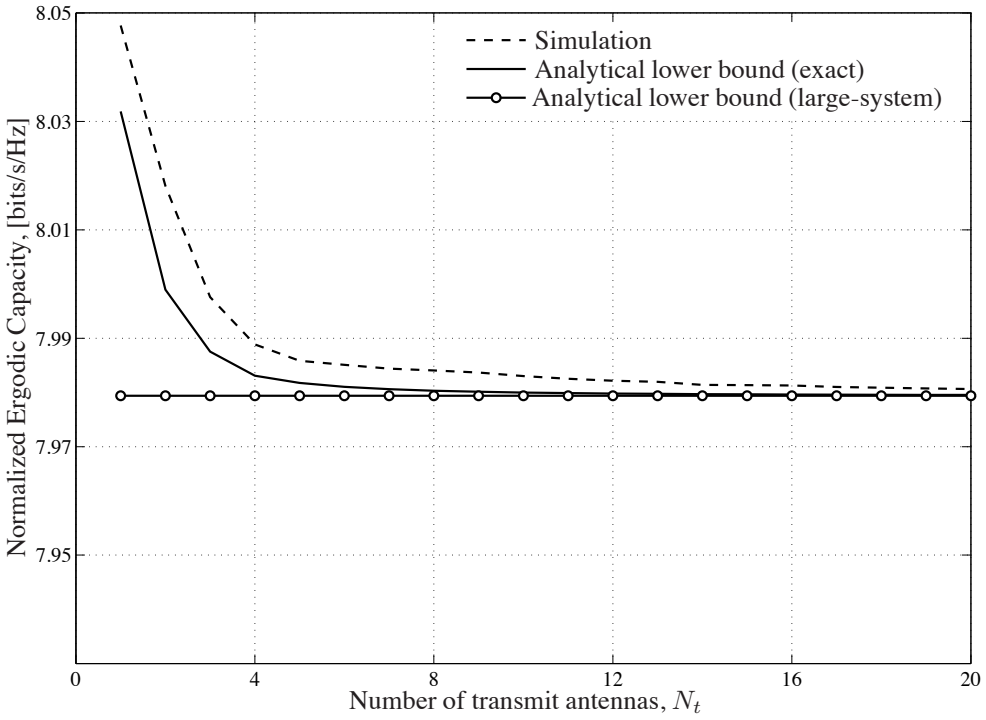

Figure 3.4: Simulated ergodic capacity, analytical lower bound, analytical large-system lower bound, and its asymptote against the number of transmit antennas, N_t ($\gamma = 25$dB, $L = 1$, $\beta = 2$, $\mu_i = \mu = 1$, $\lambda_i = \lambda = 3$, $D_i = D = 1500$m ($\forall i = 1, \ldots, L$), and $\upsilon = 4$).

Corollary 3.4. *When the number of receive antennas and radio ports grow large (i.e., $N_r \to \infty, L \to \infty$), while N_t is kept fixed, the normalized ergodic capacity lower bound w.r.t. radio ports L, is given by*

$$\frac{\mathcal{C}_{\mathrm{LB}}}{L} \overset{L,N_r\to\infty}{=} N_t \log_2\left(1 + aR_0^{-\upsilon} \exp\left(\frac{\upsilon}{2}\right)\right) \tag{3.68}$$

where $a \triangleq \gamma\mu\beta^{\beta}(\beta-1)^{(1-\beta)} \exp\left(\exp\left(\frac{2\lambda}{\mu}\right)\mathtt{Ei}\left(\frac{-2\lambda}{\mu}\right) - 1\right)$.

Proof. First, we rearrange the large-system lower bound in (3.63) as

$$\mathcal{C}_{\mathrm{LB}} = LN_t \log_2\left(1 + a \exp\left(\underbrace{\frac{1}{L}\sum_{i=1}^{L} \ln D_i^{-\upsilon}}_{I_3}\right)\right). \tag{3.69}$$

When $L \to \infty$, the argument in the exponential term (i.e., I_3) is nothing but an ensemble average w.r.t. D_i (distribution of distances). Next, we give the corresponding probability distribution of the distance between radio ports and base station as [71, Eq. (7)]

$$p_D(x) = \frac{2x}{R_0^2}, \quad 0 \le x \le R_0. \tag{3.70}$$

Now, we can express (3.69) as

$$\frac{\mathcal{C}_{\mathrm{LB}}}{L} \overset{L,N_r\to\infty}{=} N_t \log_2\left(1 + a\exp\left(\mathcal{E}_{D_i}\left[\ln D_i^{-\upsilon}\right]\right)\right). \tag{3.71}$$

We now recall L'Hospital's rule to get

$$\lim_{x\to 0^+} x\ln(x) = \lim_{x\to 0^+} \frac{\ln(x)}{1/x} = \lim_{x\to 0^+} \frac{1/x}{-1/x^2} = 0. \tag{3.72}$$

Combining [1, Eq. (2.723.1)] with (3.72), we can obtain the following

$$\mathcal{E}_{D_i}\left[\ln D_i^{-\upsilon}\right] = -\frac{2\upsilon}{R_0^2}\int_0^{R_0} \ln(D_i)\, D_i\, dD_i \tag{3.73}$$

$$= -\frac{2\upsilon}{R_0^2}\left[\frac{D_i^2\ln(D_i)}{2} - \frac{D_i^2}{4}\right]_0^{R_0} = -\frac{\upsilon}{R_0^2}\left(\frac{R_0^2\ln(R_0^2)}{2} - \frac{R_0^2}{2}\right) \tag{3.74}$$

$$= -\upsilon\ln(R_0) + \frac{\upsilon}{2}. \tag{3.75}$$

Substituting (3.75) into (3.71) gives

$$\frac{\mathcal{C}_{\mathrm{LB}}}{L} \overset{L,N_r\to\infty}{=} N_t \log_2\left(1 + a\exp\left(-\upsilon\ln(R_0) + \frac{\upsilon}{2}\right)\right). \tag{3.76}$$

Now, we can easily obtain (3.68) by appropriate simplifications. □

From (3.68), we can clearly infer that a large cell radius R_0 decreases the ergodic capacity logarithmically.

3.3.4 Wideband slope $\mathcal{S}_0^{\mathtt{opt}}$ characteristics

In this subsection, we analyze the effect of the large-scale fading parameters (μ_i, λ_i) and distance (D_i) on the wideband slope.

(i) *Fixed $D_i = D$; μ_i, λ_i are varying for all L ports:*

$$\mathcal{S}_0^{\mathtt{opt}} = \frac{2}{\frac{1}{N_r} + \frac{1}{N_t}\left(\frac{\sum_{i=1}^{L}\left(\mu_i^2 + \frac{\mu_i^3}{\lambda_i}\right)}{\left(\sum_{i=1}^{L}\mu_i\right)^2}\right)}. \tag{3.77}$$

From this specific case analysis we can infer the following: When all radio ports are equally placed (i.e., *symmetric deployment*) then the values of distances do not have any impact on the wideband slope.

(ii) *Fixed $\mu_i = \mu, \lambda_i = \lambda$; D_i is varying for all L ports:*

$$\mathcal{S}_0^{\mathtt{opt}} = \frac{2}{\frac{1}{N_r} + \frac{1}{N_t}\left(1+\frac{\mu}{\lambda}\right)\underbrace{\left(\frac{\sum_{i=1}^{L} D_i^{-2v}}{\left(\sum_{i=1}^{L} D_i^{-v}\right)^2}\right)}_{I_4}}. \tag{3.78}$$

This specific case analysis clearly indicates that the wideband slope depends only on the distances power ratio (i.e., I_4) rather than the actual distances, when all other fading parameters are kept fixed. Note that this ratio is always smaller than 1 for $L > 1$ and the wideband slope increases with D_i and/or L. Furthermore, when all radio-ports are equally placed (i.e., *symmetric deployment*) then the ratio depends only on the number of radio ports L (i.e., I_4 becomes equal to $1/L$), which agrees with the analysis of (3.77).

3.4 Achievable sum rate analysis of ZF receivers

Linear ZF receiver refers to a form of linear equalization algorithm used in communication systems which applies the inverse of the channel frequency response to the received signal, to restore the original transmitted signal at the receiver. The name 'zero-forcing' corresponds to bringing down the inter-symbol interference (ISI) to zero level in a noise free case. This is particularly useful when ISI is significant compared to the noise impairing the communication channel. Linear ZF receivers have many useful applications, especially for MIMO systems. For example, this has been studied for IEEE 802.11n (MIMO), where prior knowledge of channel allows recovery of the two or more data streams, which will be received on top of each other on each antenna.

In this section, we investigate the sum rate performance of D-MIMO ZF receivers over composite RIG fading channels. For the case under consideration, the ZF filter is expressed as $\mathbf{G} = (P/LN_t)^{-1/2}\mathbf{Z}^{\dagger}$, where P is the total transmit power. The instantaneous received SNR at the i-th ZF filter output ($1 \leq i \leq LN_t$) is equal to [14]

$$\gamma_i^{\mathtt{zf}} \triangleq \frac{\gamma}{LN_t\left[(\mathbf{Z}^H\mathbf{Z})^{-1}\right]_{ii}} = \frac{\gamma\left[\mathbf{\Xi}\right]_{ii}}{LN_t\left[(\mathbf{H}^H\mathbf{H})^{-1}\right]_{ii}} \tag{3.79}$$

where $\gamma = P/N_0$ is the average SNR and N_0 is the noise power. The second equality follows from the fact that $\mathbf{\Xi}$ is diagonal. Assume that the independent decoding at the receiver and the achievable sum rate is determined as

$$\mathcal{R}^{\mathtt{zf}} \triangleq \sum_{i=1}^{LN_t} \mathcal{E}\left[\log_2(1+\gamma_i^{\mathtt{zf}})\right] \tag{3.80}$$

where the expectation is taken-over all channel realizations of $\mathbf{H}$, $\boldsymbol{\Xi}$ and the channel is assumed to be ergodic. The main challenge in analytically evaluating (3.80) is the lack of closed-form expressions for the p.d.f. of $\gamma_i^{\mathtt{zf}}$ in the case of RIG fading. Therefore, analysis of ZF receiver becomes tedious. We overcome this problem in the following section by deriving some new, tractable bounds on the sum rate of D-MIMO ZF receivers.

3.4.1 Exact analysis

The sum rate generic bounds of MIMO ZF receivers were initially proposed in [72] for the case of point-to-point MIMO systems. In [72], the authors did not consider the effects of large-scale fading in their generic bounds, whereas in D-MIMO systems, the effects of large-scale fading are very critical. Hence, let us propose the following new sum rate bounds for D-MIMO ZF receivers over composite RIG fading channels. Capitalizing on the results of [72], we now derive both upper and lower sum rate bounds in the following proposition.

Proposition 3.5. *For D-MIMO systems with ZF receivers in RIG fading channels, the achievable sum rate in (3.5) is upper bounded by $\mathcal{R}_{\mathrm{UB}}^{\mathtt{zf}}$ and lower bounded by $\mathcal{R}_{\mathrm{LB}}^{\mathtt{zf}}$, with*

$$\mathcal{R}_{\mathrm{UB}}^{\mathtt{zf}} = LN_t \log_2\left(\frac{1}{N_r - LN_t} + \frac{\gamma}{N_t L^2}\sum_{i=1}^{L}\mu_i D_i^{-v}\right) + \frac{LN_t}{\ln 2}\psi(N_r - LN_t + 1) \tag{3.81}$$

$$\mathcal{R}_{\mathrm{LB}}^{\mathtt{zf}} = N_t \sum_{i=1}^{L}\log_2\left(1 + \frac{\gamma\mu_i}{LN_t D_i^v}\exp\left(\exp\left(\frac{2\lambda_i}{\mu_i}\right)\mathtt{Ei}\left(-\frac{2\lambda_i}{\mu_i}\right) + \psi(N_r - LN_t + 1)\right)\right). \tag{3.82}$$

Proof. Applying the generic bounding techniques of [72, Th. 1] and [72, Th. 3], and thereafter taking into account (3.79), gives

$$\begin{aligned}\mathcal{R}_{\mathrm{UB}}^{\mathtt{zf}} = {} & LN_t \log_2\left(\mathcal{E}\left[\Omega^{-1}\right] + \frac{\gamma}{(LN_t)^2}\mathcal{E}\left[\mathrm{tr}(\boldsymbol{\Xi})\right]\right) \\ & + \sum_{i=1}^{LN_t}\mathcal{E}\left[\log_2\left(\det\left(\mathbf{H}^H\mathbf{H}\right)\right) - \log_2\left(\det\left(\mathbf{H}_i^H\mathbf{H}_i\right)\right)\right]\end{aligned} \tag{3.83}$$

$$\begin{aligned}\mathcal{R}_{\mathrm{LB}}^{\mathtt{zf}} = {} & \sum_{i=1}^{LN_t}\log_2\left(1 + \frac{\gamma}{LN_t}\exp\left(\mathcal{E}\left[\ln\left([\boldsymbol{\Xi}]_{ii}\right)\right.\right.\right. \\ & \left.\left.\left. + \ln\left(\det\left(\mathbf{H}^H\mathbf{H}\right)\right) - \ln\left(\det\left(\mathbf{H}_i^H\mathbf{H}_i\right)\right)\right]\right)\right)\end{aligned} \tag{3.84}$$

where Ω is an unordered eigenvalue of $\mathbf{H}^H\mathbf{H}$. The first negative moment of Ω is given by [72, Prop. 1]

$$\mathcal{E}\left[\Omega^{-1}\right] = \frac{1}{N_r - LN_t}. \tag{3.85}$$

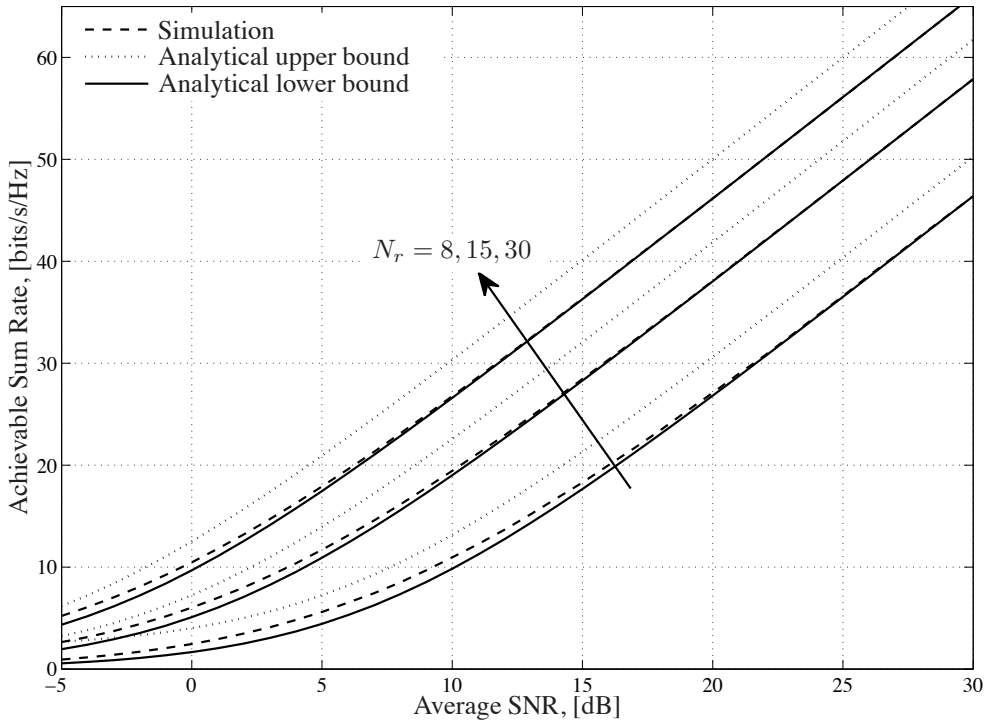

Figure 3.5: ZF receivers: Simulated sum rate, analytical upper and lower bounds against the average SNR ($N_t = 2$, $L = 3$, $\mu_i = \mu = 4$, $\lambda_i = \lambda = 3$, $D_i = D = 1500$m ($\forall i = 1, \ldots, L$), and $\upsilon = 4$).

Combining (3.85), (A.8), and (3.27) with (3.83) and basic simplifications give (3.81). We can obtain (3.82) by combining (A.7) and (3.27) with (3.84) and then simplifying it. □

Clearly, the sum rate tends to monotonically increase with the mean and scale parameters of large-scale fading. The higher Tx-Rx distances tend to effectively reduce the sum rate due to the increased path-loss attenuation.

In Fig. 3.5, we examine the tightness of both bounds by comparing the simulated sum rate with the analytical upper bound (3.81) and the analytical lower bound (3.82). We can easily observe that the performance of D-MIMO ZF receivers is systematically improved with the number of receive antennas, which is due to the mitigation of the noise enhancement effect. The upper bound remains sufficiently tight across the entire SNR range. On the other hand, the lower bound becomes tighter at high-SNRs and/or when the number of receive antennas grow large. These observations are in line with the results of [12], [59], and [67].

In Fig. 3.6, we examine the effect of the number of radio ports L on the sum rate for

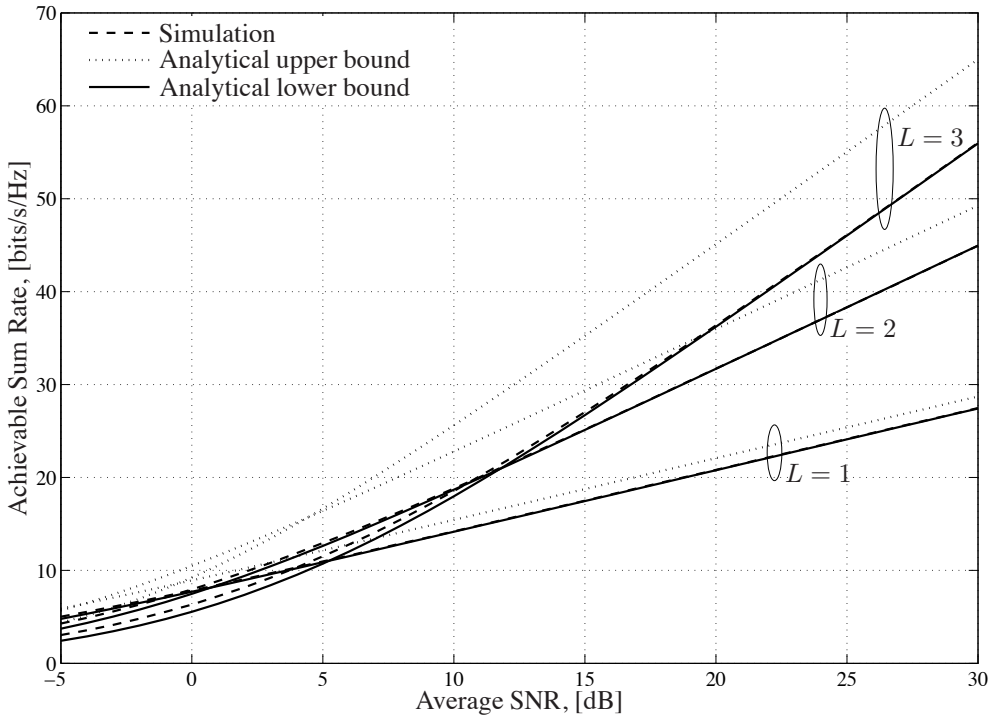

Figure 3.6: ZF receivers: Simulated sum rate, analytical upper/lower bounds against the average SNR ($N_r = 12$, $N_t = 2$, $\mu_i = \mu = 4$, $\lambda_i = \lambda = 3$, $D_i = D = 1500$m ($\forall i = 1, \ldots, L$), and $\upsilon = 4$).

$N_r = 12$ and $N_t = 2$. When $L = 1$ (i.e., point-to-point MIMO systems), both the bounds become almost exact across the entire SNR range. When L grows large, the upper bound becomes looser due to the scaling of SNR inside the first term of upper bound (3.81). In all cases, the lower bound remains sufficiently tight across the entire SNR range. An another important observation from this analysis is that, small values of L seem to have beneficial impact on the sum rate at low-SNRs, whereas higher L yields higher sum rate only when SNR increases. This is expected since at low-SNRs, the system is dominated by interference and higher values of L increase the interference. At high-SNRs, higher L implies higher scaling of the sum rate.

3.4.2 Lower bound – Distance parameter analysis

In order to better assess the effects of the radio port distances, we analyze the lower bound $\mathcal{R}_{\mathrm{LB}}^{\mathtt{zf}}$ with the with the aid of majorization theory.

Corollary 3.5. *When $\mu_i = \mu$ and $\lambda_i = \lambda$, the lower bound $\mathcal{R}_{\mathrm{LB}}^{\mathtt{zf}}$ is Schur-convex function with regard to D_i, where $i = 1, \ldots, L$.*

Proof. When $\mu_i = \mu$ and $\lambda_i = \lambda$, the lower bound (3.82) reduces to

$$\mathcal{R}_{\mathrm{LB}}^{\mathtt{zf}} = N_t \sum_{i=1}^{L} \log_2 \left(1 + \frac{d}{D_i^v}\right) \tag{3.86}$$

where $d \triangleq \frac{\gamma\mu}{LN_t} \exp\left(\exp\left(\frac{2\lambda}{\mu}\right) \mathtt{Ei}\left(-\frac{2\lambda}{\mu}\right) + \psi(N_r - LN_t + 1)\right)$. Let us define the function $f(x) \triangleq \log_2(1 + \frac{d}{x^v})$ and its second derivative is

$$\frac{d^2 f(x)}{dx^2} = \frac{dv}{\ln 2} \frac{((v+1)x^v + d)}{(x^{v+1} + dx)^2} > 0. \tag{3.87}$$

Hence, $f(x)$ is convex w.r.t x. As such, we can prove that lower bound $\mathcal{R}_{\mathrm{LB}}^{\mathtt{zf}}$ is Schur-convex function by invoking the result from Lemma A.3.5. □

Combining Corollary 3.5 with the majorization theory Lemmas A.3.3 and A.3.4, we can infer that radio ports should be placed at unequal distances to the base station when they experience the same level of large-scale fading effects; this implies that a *non-symmetric deployment* of radio ports can be implemented in practice to maximize the sum rate. This result agrees with the results corresponding on optimal receivers, which we have already proved in Section 3.3.2.

In Fig. 3.7, we investigate the impact of the radio ports' deployment on the sum rate. In this analysis, we consider two different type of configurations with the same total distance constraint. The first configuration is a *symmetrical configuration*, where all radio ports are placed in different locations with same distance to the base station ($D_1 = D_2 = D_3 = 1500$m) and the second configuration is a *anti-symmetrical configuration* ($D_1 = 1000$m, $D_2 = 1500$m, $D_3 = 2000$m). As suggested by Corollary 3.5 and the majorization theory lemmas, the anti-symmetrical configuration yields higher sum rate due to the weaker path-loss effects (i.e., it is always beneficial to put radio ports close to the base station to get stronger signals). On the other hand, both bounds, especially the upper bound, are tighter for the symmetrical configuration across the entire SNR range.

3.4.3 Lower bound – Large system analysis

In this section, we analyze the lower bound analytical expression in the large-system regime. We assume, either the number of receive or transmit antennas or both grow to infinity in the large-system regime.

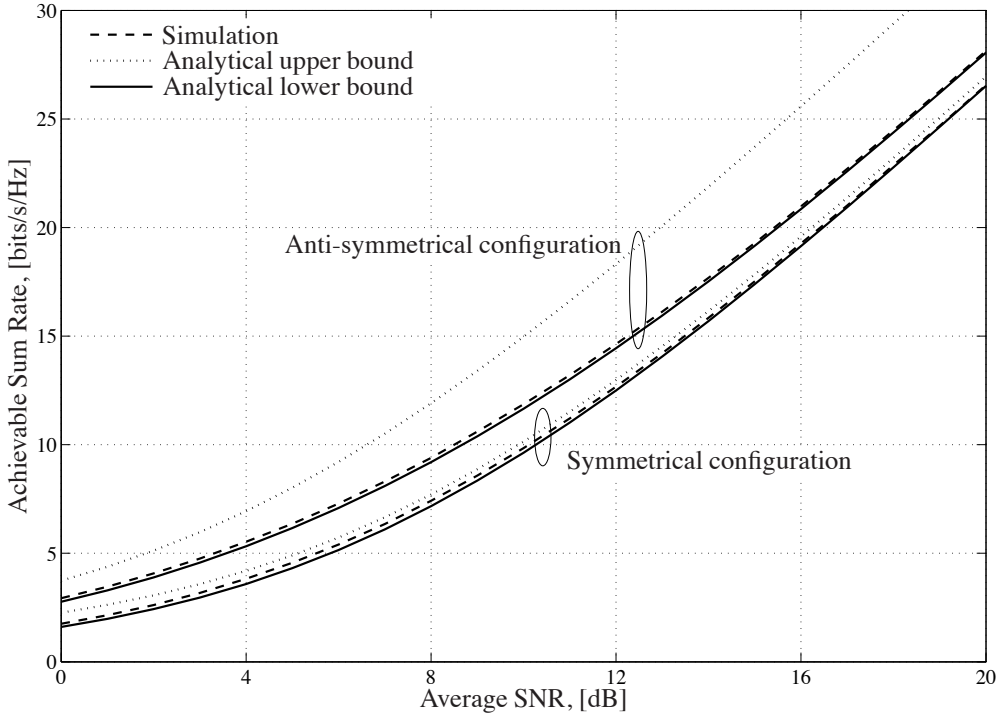

Figure 3.7: ZF receivers: Simulated sum rate, analytical upper/lower bounds against the average SNR for two different configurations ($N_r = 12$, $L = 3$, $N_t = 2$, $\mu_i = \mu = 4$, $\lambda_i = \lambda = 3$, $(\forall i = 1, \ldots, L)$, $\upsilon = 4$ with (a) anti-symmetrical configuration: $D_1 = 1000$m, $D_2 = 1500$m, $D_3 = 2000$m and (b) symmetrical configuration: $D_1 = D_2 = D_3 = 1500$m).

Corollary 3.6. *When the number of receive antennas grows large (i.e., $N_r \to \infty$) and N_t, L are kept fixed, while the effective SNR is given by $\gamma_u \triangleq \gamma/N_r$, the lower bound $\mathcal{R}_{\mathrm{LB}}^{\mathtt{zf}}$ becomes*

$$\mathcal{R}_{\mathrm{LB}}^{\mathtt{zf}} \overset{N_r \to \infty}{\approx} LN_t \log_2\left(\frac{\gamma}{LN_t}\right) + N_t \sum_{i=1}^{L} \Bigg(\log_2(\mu_i) - \upsilon \log_2(D_i) + \frac{1}{\ln 2} \exp\left(\frac{2\lambda_i}{\mu_i}\right) \mathtt{Ei}\left(\frac{-2\lambda_i}{\mu_i}\right) \Bigg). \tag{3.88}$$

Proof. By applying (3.62) into the lower bound (3.82) and thereafter appropriate simplifications. □

Clearly, Corollary 3.6 indicates that the small-scale Rayleigh fading effects are averaged out and only the slowing varying large-scale fading effects remains when $N_r \to \infty$. Even though the transmit power is scaled down with the number of receive antennas, we can still average out the effects of fading and, at the same time, serve L radio ports (e.g., users). On the other hand, a linear increase with the number of transmit antennas per radio port and a logarithmic increase with the SNR can still be acquired. These results are in line

with the results corresponding to optimal receivers, provided in Section 3.3.3 and previous results on i.i.d. Rayleigh MIMO channels of optimal receivers [11, Eq. (13)], and [60, Eq. (8)].

We now examine the case when both N_r and LN_t grow large with a fixed and finite ratio, such that $\beta = \frac{N_r}{LN_t} > 1$. More specifically, when $LN_t \to \infty$ we need to separately analyze the two cases based on $N_t \to \infty$ (keep L fixed) and $L \to \infty$ (keep N_t fixed). In the former case, it can be shown that

$$\frac{\mathcal{R}_{\mathrm{LB}}^{\mathtt{zf}}}{N_t} \overset{N_r, N_t \to \infty}{=} \sum_{i=1}^{L} \log_2 \left(1 + \frac{\gamma \mu_i (\beta - 1)}{D_i^{\upsilon}} \exp \left(\exp \left(\frac{2\lambda_i}{\mu_i} \right) \mathtt{Ei} \left(-\frac{2\lambda_i}{\mu_i} \right) \right) \right). \tag{3.89}$$

For any $\beta > 1$, the sum rate is shown to scale linearly with N_t, due to the increased interference cancellation capabilities of ZF receivers, which is consistent with [11], [60], and [72].

In Fig. 3.8, the simulated sum rate of (3.80) is plotted along with exact lower bound in (3.82) and its asymptote in (3.89), against the number of transmit antennas, N_t. We can easily observe that the sum rate curve converges fast to the deterministic asymptote, for moderate number of transmit antennas (i.e., around $N_t = 30$). Note also that the exact lower bound remains sufficiently tight regardless of the number of transmit antennas.

In the second case, we assume that radio ports are uniformly distributed in a circle of radius R_0, centered by the base station. As such, the corresponding p.d.f. is already given in (3.70). We also assume that all radio ports experience same large-scale effects (i.e., $\mu_i = \mu$ and $\lambda_i = \lambda$, where $i = 1, \ldots, L$). Now, we follow the same methodology, which we have already proved for Corollary 3.4. Thus, the normalized lower bound with regard to radio ports L, is given by

$$\frac{\mathcal{R}_{\mathrm{LB}}^{\mathtt{zf}}}{L} \overset{N_r, L \to \infty}{=} N_t \, \mathcal{E}_{D_i} \left[\log_2 \left(1 + \frac{\gamma \mu (\beta - 1)}{D_i^{\upsilon}} \exp \left(\exp \left(\frac{2\lambda}{\mu} \right) \mathtt{Ei} \left(-\frac{2\lambda}{\mu} \right) \right) \right) \right] \tag{3.90}$$

$$= \frac{N_t}{2c \ln 2} \left(c\upsilon - 2R_0^{\upsilon} \Phi \left(-\frac{R_0^{\upsilon}}{c}, 1, \frac{2+\upsilon}{\upsilon} \right) + 2c \ln \left(1 + \frac{c}{R_0^{\upsilon}} \right) \right) \tag{3.91}$$

where $c \triangleq \gamma \mu (\beta - 1) \exp \left(\exp \left(\frac{2\lambda}{\mu} \right) \mathtt{Ei} \left(-\frac{2\lambda}{\mu} \right) \right)$ and $\Phi(z, s, \alpha) \triangleq \sum_{k=0}^{\infty} \frac{z^k}{(\alpha + k)^s}$ for $|z| < 1$ and $\alpha \neq 0, -1, -2, \ldots$ is the Lerch transcendent [1, Eq. (9.550)]. For different values of

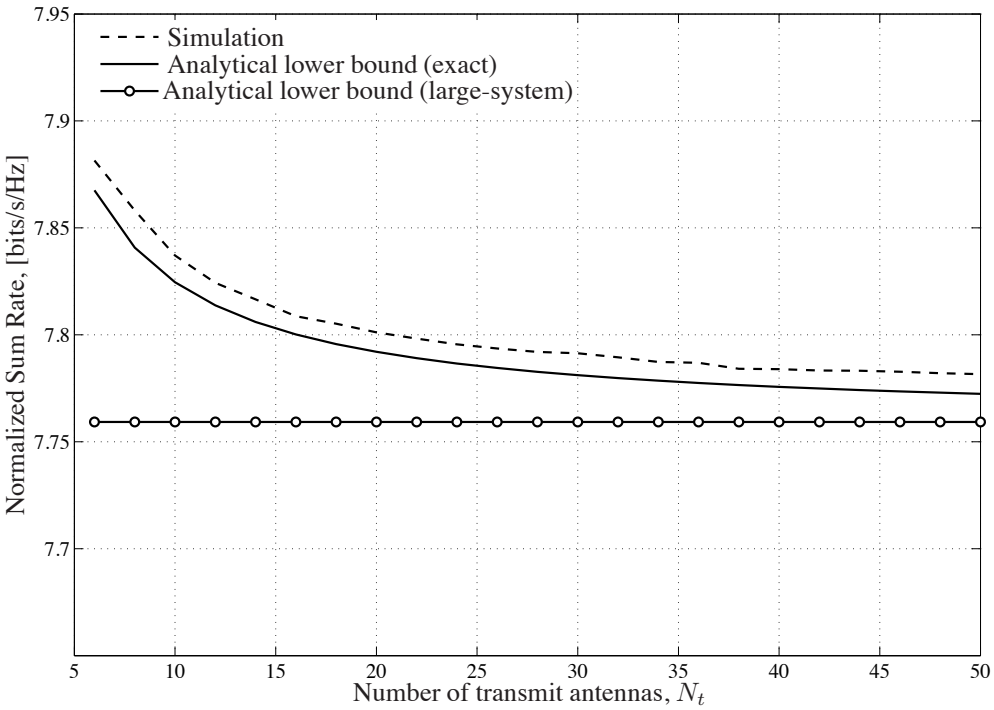

Figure 3.8: ZF receivers: Simulated sum rate, exact and asymptotic lower bounds against the number of transmit antennas, N_t ($\gamma = 15$dB, $L = 2$, $\beta = 2$, $\mu_i = \mu = 1$, $\lambda_i = \lambda = 10$ ($\forall i = 1, \ldots, L$), $D_i = [1000\text{m}, 1500\text{m}]$, and $\upsilon = 4$).

the path-loss exponent υ, we can obtain the following set of useful expressions:

$$\frac{\mathcal{R}_{\text{LB}}^{\texttt{zf}}}{L} \overset{N_r, L\to\infty}{=} \frac{N_t}{R_0^2 \ln 2}\left(c \ln\left(1+\frac{R_0^2}{c}\right) + R_0^2 \ln\left(1+\frac{c}{R_0^2}\right)\right), \qquad \upsilon = 2 \tag{3.92}$$

$$= \frac{N_t}{R_0^2 \ln 2}\left(2\sqrt{c}\arctan\left(\frac{R_0^2}{\sqrt{c}}\right) + R_0^2 \ln\left(1+\frac{c}{R_0^4}\right)\right), \qquad \upsilon = 4 \tag{3.93}$$

$$= \frac{N_t}{\ln 2}\left(3\,{}_2F_1\left(\frac{1}{3}, 1; \frac{4}{3}; -\frac{R_0^6}{c}\right) + \ln\left(1+\frac{c}{R_0^6}\right)\right), \qquad \upsilon = 6 \tag{3.94}$$

where ${}_pF_q(\cdot)$ is the generalized hypergeometric function with p, q non-negative integers [1, Eq. (9.14.1)].

3.4.4 Upper bound – High-SNR analysis

In order to get some additional insights into the tightness of the upper bound $\mathcal{R}_{\text{UB}}^{\texttt{zf}}$, we consider the following bounding error at high-SNRs, which is quantified as a fixed rate

offset

$$\Delta\mathcal{R}^{\mathtt{zf}} \triangleq \mathcal{R}^{\mathtt{zf}}_{\mathrm{UB}} - \mathcal{R}^{\mathtt{zf}} \tag{3.95}$$

$$\overset{\gamma\to\infty}{=} LN_t \log_2\left(\frac{1}{L}\sum_{i=1}^{L}\mu_i D_i^{-\upsilon}\right) - N_t\sum_{i=1}^{L}\left(\log_2(\mu_i) - \upsilon\log_2(D_i) + \frac{1}{\ln 2}\exp\left(\frac{2\lambda_i}{\mu_i}\right)\mathtt{Ei}\left(\frac{-2\lambda_i}{\mu_i}\right)\right) \tag{3.96}$$

where (3.96) follows by taking $\gamma \to \infty$ in (3.81) and (3.82), and basic simplifications. We can infer that the offset is only a function of the large-scale fading parameters, Tx-Rx distances, the number of radio ports and the number of transmit antennas, and is independent of the number of receive antennas. In general, the upper bound $\mathcal{R}^{\mathtt{zf}}_{\mathrm{UB}}$ is tighter for small number of radio ports, low number of transmit antennas and small Tx-Rx distances. For the special case $L = 1$, (3.96) simplifies to

$$\Delta\mathcal{R}^{\mathtt{zf}} \overset{\gamma\to\infty}{=} \frac{N_t}{\ln 2}\exp\left(\frac{2\lambda_1}{\mu_1}\right)\mathtt{Ei}\left(\frac{-2\lambda_1}{\mu_1}\right). \tag{3.97}$$

From (3.97), we can infer that, when L is fixed, the upper bound is tighter for a smaller number of transmit antennas and smaller large-scale fading parameters. In other words, the upper bound is tighter when the fluctuations of large-scale fading are not very severe.

3.4.5 Low-SNR analysis

We now examine the sum rate performance of D-MIMO ZF receivers in the power-limited (wideband) regime. We have already introduced the low-SNR characterization in Section 3.2.2 and hence, we directly give the following proposition.

Proposition 3.6. *For D-MIMO systems with ZF receivers in RIG fading channels, the minimum energy per information bit and the wideband slope are respectively*

$$\frac{E_b}{N_0}^{\mathtt{zf}}_{\mathtt{min}} = \frac{L\ln 2}{N_r - LN_t + 1}\left(\sum_{i=1}^{L}\mu_i D_i^{-\upsilon}\right)^{-1} \tag{3.98}$$

$$\mathcal{S}_0^{\mathtt{zf}} = \frac{2N_t(N_r - LN_t + 1)\left(\sum_{i=1}^{L}\mu_i D_i^{-\upsilon}\right)^2}{(N_r - LN_t + 2)\left(\sum_{i=1}^{L}\left(\mu_i^2 + \frac{\mu_i^3}{\lambda_i}\right)D_i^{-2\upsilon}\right)}. \tag{3.99}$$

Proof. First, we rewrite (3.80) as

$$\mathcal{R}^{\mathtt{zf}}(\gamma) = \frac{1}{\ln 2}\sum_{i=1}^{LN_t}\mathcal{E}\left[\ln\left(1 + \gamma\frac{1}{LN_t}\frac{\xi_i x_i}{D_i^{\upsilon}}\right)\right] \tag{3.100}$$

where $x_i = 1/\left[(\mathbf{H}^H\mathbf{H})^{-1}\right]_{ii}$. The p.d.f. of x_i was defined in [14, Th. 1]

$$p(x_i) = \frac{e^{-x_i}}{(N_r - LN_t)!}\, x_i^{N_r - LN_t}. \tag{3.101}$$

By taking the first derivate of (3.100) w.r.t. $\gamma \to 0$, we can obtain

$$\dot{\mathcal{R}}^{\mathtt{zf}}(0) = \frac{1}{\ln 2}\sum_{i=1}^{LN_t}\mathcal{E}\left[\frac{\frac{1}{LN_t}\frac{\xi_i x_i}{D_i^v}}{1+\gamma\frac{1}{LN_t}\frac{\xi_i x_i}{D_i^v}}\bigg|_{\gamma=0}\right] = \frac{1}{LN_t\ln 2}\sum_{i=1}^{LN_t}\mathcal{E}\left[\frac{\xi_i x_i}{D_i^v}\right] \tag{3.102}$$

$$= \frac{N_r - LN_t + 1}{LN_t\ln 2}\sum_{i=1}^{LN_t}\frac{\mu_i}{D_i^v}. \tag{3.103}$$

The expectation in (3.102) should be taken w.r.t. ξ_i and x_i. Using (A.4) and [1, Eq. (3.381.4)], we can obtain (3.103) from (3.102) after basic simplifications. Similarly, we can obtain the second derivative of (3.100) as

$$\ddot{\mathcal{R}}^{\mathtt{zf}}(0) = -\frac{1}{\ln 2}\sum_{i=1}^{LN_t}\mathcal{E}\left[\frac{\left(\frac{1}{LN_t}\frac{\xi_i x_i}{D_i^v}\right)^2}{\left(1+\gamma\frac{1}{LN_t}\frac{\xi_i x_i}{D_i^v}\right)^2}\bigg|_{\gamma=0}\right] = \frac{1}{(LN_t)^2\ln 2}\sum_{i=1}^{LN_t}\mathcal{E}\left[\left(\frac{\xi_i x_i}{D_i^v}\right)^2\right] \tag{3.104}$$

$$= -\frac{(N_r - LN_t + 2)(N_r - LN_t + 1)}{(LN_t)^2\ln 2}\sum_{i=1}^{LN_t}\frac{\mu_i^2 + \frac{\mu_i^3}{\lambda_i}}{D_i^{2v}}. \tag{3.105}$$

Using (A.5) and [1, Eq. (3.381.4)], we can obtain (3.105) from (3.104) after appropriate simplifications. To conclude the proof, we combine (3.103) and (3.105) with the definitions in (3.30). □

Note that $\frac{E_b}{N_0}^{\mathtt{zf}}_{\mathtt{min}}$ in (3.98) depends on the number of receive antennas, number of radio ports, large-scale fading mean parameter, and the number of transmit antennas N_t, whereas for optimal receivers, (3.31) is independent of N_t. This is a key difference between optimal and ZF receivers and is in agreement with [61], [62]. For fixed N_r, having more number of transmit antennas is not beneficial for ZF receivers since the minimum energy per information bit increases due to the additional power that is required to cancel out the extra interferers.

For the specific case $LN_t = 1$, ZF detection becomes optimal ((3.98) becomes equal to (3.31)). This is due to the fact that single transmit antenna transmission scheme is optimal since there are no interfering streams to be cancelled out. Additionally, we can compare

$\mathcal{S}_0^{\mathtt{zf}}$ with $\mathcal{S}_0^{\mathtt{opt}}$ to verify this behavior in terms of wideband slope. It is thus of interest to consider the following ratio when $LN_t = 1$

$$\frac{\mathcal{S}_0^{\mathtt{zf}}}{\mathcal{S}_0^{\mathtt{opt}}} = \frac{N_r + \frac{1}{\left(1+\frac{\mu}{\lambda}\right)}}{N_r + 1}. \tag{3.106}$$

Note also that the above ratio becomes one for i.i.d. Rayleigh fading conditions.

For i.i.d. Rayleigh fading conditions ($L = 1, \mathbf{\Xi} = \mathbf{I}_{N_t}$), the two low-SNR metrics simplify to

$$\frac{E_b}{N_0}^{\mathtt{zf}}_{\mathtt{min}} = \frac{\ln 2}{N_r - N_t + 1} \quad \text{and} \quad \mathcal{S}_0^{\mathtt{zf}} = \frac{2N_t(N_r - N_t + 1)}{N_r - N_t + 2} \tag{3.107}$$

which coincide with [73, Eq. (25)] and [73, Eq. (26)], respectively.

3.4.6 High-SNR analysis

In this case, we examine the sum rate performance of ZF receivers in the high-SNR regime. We have already introduced the high-SNR parameters in Section 3.2.3 and hence, we can directly give the following proposition.

Proposition 3.7. *For D-MIMO systems with ZF receivers in RIG fading channels, the high-SNR slope and offset parameters are respectively given by*

$$\mathcal{S}_\infty^{\mathtt{zf}} = LN_t \tag{3.108}$$

$$\begin{aligned}\mathcal{L}_\infty^{\mathtt{zf}} &= \log_2(LN_t) - \frac{1}{\ln 2}\psi\left(N_r - LN_t + 1\right) \\ &\quad - \frac{1}{L}\sum_{i=1}^{L}\left(\log_2(\mu_i) - v\log_2(D_i) + \frac{1}{\ln 2}\exp\left(\frac{2\lambda_i}{\mu_i}\right)\mathtt{Ei}\left(\frac{-2\lambda_i}{\mu_i}\right)\right).\end{aligned} \tag{3.109}$$

Proof. For MIMO systems with ZF receivers, the slope and offset parameters are obtained by

$$\mathcal{S}_\infty^{\mathtt{zf}} = \min(N_r, LN_t) = LN_t \tag{3.110}$$

and

$$\mathcal{L}_\infty^{\mathtt{zf}} = \log_2(LN_t) - \frac{1}{LN_t \ln 2}\sum_{i=1}^{LN_t}\mathcal{E}\Big[\ln\left([\mathbf{\Xi}]_{ii}\right) + \ln\left(\det\left(\mathbf{H}^H\mathbf{H}\right)\right) - \ln\left(\det\left(\mathbf{H}_i^H\mathbf{H}_i\right)\right)\Big]. \tag{3.111}$$

Since $\mathbf{H}_i$ is Rayleigh distributed, the term $\mathbf{H}_i^H\mathbf{H}_i$ follows a central Wishart distribution (zero-mean) [60]. Using [60, Eq. (A.8.1)], the last term in (3.111) is expressed as

$$\mathcal{E}\Big[\ln\left(\det\left(\mathbf{H}_i^H\mathbf{H}_i\right)\right)\Big] = \sum_{k=0}^{LN_t-2}\psi(N_r-k). \tag{3.112}$$

Substituting (A.7), (3.27), and (3.112) into (3.111) gives

$$\begin{aligned}\mathcal{L}_{\infty}^{\mathtt{zf}} &= \log_2(LN_t) - \frac{1}{\ln 2}\sum_{k=0}^{LN_t-1}\psi(N_r-k) + \frac{1}{\ln 2}\sum_{k=0}^{LN_t-2}\psi(N_r-k)\\ &\quad - \frac{1}{LN_t\ln 2}\left(-N_t v\sum_{i=1}^{L}\ln D_i + N_t\sum_{i=1}^{L}\left(\ln(\mu_i) + \exp\left(\frac{2\lambda_i}{\mu_i}\right)\mathtt{Ei}\left(\frac{-2\lambda_i}{\mu_i}\right)\right)\right).\end{aligned} \tag{3.113}$$

Thus, the proof of (3.109) is concluded by simplifying (3.113). □

Note that (3.108) verifies that the high-SNR sum rate increases linearly with the minimum number of antennas, which agrees with [6], [59], [60], and [66].

3.5 Achievable sum rate analysis of MMSE receivers

Linear ZF receiver removes all ISI, and is ideal when the channel is noise free. However, when the channel is noisy, ZF receiver amplifies the noise when the channel frequency response has a small magnitude, in the attempt to invert the channel completely. A more balanced linear receiver in this case is *MMSE receiver*, which does not usually eliminate ISI completely but instead minimizes the total power of the noise and ISI components in the output. Linear MMSE receiver minimizes the squared error in the presence of noise in the channel, and becomes equivalent to ZF receiver when no noise is present. In addition, the performance of MMSE receiver is very similar to ZF receiver at high SNRs, but far more robust at low SNRs [3].

In this section, the sum rate performance of D-MIMO MMSE receivers in RIG fading channels is analyzed. The instantaneous received SNR at the i-th MMSE filter output ($1 \le i \le LN_t$) is equal to [16]

$$\gamma_i^{\mathtt{mmse}} \triangleq \frac{1}{\left[\left(\mathbf{I}_{LN_t} + \frac{\gamma}{LN_t}\mathbf{Z}^H\mathbf{Z}\right)^{-1}\right]_{ii}} - 1 \tag{3.114}$$

Assuming independent decoding at the receiver, the achievable sum rate is expressed as

$$\mathcal{R}^{\texttt{mmse}} \triangleq \sum_{i=1}^{LN_t} \mathcal{E}\left[\log_2(1+\gamma_i^{\texttt{mmse}})\right] \tag{3.115}$$

where the expectation is taken-over all channel realizations of $\mathbf{H}$, $\boldsymbol{\Xi}$ and the channel is assumed to be ergodic. Since an exact SNR analysis is tedious for MMSE receivers operating over RIG fading channels, we present an useful analytic framework of the achievable sum rate in the following section.

3.5.1 A generic framework

We now present a generic framework for investigating the achievable sum rate of D-MIMO systems employing linear MMSE receivers.

Proposition 3.8. *For D-MIMO systems with MMSE receivers in RIG fading channels, the achievable sum rate is expressed as*

$$\begin{aligned}\mathcal{R}^{\texttt{mmse}} = LN_t\,\mathcal{E}\Big[\log_2\Big(\det\Big(\mathbf{I}_{LN_t}+\frac{\gamma}{LN_t}\boldsymbol{\Xi}\mathbf{H}^H\mathbf{H}\Big)\Big)\Big] \\ -\sum_{i=1}^{LN_t}\mathcal{E}\Big[\log_2\Big(\det\Big(\mathbf{I}_{LN_t-1}+\frac{\gamma}{LN_t}\boldsymbol{\Xi}_{ii}\mathbf{H}_i^H\mathbf{H}_i\Big)\Big)\Big].\end{aligned} \tag{3.116}$$

Proof. First, we recall that

$$\left[\mathbf{W}^{-1}\right]_{ii} = \frac{\det(\mathbf{W}_{ii})}{\det(\mathbf{W})}. \tag{3.117}$$

Using the above expression, we can rewrite (3.114) as

$$\gamma_i^{\texttt{mmse}} = \frac{\det\left(\mathbf{I}_{LN_t}+\frac{\gamma}{LN_t}\mathbf{Z}^H\mathbf{Z}\right)}{\det\left(\left(\mathbf{I}_{LN_t}+\frac{\gamma}{LN_t}\mathbf{Z}^H\mathbf{Z}\right)_{ii}\right)}-1. \tag{3.118}$$

Substitute $\mathbf{Z} \triangleq \mathbf{H}\boldsymbol{\Xi}^{1/2}$ and using the following determinant property, $\det(\mathbf{I}_n+\mathbf{A}_{n\times m}\mathbf{B}_{m\times n}) = \det(\mathbf{I}_m+\mathbf{B}_{m\times n}\mathbf{A}_{n\times m})$, we can rearrange (3.118) as follows:

$$\gamma_i^{\texttt{mmse}} = \frac{\det\left(\mathbf{I}_{LN_t}+\frac{\gamma}{LN_t}\boldsymbol{\Xi}\mathbf{H}^H\mathbf{H}\right)}{\det\left(\left(\mathbf{I}_{LN_t}+\frac{\gamma}{LN_t}\boldsymbol{\Xi}\mathbf{H}^H\mathbf{H}\right)_{ii}\right)}-1. \tag{3.119}$$

Now, substituting (3.119) into (3.115) and simplification gives

$$\begin{aligned}\mathcal{R}^{\texttt{mmse}} &= \sum_{i=1}^{LN_t} \mathcal{E}\Big[\log_2\Big(\det\Big(\mathbf{I}_{LN_t}+\frac{\gamma}{LN_t}\boldsymbol{\Xi}\mathbf{H}^H\mathbf{H}\Big)\Big)\Big] \\ &\quad - \sum_{i=1}^{LN_t} \mathcal{E}\Big[\log_2\Big(\det\Big(\mathbf{I}_{LN_t}+\frac{\gamma}{LN_t}\boldsymbol{\Xi}\mathbf{H}^H\mathbf{H}\Big)_{ii}\Big)\Big] \qquad (3.120) \\ &= \sum_{i=1}^{LN_t} \mathcal{E}\Big[\log_2\Big(\det\Big(\mathbf{I}_{LN_t}+\frac{\gamma}{LN_t}\boldsymbol{\Xi}\mathbf{H}^H\mathbf{H}\Big)\Big)\Big] \\ &\quad - \sum_{i=1}^{LN_t} \mathcal{E}\Big[\log_2\Big(\det\Big(\mathbf{I}_{LN_t-1}+\frac{\gamma}{LN_t}(\boldsymbol{\Xi}\mathbf{H}^H\mathbf{H})_{ii}\Big)\Big)\Big]. \qquad (3.121)\end{aligned}$$

Thus, we can conclude the proof, using the following matrix minor property $(\boldsymbol{\Xi}\mathbf{H}^H\mathbf{H})_{ii} = \boldsymbol{\Xi}_{ii}\mathbf{H}_i^H\mathbf{H}_i$. □

3.5.2 Low-SNR analysis

We now examine the sum rate performance of D-MIMO MMSE receivers in the power-limited (wideband) regime. We have already introduced the low-SNR analysis in Section 3.2.2 and hence, we directly give the following proposition.

Proposition 3.9. *For D-MIMO systems with MMSE receivers in RIG fading channels, the minimum energy per information bit and the wideband slope are respectively*

$$\frac{E_b}{N_0}^{\texttt{mmse}}_{\texttt{min}} = \frac{\ln 2}{N_r\left(N_t\sum_{i=1}^{L}\mu_i D_i^{-v} - \frac{1}{LN_t}\sum_{i=1}^{LN_t}\sum_{\substack{j=1\\ j\neq i}}^{LN_t}\mu_j D_j^{-v}\right)} \qquad (3.122)$$

$$\mathcal{S}_0^{\texttt{mmse}} = \frac{2LN_t}{\frac{2LN_t-1}{N_r} + L^2N_t\frac{\sum_{i=1}^{L}\left(\mu_i^2+\frac{\mu_i^3}{\lambda_i}\right)D_i^{-2v}}{\left(\sum_{i=1}^{L}\mu_i D_i^{-v}\right)^2} - \frac{(LN_t-1)^2}{LN_t}\sum_{i=1}^{LN_t}\left(\frac{\sum_{\substack{j=1\\ j\neq i}}^{LN_t}\left(\mu_j^2+\frac{\mu_j^3}{\lambda_j}\right)D_j^{-2v}}{\left(\sum_{\substack{j=1\\ j\neq i}}^{LN_t}\mu_j D_j^{-v}\right)^2}\right)}. \qquad (3.123)$$

Proof. For proving (3.122), we need to take the first derivative of (3.116) w.r.t. $\gamma \to 0$. Using (3.33), we can easily evaluate the first derivative as

$$\dot{\mathcal{R}}^{\texttt{mmse}}(0) = \frac{1}{\ln 2}\,\mathcal{E}\left[\mathrm{tr}\big(\boldsymbol{\Xi}\mathbf{H}^H\mathbf{H}\big)\right] - \frac{1}{\ln 2}\sum_{i=1}^{LN_t}\mathcal{E}\left[\frac{1}{LN_t}\mathrm{tr}\big(\boldsymbol{\Xi}_{ii}\mathbf{H}_i^H\mathbf{H}_i\big)\right]. \qquad (3.124)$$

Now, we split (3.124) as $\dot{\mathcal{R}}^{\mathtt{mmse}}(0) = \dot{\mathcal{R}}_1^{\mathtt{mmse}} - \dot{\mathcal{R}}_2^{\mathtt{mmse}}$. We have already evaluated $\dot{\mathcal{R}}_1^{\mathtt{mmse}}$ in (3.36) and hence, we evaluate $\dot{\mathcal{R}}_2^{\mathtt{mmse}}$ as

$$\dot{\mathcal{R}}_2^{\mathtt{mmse}} = \frac{1}{LN_t \ln 2} \sum_{i=1}^{LN_t} \mathcal{E}\left[\sum_{\substack{j=1 \\ j\neq i}}^{LN_t} \frac{\xi_j}{D_j^{\upsilon}} \varphi_j \right] \tag{3.125}$$

$$= \frac{1}{LN_t \ln 2} \sum_{i=1}^{LN_t} \sum_{\substack{j=1 \\ j\neq i}}^{LN_t} \frac{1}{D_j^{\upsilon}} \mathcal{E}[\xi_j]\mathcal{E}[\varphi_j]. \tag{3.126}$$

The expectations are the same as in (3.35). Therefore, we have that

$$\dot{\mathcal{R}}^{\mathtt{mmse}}(0) = \frac{N_r N_t}{\ln 2} \sum_{i=1}^{L} \frac{\mu_i}{D_i^{\upsilon}} - \frac{N_r}{LN_t \ln 2} \sum_{i=1}^{LN_t} \sum_{\substack{j=1 \\ j\neq i}}^{LN_t} \frac{\mu_j}{D_j^{\upsilon}}. \tag{3.127}$$

The inverse of (3.127) directly yields (3.122). For the wideband slope $\mathcal{S}_0^{\mathtt{mmse}}$, we invoke a classical result from random matrix theory on correlated Rayleigh MIMO channels [16, Eq. (75)]

$$\mathcal{S}_0^{\mathtt{mmse}} = \frac{2LN_tN_r}{(2LN_t - 1)\,\zeta(\mathbf{\Theta}_R) + N_r \left(LN_t \zeta(\mathbf{\Theta}_T) - \frac{LN_t - 1}{LN_t} \sum_{i=1}^{LN_t} \zeta(\mathbf{\Theta}_{Tii}) \right)}. \tag{3.128}$$

Assuming no correlation at the receiver, we can express $\mathcal{S}_0^{\mathtt{mmse}}$ by substituting $\mathbf{\Theta}_R = \mathbf{I}_{N_r}$ and $\mathbf{\Theta}_T = \mathbf{\Xi}$ into (3.128). $\zeta(\mathbf{\Xi})$ is deduced in Section 3.2.2, whilst $\zeta(\mathbf{\Xi}_{ii})$ is given by

$$\zeta(\mathbf{\Theta}_{Tii}) = \zeta(\mathbf{\Xi}_{ii}) = \frac{(LN_t - 1)\,\mathcal{E}\left[\mathrm{tr}(\mathbf{\Xi}_{ii}^2)\right]}{\mathcal{E}^2\left[\mathrm{tr}(\mathbf{\Xi}_{ii})\right]} = \frac{(LN_t - 1) \sum_{\substack{j=1 \\ j\neq i}}^{LN_t} \left(\mu_j^2 + \frac{\mu_j^3}{\lambda_j} \right) D_j^{-2\upsilon}}{\left(\sum_{\substack{j=1 \\ j\neq i}}^{LN_t} \mu_j D_j^{-\upsilon} \right)^2}. \tag{3.129}$$

Substituting (A.8) and (A.9) into (3.38) gives (3.129) and substituting all the above results into (3.128) gives the wideband slope as

$$\mathcal{S}_0^{\mathtt{mmse}} = \frac{2LN_tN_r}{(2LN_t - 1) + N_r L^2 N_t \frac{\sum_{i=1}^{L} \left(\mu_i^2 + \frac{\mu_i^3}{\lambda_i} \right) D_i^{-2\upsilon}}{\left(\sum_{i=1}^{L} \mu_i D_i^{-\upsilon} \right)^2} - \frac{N_r (LN_t - 1)^2}{LN_t} \sum_{i=1}^{LN_t} \left(\frac{\sum_{\substack{j=1 \\ j\neq i}}^{LN_t} \left(\mu_j^2 + \frac{\mu_j^3}{\lambda_j} \right) D_j^{-2\upsilon}}{\left(\sum_{\substack{j=1 \\ j\neq i}}^{LN_t} \mu_j D_j^{-\upsilon} \right)^2} \right)}. \tag{3.130}$$

Thus, the proof is concluded by simplifying (3.130). □

In Fig. 3.9, the simulated sum rate of (3.115) and the analytical low-SNR linear approximation are plotted against the transmit E_b/N_0. Clearly, we can observe that the low-SNR

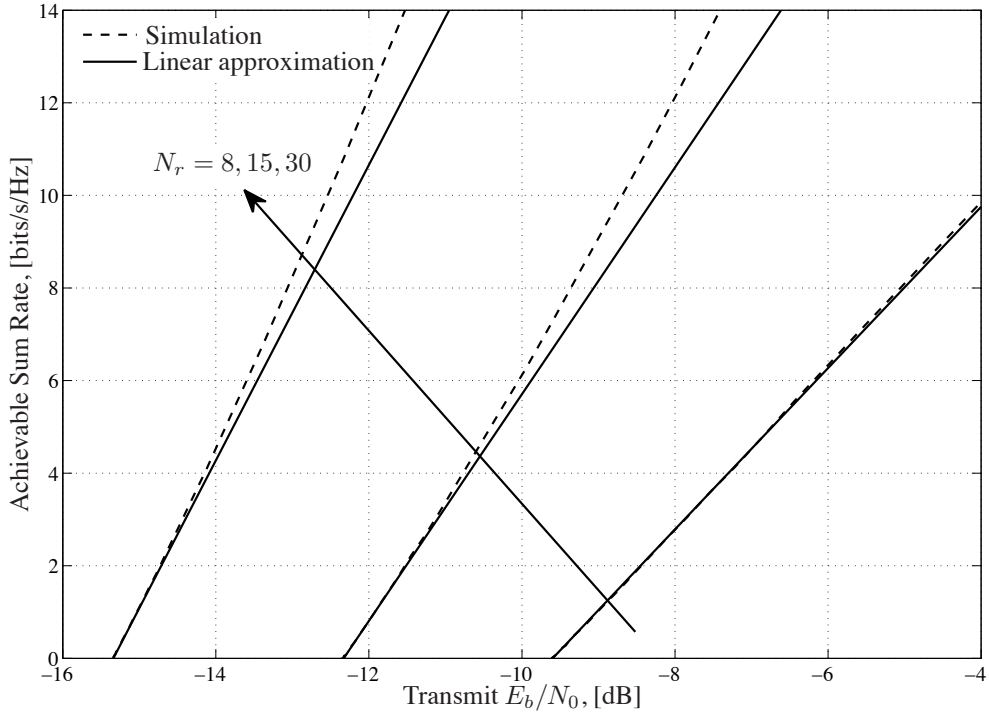

Figure 3.9: MMSE receivers: Low-SNR simulated sum rate and analytical linear approximation against the transmit E_b/N_0 ($N_t = 3$, $L = 3$, $\mu_i = \mu = 4$, $\lambda_i = \lambda = 13$, $D_i = D = 1500$m $(\forall i = 1, \ldots, L)$, and $\upsilon = 4$).

performance of MMSE receivers is systematically improved with the number of receive antennas, N_r, which is due to the additional degrees-of-freedom for canceling interference. Also, the linear approximation remains sufficiently tight across the entire SNR range.

In Fig. 3.10, we compare the performance of optimal, linear ZF and MMSE receivers in the low-SNR regime. The simulated low-SNR ergodic capacity/sum rates and the analytical linear approximations are plotted against the transmit E_b/N_0. The figure illustrates the big performance gap between optimal and ZF receivers, which is due to the high number of total transmit antennas ($LN_t = 6$), that corresponds to the number of interfering data streams. On the other hand, we can easily conclude that MMSE receivers are optimal in terms of $E_b/N_{0\mathtt{min}}$. MMSE receivers sub-optimality is only reflected via a reduced wideband slope.

We now compare $\mathcal{S}_0^{\mathtt{mmse}}$ with $\mathcal{S}_0^{\mathtt{opt}}$ to understand the effects of shadowing on the wideband slope. It is thus of interest to consider the following ratio for analyzing the wideband

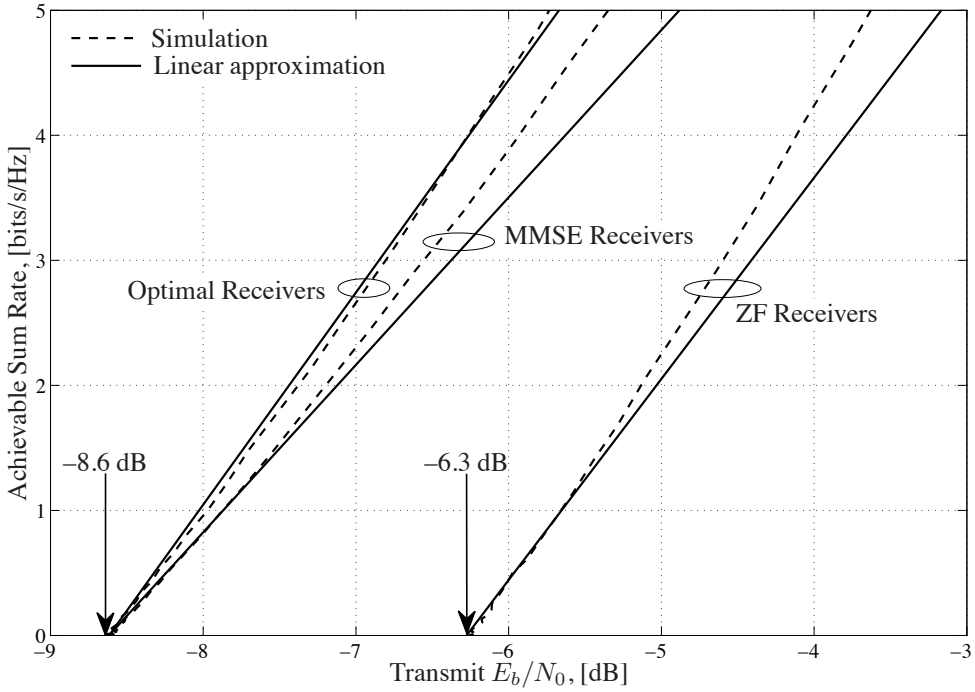

Figure 3.10: Low-SNR simulated sum rate (optimal, ZF, and MMSE) and analytical linear approximations against the transmit E_b/N_0 ($N_r = 12$, $N_t = 2$, $L = 3$, $\mu_i = \mu = 1$, $\lambda_i = \lambda = 10$ ($\forall i = 1, \ldots, L$), $D_i = [1000\text{m}, 1500\text{m}, 2000\text{m}]$, and $\upsilon = 4$).

slopes further

$$\frac{LN_t}{2LN_t - 1} \leq \frac{\mathcal{S}_0^{\texttt{mmse}}}{\mathcal{S}_0^{\texttt{opt}}} \leq \frac{LN_t + N_r}{2LN_t + N_r - 1}. \tag{3.131}$$

The result reveals that in the low-SNR regime, the shadowing decreases the ratio and subsequently reduces the achievable sum rate of MMSE receivers through a reduction in wideband slope. Interestingly, when $LN_t = 1$, the ratio becomes unity, which reveals that MMSE receivers are optimal when there is no interfering data streams to be cancelled out. It is also important to note that when $N_r \to \infty$, for fixed LN_t, MMSE receivers operate optimally, due to the additional captured power and the enhanced interference suppression capabilities of the receive array, which coincides with [16].

3.5.3 High-SNR analysis

We now examine the sum rate performance of MMSE receivers in the high-SNR regime. We recall that, at high-SNRs, both ZF and MMSE receivers behave equivalently in terms of sum rate [15]. We have already introduced the high-SNR parameters in Section 3.2.3 and hence, we can directly give the following proposition.

Proposition 3.10. *For D-MIMO systems with MMSE receivers in RIG fading channels, the high-SNR slope and offset parameters are respectively given by*

$$\mathcal{S}_{\infty}^{\mathtt{mmse}} = LN_t \tag{3.132}$$

$$\begin{aligned}\mathcal{L}_{\infty}^{\mathtt{mmse}} &= \log_2(LN_t) - \frac{1}{\ln 2}\psi(N_r - LN_t + 1) \\ &\quad - N_t \sum_{i=1}^{L} \left(\log_2 \mu_i - \upsilon \log_2 D_i + \frac{1}{\ln 2} \exp\left(\frac{2\lambda_i}{\mu_i}\right) \mathtt{Ei}\left(\frac{-2\lambda_i}{\mu_i}\right)\right) \\ &\quad + \frac{1}{LN_t} \sum_{i=1}^{LN_t} \sum_{\substack{j=1 \\ j\neq i}}^{LN_t} \left(\log_2 \mu_j - \upsilon \log_2 D_j + \frac{1}{\ln 2} \exp\left(\frac{2\lambda_j}{\mu_j}\right) \mathtt{Ei}\left(\frac{-2\lambda_j}{\mu_j}\right)\right).\end{aligned} \tag{3.133}$$

Proof. For MIMO systems with MMSE receivers, the slope and offset parameters are obtained by [16, Eq. (19), (20)] as follows:

$$\mathcal{S}_{\infty}^{\mathtt{mmse}} = \min(N_r, LN_t) \tag{3.134}$$

$$\begin{aligned}\mathcal{L}_{\infty}^{\mathtt{mmse}} &= \log_2(LN_t) - \mathcal{E}\Big[\log_2\Big(\det\Big(\mathbf{\Xi}\mathbf{H}^H\mathbf{H}\Big)\Big)\Big] \\ &\quad + \frac{1}{LN_t}\sum_{i=1}^{LN_t} \mathcal{E}\Big[\log_2\Big(\det\Big(\mathbf{\Xi}_{ii}\mathbf{H}_i^H\mathbf{H}_i\Big)\Big)\Big].\end{aligned} \tag{3.135}$$

For the offset calculations, using the following identity $\det(\mathbf{AB}) = \det(\mathbf{A})\det(\mathbf{B})$, we can rewrite (3.135) as

$$\begin{aligned}\mathcal{L}_{\infty}^{\mathtt{mmse}} &= \log_2(LN_t) - \mathcal{E}\Big[\log_2\Big(\det\Big(\mathbf{\Xi}\mathbf{H}^H\mathbf{H}\Big)\Big)\Big] \\ &\quad + \frac{1}{LN_t \ln 2}\sum_{i=1}^{LN_t} \mathcal{E}\big[\ln(\det(\mathbf{\Xi}_{ii}))\big] + \frac{1}{LN_t \ln 2}\sum_{i=1}^{LN_t} \mathcal{E}\Big[\ln\Big(\det\Big(\mathbf{H}_i^H\mathbf{H}_i\Big)\Big)\Big].\end{aligned} \tag{3.136}$$

Since $\mathbf{\Xi}_{ii}$ is also diagonal, we can apply (3.26) directly to evaluate the above expectation as follows:

$$\sum_{i=1}^{LN_t} \mathcal{E}\big[\ln(\det(\mathbf{\Xi}_{ii}))\big] = \sum_{i=1}^{LN_t}\sum_{\substack{j=1 \\ j\neq i}}^{LN_t} \left(\log_2 \mu_j - \upsilon \log_2 D_j + \frac{1}{\ln 2} \exp\left(\frac{2\lambda_j}{\mu_j}\right) \mathtt{Ei}\left(\frac{-2\lambda_j}{\mu_j}\right)\right). \tag{3.137}$$

Combining (3.23), (3.137), and (3.112) with (3.136) gives

$$\begin{aligned}\mathcal{L}_{\infty}^{\mathtt{mmse}} &= \log_2(LN_t) - \frac{1}{\ln 2}\sum_{k=0}^{LN_t-1}\psi(N_r-k) + \frac{1}{LN_t \ln 2}\sum_{i=1}^{LN_t}\sum_{k=0}^{LN_t-2}\psi(N_r-k) \\ &\quad - N_t \sum_{i=1}^{L} \left(\log_2 \mu_i - \upsilon \log_2 D_i + \frac{1}{\ln 2} \exp\left(\frac{2\lambda_i}{\mu_i}\right) \mathtt{Ei}\left(\frac{-2\lambda_i}{\mu_i}\right)\right) \\ &\quad + \frac{1}{LN_t} \sum_{i=1}^{LN_t} \sum_{\substack{j=1 \\ j\neq i}}^{LN_t} \left(\log_2 \mu_j - \upsilon \log_2 D_j + \frac{1}{\ln 2} \exp\left(\frac{2\lambda_j}{\mu_j}\right) \mathtt{Ei}\left(\frac{-2\lambda_j}{\mu_j}\right)\right).\end{aligned} \tag{3.138}$$

Thus, the proof of (3.133) is concluded by simplifying (3.138). □

Similar to optimal and ZF receivers, the high-SNR sum rate increases linearly with the minimum number of antennas. As anticipated, higher Tx-Rx distances effectively reduce the sum rate due to the increased path-loss attenuation.

Chapter 4

Effective Capacity Analysis of MISO Systems

A plethora of emerging applications, such as video tele-conferencing and VoIP, impose stringent delay constraints that have to be appropriately accounted for, using a suitable metric. Unfortunately, the classical Shannon's ergodic capacity fails to do so. Hence, the concept of *effective capacity* arises which can efficiently characterize communication systems in terms of data rate, delay and delay-violation probability. In this thesis, we will be using the terminology *effective rate* instead of effective capacity, since we perform no optimization over the input covariance matrix $\mathbf{Q} = \mathcal{E}[\mathbf{x}\mathbf{x}^H]$. For a detailed discussion, interested readers are referred to [17].

In this chapter, we present a detailed effective rate analysis of MISO systems operating over RIG and $\mathcal{G}$ fading channels in two different channel formulations. Since an exact analysis is tedious, we derive new analytical expressions for the effective rate in the asymptotically low- and high-SNR regimes. By doing so, we are able to obtain additional physical insights into the implications of several parameters (e.g. fading parameters, number of antennas, delay constraints) on the system performance.

4.1 MISO system model

4.1.1 RIG fading channels

Consider a typical MISO system with N_t transmit antennas whose input-output relationship is expressed as

$$y = \mathbf{h}\boldsymbol{\Xi}^{1/2}\mathbf{x} + \mathbf{n} \tag{4.1}$$

where $\mathbf{x} \in \mathbb{C}^{N_t \times 1}$ is the transmitted signal vector, while $\mathbf{n}$ is the complex AWGN with zero-mean and variance N_0. The large-scale coefficients are represented by the diagonal matrix $\boldsymbol{\Xi} \in \mathbb{R}^{N_t \times N_t}$ whose structure is $\boldsymbol{\Xi} = \text{diag}\{\mathbf{I}_{N_t}\xi_i/D_i^v\}$ for $i = 1, \ldots, N_t$. The large-scale coefficients ξ_i are modeled as independent IG RVs, $\xi_i \sim \text{IG}(\mu_i, \lambda_i)$ according to (3.2).

The entries of the channel fading vector $\mathbf{h} \in \mathbb{C}^{1 \times N_t}$ are assumed to be i.i.d. Rayleigh RVs, i.e., $h_i \sim \mathcal{CN}(0, 1)$, where $i = 1, \ldots, N_t$. We now invoke that a squared Rayleigh RV follows the Gamma distribution with scale parameter 1 [30]. As such, i.i.d. Gamma RVs with scale parameter 1 are distributed as $\varphi_i \sim \text{Gamma}(1, 1)$, or

$$p(\varphi_i) = \exp(-\varphi_i), \quad \varphi_i \geq 0. \tag{4.2}$$

We assume that the transmitter sends uncorrelated circularly symmetric zero-mean complex Gaussian signals and uniform power allocation across the transmit antennas; hence, the effective rate can be expressed as [74]

$$\mathcal{R}(\theta, \gamma) = -\frac{1}{A}\log_2\left(\mathcal{E}\left[\left(1 + \frac{\gamma}{N_t}\mathbf{h}\boldsymbol{\Xi}\mathbf{h}^H\right)^{-A}\right]\right) \text{ bits/s/Hz} \tag{4.3}$$

where $A \triangleq \theta TB/\ln 2$, with B denoting the bandwidth of the system, while γ is the average transmit SNR.

4.1.2 $\mathcal{G}$ fading channels

In this section, we consider the entries of the channel vector $\mathbf{h}$ to be i.i.d. Nakagami-m/IG RVs with fading parameters μ, λ, and $m \geq 0.5$. We also assume that the large-scale coefficients in this fading channel are kept constant throughout this chapter. As such, we express a typical MISO system with N_t transmit antennas input-output model as,

$$y = \mathbf{h}\mathbf{x} + \mathbf{n} \tag{4.4}$$

where $\mathbf{x} \in \mathbb{C}^{N_t \times 1}$ is the transmitted signal vector, while $\mathbf{n}$ is the complex AWGN with zero-mean and variance N_0. Then, the p.d.f. of $x = |h_i|^2$, where $i = 1, \ldots, N_t$, is given by [55, Eq. (6)]

$$p_{|h_i|^2}(x) = \frac{Cx^{m-1}}{\left(\sqrt{\alpha + \beta x}\right)^{m+\frac{1}{2}}} K_{m+\frac{1}{2}}\left(b\sqrt{\alpha + \beta x}\right), \quad x > 0 \tag{4.5}$$

where $K_v(\cdot)$ denotes the v-th order modified Bessel function of second kind [1, Eq. (8.407.1)] and the following constants have been used:

$$C \triangleq \frac{(\mu\lambda)^{\frac{1+2m}{4}}}{\Gamma(m)}\sqrt{\frac{2\lambda}{\pi\mu}}\exp\left(\frac{\lambda}{\mu}\right)\left(\frac{m}{\mu}\right)^m, \; b \triangleq \frac{1}{\mu}\sqrt{\frac{\lambda}{\mu}}, \; \alpha \triangleq \mu\lambda, \; \beta \triangleq 2m\mu. \tag{4.6}$$

Using the moment generating function (m.g.f.) of the $\mathcal{G}$ distribution [55, Eq. (9)], we obtain the first two moments of the squared $\mathcal{G}$ envelope (i.e. $|h_i|^2$) as follows:

$$\mathcal{E}\left[|h_i|^2\right] = \mu \tag{4.7}$$

$$\mathcal{E}\left[\left(|h_i|^2\right)^2\right] = \mu^2\left(1+\frac{1}{m}\right)\left(1+\frac{\mu}{\lambda}\right). \tag{4.8}$$

Now, using [55, Eq. (7)] and [55, Eq. (9)], we introduce the m.g.f. of the sum of the squared $\mathcal{G}$ envelope (i.e. $z = \mathbf{h}\mathbf{h}^H = \sum_{i=1}^{N_t}|h_i|^2$) as follows:

$$\mathcal{E}\left[\left(\mathbf{h}\mathbf{h}^H\right)^k\right] = \mathcal{E}\left[z^k\right] = \sqrt{\frac{2\lambda}{\pi\mu}}\exp\left(\frac{\lambda}{\mu}\right)\left(\frac{\mu}{m}\right)^k\frac{\Gamma(mN_t+k)}{\Gamma(mN_t)}K_{k-\frac{1}{2}}\left(\frac{\lambda}{\mu}\right) \tag{4.9}$$

while the k-th negative moment is given by

$$\mathcal{E}\left[z^{-k}\right] = \sqrt{\frac{2\lambda}{\pi\mu}}\exp\left(\frac{\lambda}{\mu}\right)\left(\frac{\mu}{m}\right)^{-k}\frac{\Gamma(mN_t-k)}{\Gamma(mN_t)}K_{-k-\frac{1}{2}}\left(\frac{\lambda}{\mu}\right) \tag{4.10}$$

$$= \left(\frac{m}{\mu}\right)^k\frac{\Gamma(mN_t-k)}{\Gamma(mN_t)}\sum_{n=0}^{k}\frac{(k+n)!}{n!\,(k-n)!}\left(\frac{\mu}{2\lambda}\right)^n. \tag{4.11}$$

By using (4.9), we give the first two moments of the sum of squared $\mathcal{G}$ envelope as follows:

$$\mathcal{E}\left[z\right] = N_t\mu \tag{4.12}$$

$$\mathcal{E}\left[z^2\right] = N_t^2\mu^2\left(1+\frac{1}{mN_t}\right)\left(1+\frac{\mu}{\lambda}\right). \tag{4.13}$$

We now assume that the transmitter sends uncorrelated circularly symmetric zero-mean complex Gaussian signals and uniform power allocation across the transmit antennas. Then, the effective rate in this fading channel is expressed as [74]

$$\mathcal{R}(\theta,\gamma) = -\frac{1}{A}\log_2\left(\mathcal{E}\left[\left(1+\frac{\gamma}{N_t}\mathbf{h}\mathbf{h}^H\right)^{-A}\right]\right)\ \text{bits/s/Hz} \tag{4.14}$$

where $A \triangleq \theta TB/\ln 2$ with B denoting the bandwidth of the system, while γ is the average transmit SNR.

4.2 Low-SNR analysis

In this section, we present a detailed effective rate analysis of MISO systems in RIG and $\mathcal{G}$ fading channels in the low-SNR regime. Following the generic methodology of [17],

we can assess the low-SNR performance via a second-order expansion of the effective rate around $\gamma \to 0^+$ according to

$$\mathcal{R}(\theta,\gamma) = \dot{\mathcal{R}}(\theta,0)\gamma + \ddot{\mathcal{R}}(\theta,0)\frac{\gamma^2}{2} + o(\gamma^2) \tag{4.15}$$

where $\dot{\mathcal{R}}(\theta,0)$ and $\ddot{\mathcal{R}}(\theta,0)$ denote the first- and second-order derivatives of the effective rate in (4.3) (or in (4.14)) w.r.t. the SNR γ, respectively. We point out that these derivative expressions are inherently related with the notions of the *minimum normalized energy per information bit to reliably convey any positive rate* and the *wideband slope* respectively, originally proposed in [61]. For the case of QoS constraints, the latter two metrics are respectively defined as,

$$\frac{E_b}{N_0}_{\min} \triangleq \lim_{\gamma\to 0}\frac{\gamma}{\mathcal{R}(\theta,\gamma)} = \frac{1}{\dot{\mathcal{R}}(\theta,0)} \quad \text{and} \quad \mathcal{S}_0 = -2\ln 2\frac{\left(\dot{\mathcal{R}}(\theta,0)\right)^2}{\ddot{\mathcal{R}}(\theta,0)}. \tag{4.16}$$

4.2.1 RIG fading channels

Proposition 4.1. *For MISO systems in RIG fading channels, the minimum energy per information bit and the wideband slope are*

$$\frac{E_b}{N_0}_{\min}^{\mathtt{RIG}} = \ln 2\, N_t \left(\sum_{i=1}^{N_t}\mu_i\right)^{-1} \tag{4.17}$$

$$\mathcal{S}_0^{\mathtt{RIG}} = \frac{2\left(\sum_{i=1}^{N_t}\mu_i\right)^2}{(A+1)\left(\left(2\sum_{i=1}^{N_t}\left(\mu_i^2+\frac{\mu_i^3}{\lambda_i}\right)\right)+\left(\sum_{i=1}^{N_t}\sum_{\substack{j=1\\ j\neq i}}^{N_t}\mu_i\mu_j\right)\right) - A\left(\sum_{i=1}^{N_t}\mu_i\right)^2}. \tag{4.18}$$

Proof. Recalling that, for IG distributed RVs, the first two moments about zero are $\mathcal{E}[\xi_i] = \mu_i$ and $\mathcal{E}[\xi_i^2] = \mu_i^2 + \frac{\mu_i^3}{\lambda_i}$, respectively [33]. For Gamma distributed RVs with scale parameter 1, the first two moments about zero are $\mathcal{E}[\varphi_i] = 1$ and $\mathcal{E}[\varphi_i^2] = 2$, respectively [30].

Using the results in [74, Appendix I], we can easily find the first- and second-order derivatives in (4.16). Thus, the former is given by

$$\dot{\mathcal{R}}(\theta,0) = \frac{1}{\ln 2\, N_t}\mathcal{E}\left[\mathbf{h}\boldsymbol{\Xi}\mathbf{h}^H\right] = \frac{1}{\ln 2\, N_t}\mathcal{E}\left[\mathrm{tr}\left(\boldsymbol{\Xi}\mathbf{h}^H\mathbf{h}\right)\right] \tag{4.19}$$

$$= \frac{1}{\ln 2\, N_t}\mathcal{E}\left[\sum_{i=1}^{N_t}\xi_i\varphi_i\right] = \frac{1}{\ln 2\, N_t}\sum_{i=1}^{N_t}\mathcal{E}\left[\xi_i\right]\mathcal{E}\left[\varphi_i\right] \tag{4.20}$$

$$= \frac{1}{\ln 2\, N_t}\sum_{i=1}^{N_t}\mu_i \tag{4.21}$$

where in (4.20), we have used the statistical independence property. Now, we can easily get (4.17) using (4.21). Next, the second-order derivative in (4.16) is given by

$$\ddot{\mathcal{R}}(\theta,0) = -\frac{1}{\theta TB}\frac{A(A+1)}{{N_t}^2}\mathcal{E}\left[\left(\mathbf{h}\boldsymbol{\Xi}\mathbf{h}^H\right)^2\right] + \frac{1}{\theta TB}\frac{A^2}{{N_t}^2}\left(\mathcal{E}\left[\mathbf{h}\boldsymbol{\Xi}\mathbf{h}^H\right]\right)^2 \tag{4.22}$$

$$= -\frac{1}{\theta TB}\frac{A(A+1)}{{N_t}^2}\underbrace{\mathcal{E}\left[\mathrm{tr}^2\left(\boldsymbol{\Xi}\mathbf{h}^H\mathbf{h}\right)\right]}_{I_1} + \frac{1}{\theta TB}\frac{A^2}{{N_t}^2}\left(\sum_{i=1}^{N_t}\mu_i\right)^2. \tag{4.23}$$

The expectation term in (4.23) is evaluated by

$$I_1 = \mathcal{E}\left[\left(\sum_{i=1}^{N_t}\xi_i\varphi_i\right)^2\right] = \mathcal{E}\left[\sum_{i=1}^{N_t}\left(\xi_i\varphi_i\right)^2\right] + \mathcal{E}\left[\sum_{i=1}^{N_t}\sum_{\substack{j=1\\j\neq i}}^{N_t}\xi_i\xi_j\varphi_i\varphi_j\right] \tag{4.24}$$

$$= \sum_{i=1}^{N_t}\mathcal{E}\left[\xi_i^2\right]\mathcal{E}\left[\varphi_i^2\right] + \sum_{i=1}^{N_t}\sum_{\substack{j=1\\j\neq i}}^{N_t}\mathcal{E}\left[\xi_i\right]\mathcal{E}\left[\varphi_i\right]\mathcal{E}\left[\xi_j\right]\mathcal{E}\left[\varphi_j\right] \tag{4.25}$$

$$= 2\sum_{i=1}^{N_t}\left(\mu_i^2 + \frac{\mu_i^3}{\lambda_i}\right) + \sum_{i=1}^{N_t}\sum_{\substack{j=1\\j\neq i}}^{N_t}\mu_i\mu_j \tag{4.26}$$

where in (4.25), we have used the statistical independence property. Substituting (4.26) into (4.23) gives

$$\ddot{\mathcal{R}}(\theta,0) = -\frac{1}{\theta TB}\frac{A(A+1)}{{N_t}^2}\left(\left(2\sum_{i=1}^{N_t}\left(\mu_i^2 + \frac{\mu_i^3}{\lambda_i}\right)\right) + \left(\sum_{i=1}^{N_t}\sum_{\substack{j=1\\j\neq i}}^{N_t}\mu_i\mu_j\right)\right) + \frac{1}{\theta TB}\frac{A^2}{{N_t}^2}\left(\sum_{i=1}^{N_t}\mu_i\right)^2. \tag{4.27}$$

Now, using the first- and second-order derivatives in (4.23) and (4.27) respectively, we can easily find the wideband slope as

$$\mathcal{S}_0^{\mathtt{RIG}} = \frac{-2\ln 2\left(\frac{1}{\ln 2\ N_t}\sum_{i=1}^{N_t}\mu_i\right)^2}{-\frac{1}{\theta TB}\frac{A(A+1)}{{N_t}^2}\left(\left(2\sum_{i=1}^{N_t}\left(\mu_i^2+\frac{\mu_i^3}{\lambda_i}\right)\right)+\left(\sum_{i=1}^{N_t}\sum_{\substack{j=1\\j\neq i}}^{N_t}\mu_i\mu_j\right)\right)+\frac{1}{\theta TB}\frac{A^2}{{N_t}^2}\left(\sum_{i=1}^{N_t}\mu_i\right)^2} \tag{4.28}$$

$$= \frac{2\left(\sum_{i=1}^{N_t}\mu_i\right)^2}{\frac{sA(A+1)}{{N_t}^2}\left(\left(2\sum_{i=1}^{N_t}\left(\mu_i^2+\frac{\mu_i^3}{\lambda_i}\right)\right)+\left(\sum_{i=1}^{N_t}\sum_{\substack{j=1\\j\neq i}}^{N_t}\mu_i\mu_j\right)\right)-\frac{sA^2}{{N_t}^2}\left(\sum_{i=1}^{N_t}\mu_i\right)^2} \tag{4.29}$$

where $s = \frac{\ln 2\ N_t^2}{\theta TB}$. Thus, we can conclude the proof after simplifying the above expression. □

We can easily observe that $\frac{E_b}{N_0}^{\mathtt{RIG}}_{\mathtt{min}}$ is independent of delay constraints, whereas $\mathcal{S}_0^{\mathtt{RIG}}$ is a monotonically decreasing function in A, which implies that the strict delay constraints effectively reduce $\mathcal{S}_0^{\mathtt{RIG}}$ and, in turn, the effective rate.

Corollary 4.1. *For MISO systems in RIG fading channels with constant large-scale fading parameters, the low-SNR metrics are given by*

$$\frac{E_b}{N_0}^{\mathtt{RIG}}_{\mathtt{min}} = \frac{\ln 2}{\mu} \tag{4.30}$$

$$\mathcal{S}_0^{\mathtt{RIG}} = \frac{2}{\frac{A+1}{N_t}\left(1+\frac{2\mu}{\lambda}\right)+1}. \tag{4.31}$$

Proof. The proof is trivial and therefore omitted. □

Interestingly, $\frac{E_b}{N_0}^{\mathtt{RIG}}_{\mathtt{min}}$ is now independent of number of transmit antennas, whereas $\mathcal{S}_0^{\mathtt{RIG}}$ is a monotonically decreasing function in A and an increasing function in N_t. This implies that strict delay constraints affect the effective rate in terms of $\mathcal{S}_0^{\mathtt{RIG}}$ whereas the effective rate can be improved by increasing the number of transmit antennas.

4.2.2 $\mathcal{G}$ fading channels

In this section, capitalizing on the results of [55], we analyze the effective rate of MISO systems in $\mathcal{G}$ fading channels.

Proposition 4.2. *For MISO systems in $\mathcal{G}$ fading channels, the minimum energy per information bit and the wideband slope are*

$$\frac{E_b}{N_0}^{\mathcal{G}}_{\mathtt{min}} = \frac{\ln 2}{\mu} \tag{4.32}$$

$$\mathcal{S}_0^{\mathcal{G}} = \frac{2}{\frac{A+1}{N_t}\left(\frac{1}{m}\left(1+\frac{\mu}{\lambda}\right)+\frac{\mu}{\lambda}\right)+1}. \tag{4.33}$$

Proof. Using the results in [74, Appendix I], we can easily find the first- and second-order derivatives of the effective rate in (4.14) w.r.t. SNR γ. Thus, the former is given by

$$\dot{\mathcal{R}}(\theta,0) = \frac{1}{\ln 2\, N_t}\mathcal{E}\left[\mathbf{h}\mathbf{h}^H\right] \tag{4.34}$$

$$= \frac{1}{\ln 2\, N_t}\mathcal{E}\left[\sum_{i=1}^{N_t}|h_i|^2\right] = \frac{1}{\ln 2\, N_t}N_t\,\mathcal{E}\left[|h_1|^2\right] \tag{4.35}$$

$$= \frac{\mu}{\ln 2} \tag{4.36}$$

where in (4.35), we have used the statistical independence property. We obtained (4.36) using (4.7) and thus, we can easily get (4.32). Next, the second-order derivative of the effective rate is given by

$$\ddot{\mathcal{R}}(\theta,0) = -\frac{(A+1)}{{N_t}^2 \ln 2} \underbrace{\mathcal{E}\left[\left(\mathbf{h}\mathbf{h}^H\right)^2\right]}_{I_1} + \frac{A}{{N_t}^2 \ln 2}\left(\mathcal{E}\left[\mathbf{h}\mathbf{h}^H\right]\right)^2 \tag{4.37}$$

The expectation term in (4.37) is evaluated by

$$I_1 = \mathcal{E}\left[\left(\sum_{i=1}^{N_t}|h_i|^2\right)^2\right] = \mathcal{E}\left[\sum_{i=1}^{N_t}\left(|h_i|^2\right)^2\right] + \mathcal{E}\left[\sum_{i=1}^{N_t}\sum_{\substack{j=1\\j\neq i}}^{N_t}|h_i|^2|h_j|^2\right] \tag{4.38}$$

$$= \sum_{i=1}^{N_t}\mathcal{E}\left[\left(|h_i|^2\right)^2\right] + \sum_{i=1}^{N_t}\sum_{\substack{j=1\\j\neq i}}^{N_t}\mathcal{E}\left[|h_i|^2\,|h_j|^2\right] \tag{4.39}$$

$$= N_t\mathcal{E}\left[\left(|h_1|^2\right)^2\right] + N_t(N_t-1)\left(\mathcal{E}\left[|h_1|^2\right]\right)^2 \tag{4.40}$$

$$= N_t\mu^2\left(1+\frac{1}{m}\right)\left(1+\frac{\mu}{\lambda}\right) + N_t(N_t-1)\mu^2 \tag{4.41}$$

where in (4.40), we have used the statistical independence property. We obtained (4.41) using (4.7) and (4.8). Substituting (4.41) into (4.37) gives

$$\ddot{\mathcal{R}}(\theta,0) = -\frac{(A+1)\mu^2}{N_t \ln 2}\left(\left(\left(\left(1+\frac{1}{m}\right)\left(1+\frac{\mu}{\lambda}\right)\right)+N_t-1\right)+\frac{A\mu^2}{\ln 2}\right). \tag{4.42}$$

Now, using (4.37) and (4.42), we can easily find the wideband slope as

$$\mathcal{S}_0^{\mathcal{G}} = \frac{-2\ln 2\left(\frac{\mu}{\ln 2}\right)^2}{\frac{\mu^2}{\ln 2}\left(-\frac{A+1}{N_t}\left(\left(\left(1+\frac{1}{m}\right)\left(1+\frac{\mu}{\lambda}\right)\right)+N_t-1\right)+A\right)} \tag{4.43}$$

$$= \frac{2}{\frac{A+1}{N_t}\left(\left(\left(1+\frac{1}{m}\right)\left(1+\frac{\mu}{\lambda}\right)\right)+N_t-1\right)-A}. \tag{4.44}$$

Thus, we can conclude the proof after simplifying (4.44). □

Note that, when $m=1$, the low-SNR metrics of $\mathcal{G}$ fading channels reduce to RIG fading model, as evidently we can compare with Corollary 4.1.

We can clearly observe that $\frac{E_b}{N_0}^{\mathcal{G}}_{\mathtt{min}}$ is independent of the Nakagami-m factor, delay constraints, and number of transmit antennas, whereas $\mathcal{S}_0^{\mathcal{G}}$ is an increasing function in N_t and m-factor. We can validate the impact of the m-factor using the following expression

$$\frac{d\mathcal{S}_0^{\mathcal{G}}}{dm} = \frac{2N_t(A+1)\left(1+\frac{\mu}{\lambda}\right)}{\left((A+1)\left(\left(1+\frac{\mu}{\lambda}\right)+\frac{m\mu}{\lambda}\right)+mN_t\right)^2} > 0 \tag{4.45}$$

whereas, the impact of N_t is validated by

$$\frac{d\mathcal{S}_0^{\mathcal{G}}}{dN_t} = \frac{2(A+1)\left(\frac{1}{m}\left(1+\frac{\mu}{\lambda}\right)+\frac{\mu}{\lambda}\right)}{\left((A+1)\left(\frac{1}{m}\left(1+\frac{\mu}{\lambda}\right)+\frac{\mu}{\lambda}\right)+N_t\right)^2} > 0. \tag{4.46}$$

Now, we can obtain the minimum value of wideband slope for $m = 0.5$ as

$$\mathcal{S}_0^{\mathcal{G}} = \frac{2}{(A+1)\left(2+\frac{3\mu}{\lambda}\right)+N_t} \tag{4.47}$$

and we can obtain its maximum value for $m \to \infty$ (i.e. AWGN channel) as

$$\mathcal{S}_0^{\mathcal{G}} = \frac{2}{(A+1)\frac{\mu}{\lambda}+N_t}. \tag{4.48}$$

Thus, we get the following bounds

$$\frac{2}{(A+1)\left(2+\frac{3\mu}{\lambda}\right)+N_t} \leq \mathcal{S}_0^{\mathcal{G}} \leq \frac{2}{(A+1)\frac{\mu}{\lambda}+N_t}. \tag{4.49}$$

We can easily validate monotonically decreasing function in A using the following expression

$$\frac{d\mathcal{S}_0^{\mathcal{G}}}{dA} = \frac{-2N_t\left(\frac{1}{m}\left(1+\frac{\mu}{\lambda}\right)+\frac{\mu}{\lambda}\right)}{\left((A+1)\left(\frac{1}{m}\left(1+\frac{\mu}{\lambda}\right)+\frac{\mu}{\lambda}\right)+N_t\right)^2} < 0. \tag{4.50}$$

It is also important to analyze the case when $A = 0$, i.e., no delay constraint, in which wideband slope reduces to

$$\mathcal{S}_0^{\mathcal{G}} = \frac{2N_t}{\frac{1}{m}\left(1+\frac{\mu}{\lambda}\right)+\frac{\mu}{\lambda}+N_t}. \tag{4.51}$$

When $A = 1$, the wideband slope becomes

$$\mathcal{S}_0^{\mathcal{G}} = \frac{2N_t}{\frac{2}{m}\left(1+\frac{\mu}{\lambda}\right)+\frac{2\mu}{\lambda}+N_t}. \tag{4.52}$$

We now validate the analytical expressions presented in Section 4.2.1 and Section 4.2.2 through set of Monte-Carlo simulations. For Section 4.2.1, we first generate 10,000 random realizations of $\boldsymbol{\Xi}$ and $\mathbf{h}$ according to (3.2) and (4.2), respectively. For Section 4.2.2, we generate 10,000 random realizations of channel vector $\mathbf{h}$ according to (4.5). In Fig. 4.1, the simulated low-SNR effective rate of (4.3) is compared with the analytical linear approximation in (4.15) for $N_t = 6$ and $A = 4$. We change only the large-scale fading

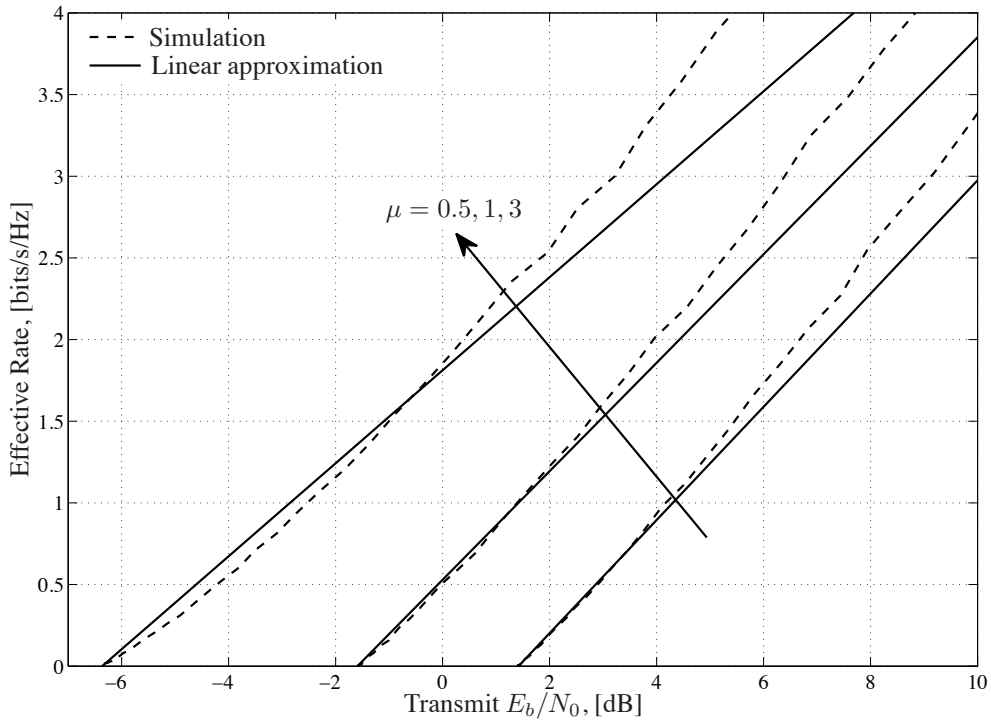

Figure 4.1: Low-SNR effective rate and analytical linear approximation against the transmit E_b/N_0 ($N_t = 6$, $A = 4$, $\lambda = 10$, and $m = 1$).

mean parameter, μ, and keep all other parameters constant. We can clearly observe that the low-SNR effective rate increases, whereas the wideband slope decreases when μ gets larger. On the other hand, the analytical approximation becomes tighter for small values of μ.

In Fig. 4.2, the simulated low-SNR effective rate of (4.3) is compared with the analytical linear approximation in (4.15) for $N_t = 6$ with different delay constraints. The graph indicates the accuracy of the analytical expressions and that the range for a good approximation improves if the QoS requirement loosens. On the other hand, when the QoS requirement becomes harsher (i.e. when A becomes larger), the wideband slope decreases and therefore the effective rate is reduced. The analytical approximation becomes tighter for small values of A and this we can evidently see in Fig. 4.3. The figure implies that the tighter delay constraint causes a severe decrease in the effective rate. This effective rate can be improved by increasing the number of transmit antennas.

Note that, in Fig. 4.1, Fig. 4.2 and Fig. 4.3, we considered the case $m = 1$ and therefore the results are applicable for both Sections 4.2.1 and 4.2.2.

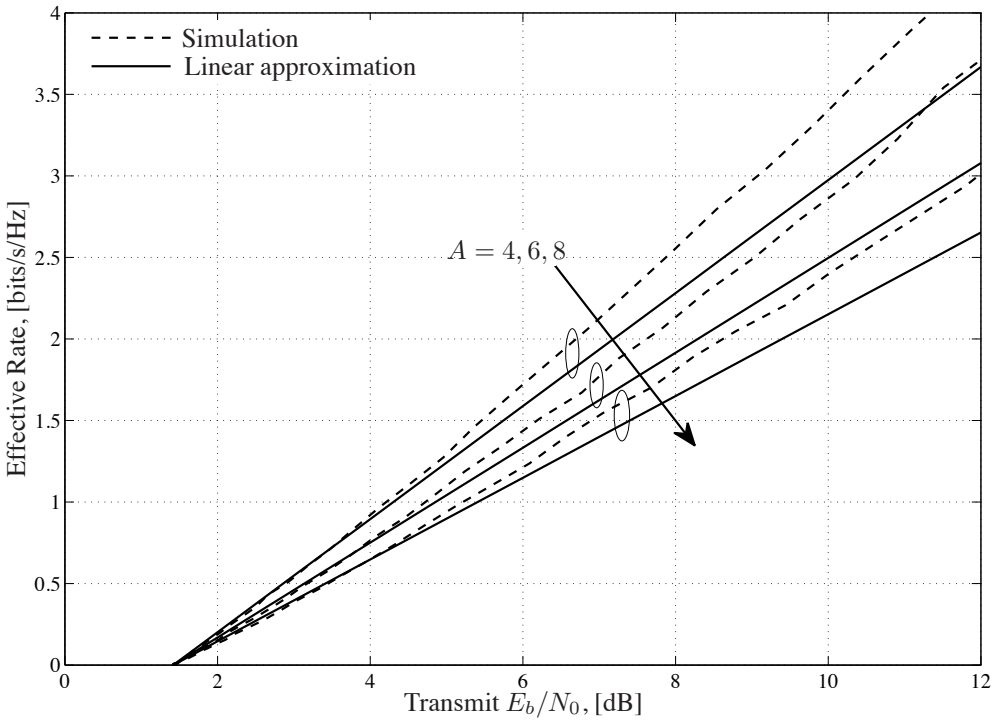

Figure 4.2: Low-SNR effective rate and analytical linear approximation against the transmit E_b/N_0 ($N_t = 6, m = 1, \lambda = 10$, and $\mu = 0.5$).

In Fig. 4.4, the simulated low-SNR effective rate of (4.14) is compared with the analytical linear approximation in (4.15) for $N_t = 6$ with different m-factors in the $\mathcal{G}$ distribution. The curves validate the accuracy of the analytical linear approximations. The fading parameter m affects the effective rate through the wideband slope rather than the minimum E_b/N_0. As such, for the larger values of m, the linear approximation becomes tighter and the effective rate increases.

4.3 High-SNR analysis

In this section, capitalizing on the results of [55], we analyze the effective rate of MISO systems in $\mathcal{G}$ fading channels in the high-SNR regime.

Proposition 4.3. *For MISO systems in $\mathcal{G}$ fading channels, the effective rate at high SNRs and for $A < mN_t$, where $A \in \mathbb{N}$, is given by*

$$\mathcal{R}^{\infty}(\theta, \gamma) = \log_2\left(\frac{\gamma\mu}{mN_t}\right) - \frac{1}{A}\log_2\left(\frac{\Gamma(mN_t - A)}{\Gamma(mN_t)}\right) - \frac{1}{A}\log_2\left(\sum_{n=0}^{A}\frac{(A+n)!}{n!\,(A-n)!}\left(\frac{\mu}{2\lambda}\right)^n\right). \tag{4.53}$$

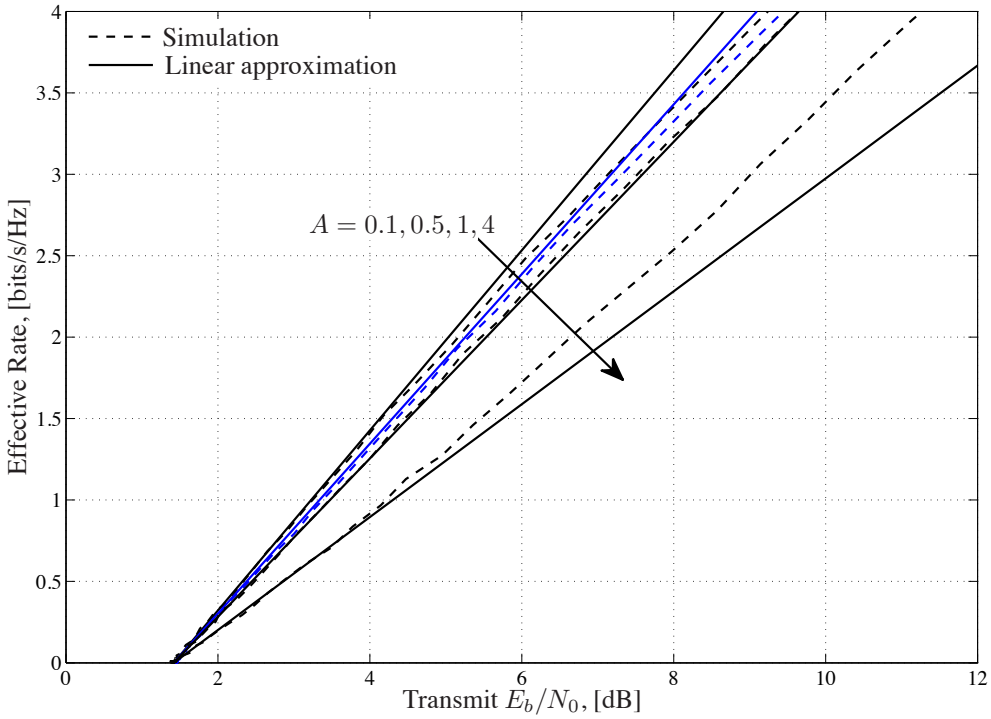

Figure 4.3: Low-SNR effective rate and analytical linear approximation against the transmit E_b/N_0 ($N_t = 6, m = 1, \lambda = 10$, and $\mu = 0.5$).

Proof. By taking γ large in (4.14) and using (4.11), we can easily get the desired result after appropriate simplifications. □

Note that the slope of the effective rate at high SNRs is equal to 1. For the particular case $A = 1$, (4.53) simplifies to

$$\mathcal{R}^{\infty}(\theta, \gamma) = \log_2(\gamma\mu) + \log_2\left(1 - \frac{1}{mN_t}\right) - \log_2\left(1 + \frac{\mu}{\lambda}\right) \tag{4.54}$$

$$= \log_2(\gamma) + \log_2\left(1 - \frac{1}{mN_t}\right) - \log_2\left(\frac{1}{\mu} + \frac{1}{\lambda}\right) \tag{4.55}$$

which indicates the beneficial impact of m, due to the reduced fading fluctuations.

In Fig. 4.5, the simulated effective rate is compared with the analytical linear approximation in (4.53) for different number of transmit antennas N_t. The curves validate the accuracy of the analytical linear approximations. The linear approximations become exact even at moderate SNRs (e.g., around $\gamma = 20$dB), while the tightness of the curves improves for higher N_t. We can easily observe that the effective rate increases with N_t, but the relative difference between the curves gets steadily smaller.

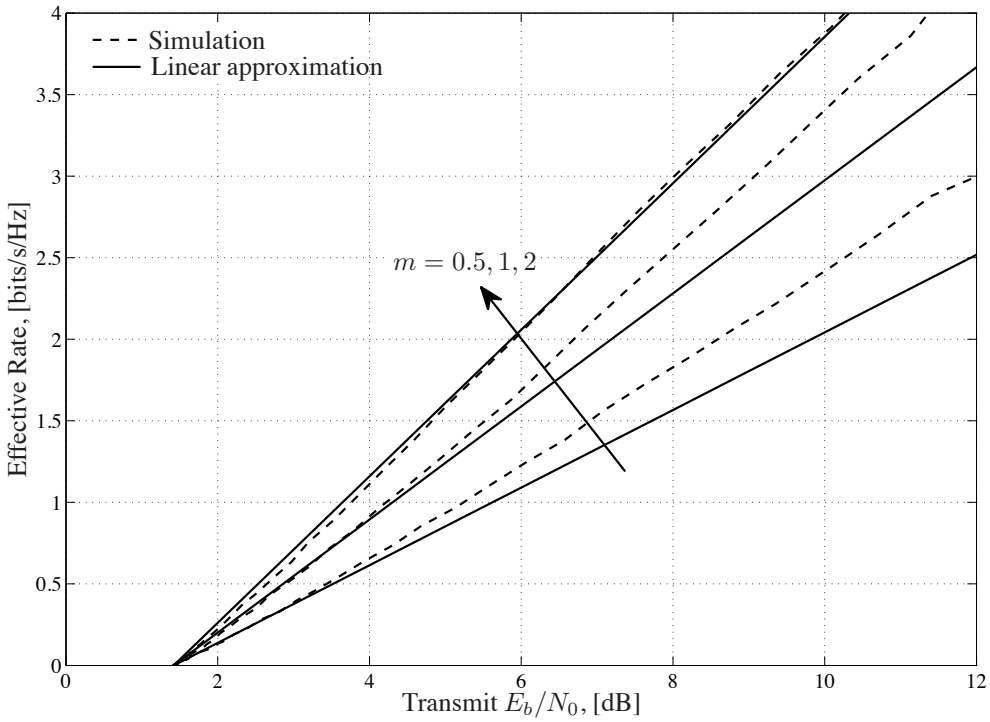

Figure 4.4: Low-SNR effective rate and analytical linear approximation against the transmit E_b/N_0 ($N_t = 6$, $A = 4$, $\lambda = 10$, and $\mu = 0.5$).

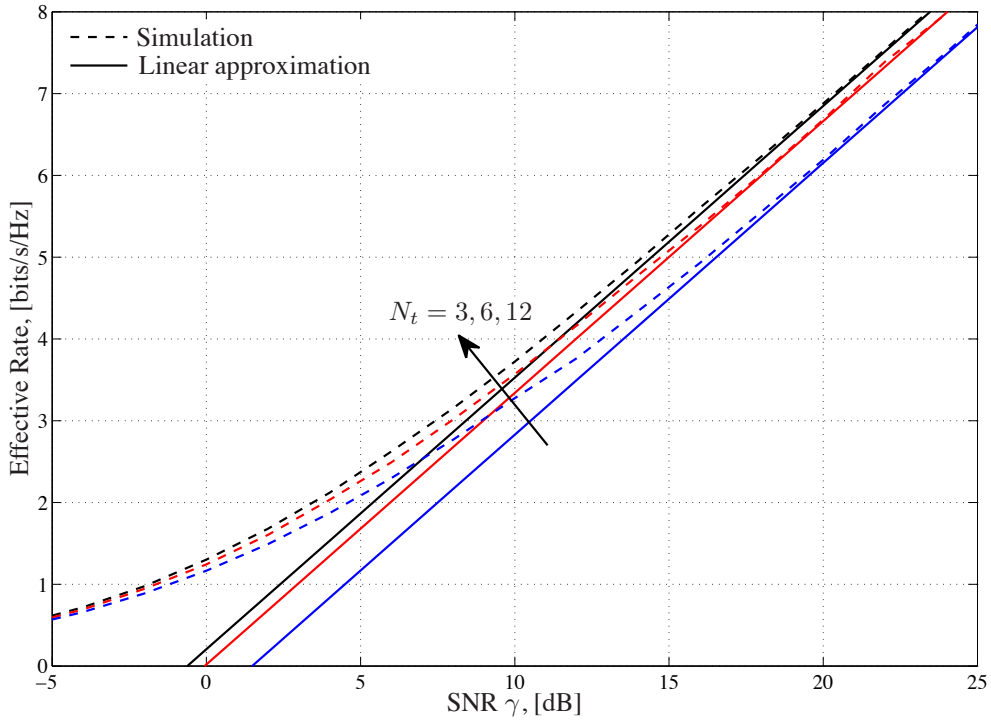

Figure 4.5: High-SNR effective rate and analytical linear approximation against the SNR ($A = 4$, $m = 2$, $\lambda = 10$, and $\mu = 2$).

Chapter 5

Conclusions

In this thesis, we have first presented a detailed performance analysis of D-MIMO systems with optimal, linear ZF, and MMSE receivers operating over RIG fading channels. It has been shown that its contributions are of both theoretical and practical interest and serve as a good starting point for future research. In this concluding chapter, all the key findings from different chapters are summarized and several future research areas are suggested.

5.1 Summary of results

- We have derived new closed-form upper and lower capacity bounds for D-MIMO systems over RIG fading channels, which can apply for any arbitrary number of antennas and remain sufficiently tight across the entire SNR range. More specifically, the implications of small- and large-scale fading effects were analyzed in detail.
- With the help of these proposed bounds, we analytically explored the "large-system" regime by assuming that either the number of receive or transmit antennas grows large. In both cases, we explicitly demonstrated that the effects of small-scale Rayleigh fading are averaged out and that the sum rate is affected only by the large-scale fading effects. It is also clearly shown that the sum rate converges to deterministic asymptotes, which are explicitly derived and validated by Monte-Carlo simulations.
- In the high-SNR regime, we explicitly demonstrated that the lower bound becomes exact and in the low-SNR regime, we derived new analytical expressions for the minimum energy per information bit to reliably convey any positive rate and the wideband slope. We also demonstrated that, at high SNRs, the sum rate reduction is manifested via an increased power offset, whereas at low SNRs, it is through a reduced wideband slope. Likewise, we have analyzed the effective rate of MISO systems operating over $\mathcal{G}$ fading channels in the high and low SNR regimes.

5.2 Future research areas

There are several areas of this thesis that can be expanded at a future stage and some of these are being outlined below:

- We have analytically investigated the sum rate of D-MIMO systems employing linear ZF and MMSE receivers over RIG fading channels, exploiting a simple but powerful connection with the ergodic MIMO mutual information achieved with optimal receivers. Hence, we can extend this RIG distribution to other measures of performance related to practical communication system design (such as outage performance analysis, average symbol/bit error rates) and to begin exploring the analytical methods by which they may be evaluated.

- The main focus of the thesis was the performance analysis of D-MIMO systems with different receivers on a single-cell scenario. We can extend the proposed RIG distribution and performance analysis to many other scenarios beyond those explicitly studied in this thesis. These include, for example, multi-cell MIMO systems, MIMO systems operating in the presence of interference [75–77], and amplify-and-forward relaying systems [56], [78].

- We also highlight the fact that the presented effective rate analysis of MISO systems can be extended to MIMO systems over $\mathcal{G}$ and RIG fading channels.

Appendix A

Standard Results and Formulae

A.1 Modified Bessel function of second kind

The modified Bessel function of second kind and of order v is denoted by $K_v(\cdot)$. The following results, taken from [1, Eq. (8.469.3)] and [1, Eq. (8.486.21)] are useful for solving integral expressions in this thesis:

$$K_v(z)\Big|_{v=\pm\frac{1}{2}} = \sqrt{\frac{\pi}{2z}}\exp(-z) \tag{A.1}$$

$$\frac{\partial}{\partial v}\left(K_v(z)\right)\Big|_{v=\pm\frac{1}{2}} = \mp\sqrt{\frac{\pi}{2z}}\exp(z)\texttt{Ei}(-2z). \tag{A.2}$$

A.2 Properties of Inverse-Gaussian distributed RVs

The positive moments of an Inverse-Gaussian (IG) distributed RV, $\xi_i \sim \mathrm{IG}(\mu_i, \lambda_i)$ can be determined by [33, Eq. (2.5)]

$$\mathcal{E}\left[\xi_i^n\right] = \mu_i^n \sum_{m=0}^{n-1} \frac{(n-1+m)!}{m!(n-1-m)!}\left(\frac{2\lambda_i}{\mu_i}\right)^{-m}. \tag{A.3}$$

Using (A.3), we can obtain the first two moments about zero as follows:

$$\mathcal{E}\left[\xi_i\right] = \mu_i \tag{A.4}$$

$$\mathcal{E}\left[\xi_i^2\right] = \mu_i^2 + \frac{\mu_i^3}{\lambda_i}. \tag{A.5}$$

The following lemma will be particularly useful in the capacity analysis of MIMO systems in RIG fading channels:

Lemma A.2.1. *The positive moments of an IG distributed RV can be alternatively expressed as*

$$\mathcal{E}\left[\xi_i^n\right] = \sqrt{\frac{2\lambda_i}{\pi\mu_i}} \exp\left(\frac{\lambda_i}{\mu_i}\right) \mu_i^n K_{n-\frac{1}{2}}\left(\frac{\lambda_i}{\mu_i}\right). \tag{A.6}$$

The first log-moment of an IG distributed RV is given by

$$\mathcal{E}\Big[\ln(\xi_i)\Big] = \ln(\mu_i) + \exp\left(\frac{2\lambda_i}{\mu_i}\right) \texttt{Ei}\left(-\frac{2\lambda_i}{\mu_i}\right). \tag{A.7}$$

The following key results will be particularly useful to obtain the dispersion of the large-scale fading random matrix $\boldsymbol{\Xi}$

$$\mathcal{E}\Big[\mathrm{tr}(\boldsymbol{\Xi})\Big] = N_t \sum_{i=1}^{L} \mathcal{E}\left[\xi_i\right] D_i^{-\upsilon} = N_t \sum_{i=1}^{L} \mu_i D_i^{-\upsilon} \tag{A.8}$$

$$\mathcal{E}\Big[\mathrm{tr}\big(\boldsymbol{\Xi}^2\big)\Big] = N_t \sum_{i=1}^{L} \mathcal{E}\left[{\xi_i}^2\right] D_i^{-2\upsilon} = N_t \sum_{i=1}^{L} \left(\mu_i^2 + \frac{\mu_i^3}{\lambda_i}\right) D_i^{-2\upsilon}. \tag{A.9}$$

Proof. Using [1, Eq. (3.471.9)], we can easily obtain (A.6) after basic simplifications. To prove (A.7), we first recall the following integral identity [79, Eq. (2.6.22.8)]

$$\int_0^\infty \ln(x) x^{-1\pm\frac{1}{2}} e^{-(px-\frac{q}{x})} dx = \sqrt{\frac{\pi}{p}} \left(\frac{p}{q}\right)^{(1\mp1)/4} \left(\frac{1}{2} e^{-2\sqrt{pq}} \ln\left(\frac{p}{q}\right) \mp e^{2\sqrt{pq}} \texttt{Ei}\left(-4\sqrt{pq}\right)\right). \tag{A.10}$$

Using (A.10), we can directly obtain (A.7) after appropriate simplifications. Finally, using (A.4) and (A.5), we can directly obtain (A.8) and (A.9), respectively. □

A.3 Basic majorization theory results

Majorization theory is one of the most powerful tools to derive inequalities and it has been widely used in wireless communications research field in recent years (see e.g., [11], [80], and [81]). We now give some basic majorization theory results, which allow us to derive our main results in this thesis. For additional definitions, examples, and other majorization theory results, interested readers are referred to [11, App. I] and [69].

Lemma A.3.1. *[69] For any vector* $\mathbf{x} \in \mathbb{R}^n$*, let* $x_{[1]} \geq x_{[2]} \geq \ldots \geq x_{[k]}$ *denote its components in decreasing order.*

Lemma A.3.2. *[69, 1.A.1] For any vector $\mathbf{x}, \mathbf{y} \in \mathbb{R}^n$, $\mathbf{x}$ is majorized by $\mathbf{y}$ (or $\mathbf{y}$ majorizes $\mathbf{x}$) if*

$$\begin{cases} \sum_{i=1}^{k} x_{[i]} & \leq & \sum_{i=1}^{k} y_{[i]}, \quad 1 \leq k \leq n-1 \\ \sum_{i=1}^{n} x_{[i]} & = & \sum_{i=1}^{n} y_{[i]}. \end{cases} \tag{A.11}$$

The notation $\mathbf{x} \prec \mathbf{y}$, or equivalently, by $\mathbf{y} \succ \mathbf{x}$, is used to denote the case where $\mathbf{y}$ majorizes $\mathbf{x}$.

Lemma A.3.3. *[69, p. 7] For any vector $\mathbf{x} \in \mathbb{R}^n$, let $\mathbf{a} \in \mathbb{R}^n$ denotes a constant vector with the i-th element given by $\mathbf{a}_{[i]} = (1/n)\sum_{k=1}^{n} x_{[k]}$. Then, $\mathbf{x}$ majorizes $\mathbf{a}$, or $\mathbf{a} \prec \mathbf{x}$. This result indicates that the vector with identical entries is majorized by any vector with the same sum value.*

Lemma A.3.4. *[69, 3.A.1] A real-valued function $f(\cdot)$ defined on a set $\mathcal{A}$ is said to be Schur-convex on $\mathcal{A}$ if*

$$\mathbf{x} \prec \mathbf{y} \quad \text{on} \quad \mathcal{A} \Rightarrow f(\mathbf{x}) \leq f(\mathbf{y}). \tag{A.12}$$

Lemma A.3.5. *[69, 3.C.1] If $\mathcal{I} \subset \mathbb{R}$ is an interval and $g : \mathcal{I} \to \mathbb{R}$ is convex, then*

$$f(\mathbf{x}) = \sum_{k=1}^{n} g\left(x_{[k]}\right) \tag{A.13}$$

is Schur-convex on $\mathcal{I}^n$. Consequently, $\mathbf{x} \prec \mathbf{y}$ on $\mathcal{I}^n$ implies $f(\mathbf{x}) \leq f(\mathbf{y})$.

Appendix B

Original publications

1. **V. Gopal**, M. Matthaiou, and C. Zhong, "Performance analysis of distributed MIMO systems in Rayleigh/Inverse Gaussian fading channels," *to appear in Proc. of IEEE Global Commun. Conf. (GLOBECOM),* Anaheim, CA, USA, Dec. 2012.

Performance Analysis of Distributed MIMO Systems in Rayleigh/Inverse-Gaussian Fading Channels

Vetriselvam Gopal*, Michail Matthaiou*, and Caijun Zhong†
*Department of Signals and Systems, Chalmers University of Technology, Gothenburg, Sweden
†Institute of Information and Communication Engineering, Zhejiang University, Hangzhou, China
E-mail: gopalv@student.chalmers.se, michail.matthaiou@chalmers.se, caijunzhong@zju.edu.cn

***Abstract*—In this paper, we pursue a performance evaluation of distributed multiple-input multiple-output (MIMO) systems in composite Rayleigh/Inverse-Gaussian fading channels. Capitalizing on some generic bounding techniques, we first derive new closed-form bounds on the ergodic capacity of optimal receivers. In order to gain useful insights into the impact of fading parameters on optimal receivers' performance, a detailed characterization in the asymptotically high and low signal-to-noise ratio regimes is also provided. In addition, we explore the "large-system" regime and provide asymptotic expressions when the number of antennas grows large. A similar performance analysis is performed for the achievable sum rate of distributed MIMO systems employing linear minimum mean-square error receivers.**

I. Introduction

The potential of combining MIMO spatial multiplexing gains with macro-diversity gains is realized by distributed MIMO (D-MIMO) systems, that promise to improve the cell coverage [1]–[3]. In D-MIMO systems, multiple antennas, placed at one end of the radio link, are deployed into multiple radio ports. In such configurations, each radio port experiences different large-scale fading (a.k.a. shadowing) effects and path-loss, due to the different propagation paths. This is the key difference compared to conventional point-to-point MIMO configurations, which makes the performance analysis of D-MIMO systems a challenging mathematical problem. As such, there are very few analytical works investigating the impact of composite fading channels (i.e., mixture of both small-scale and large-scale fading) on the performance of D-MIMO systems.

The ergodic capacity of D-MIMO systems was explored with the aid of majorization theory in [2] by deriving upper and lower capacity bounds for the case of Nakagami-m/log-normal fading channels. On the other hand, in [3], the analytically friendlier gamma distribution was used, as an alternative to the log-normal distribution, and the capacity of D-MIMO systems was investigated over Nakagami-m/Gamma fading (a.k.a. generalized-$\mathcal{K}$ fading) channels. Nevertheless, these results, based on the gamma shadowing model, are essentially approximations. More importantly, for the large variance case or in the tails of the log-normal distribution, the gamma distribution does not yield a good approximation [4]. Motivated by these intrinsic deficiencies, the Inverse-Gaussian (IG) distribution was recently proposed as a more accurate approximation to the classical log-normal model to describe large-scale fading effects [4]. In fact, the authors in [4] proved that the composite Rayleigh/IG (RIG) distribution approximates the Rayleigh/log-normal distribution more accurately than the $\mathcal{K}$ distribution in terms of the Kullback–Leibler measure of divergence. Note that the IG distribution has already been used in the context of free-space optical systems [5], whereas the composite Nakagami-m/IG distribution was first used in [6] for the performance evaluation of communications systems and in [7], in the context of relaying systems, respectively.

The main objective of this paper is to analytically investigate the performance of D-MIMO systems with optimal and linear minimum mean-squared error (MMSE) receivers over RIG fading channels. It is important to note that, to the best of authors' knowledge, the results in this paper present the first-ever analytical investigation of D-MIMO systems in RIG fading channels. Motivated by the preceding, we hereafter derive tight upper and lower sum rate bounds for this class of channels using some recent bounding techniques [2]. With the help of these proposed bounds, we analytically explore the "large-system" regime by assuming that either the number of receive or transmit antennas grows large. In both cases, we explicitly demonstrate that the effects of small-scale Rayleigh fading are averaged out and the ergodic capacity is affected only by the large-scale fading. We also investigate the asymptotically high and low signal-to-noise ratio (SNR) regimes. Our analytical results are quite informative and insightful; for example, they enable us to characterize the impact of large-scale fading parameters as well as path-loss on the sum rate.

Notation: For any matrix, $(\cdot)^H$ denotes the Hermitian transpose, $\mathrm{tr}(\cdot)$ the matrix trace, and $\det(\cdot)$ the determinant operation. The (i,j)-th minor of matrix $\mathbf{A}$ is denoted by $\mathbf{A}_{ij}$, while $\mathbf{A}_i$ is $\mathbf{A}$ with the i-th column removed. The symbol $\mathcal{E}[\cdot]$ stands for the expectation operation. The notation $\Gamma(\cdot)$ stands for the well-known Gamma function [8, Eq. (8.310.1)], while $\mathtt{Ei}(x) = -\int_{-x}^{\infty} \frac{e^{-t}}{t}\, dt$ is the exponential integral function [8, Eq. (8.211.1)]. Finally, $\psi(\cdot)$ is Euler's digamma function [8, Eq. (8.360.1)].

II. MIMO System Model

Consider a typical MIMO system with N_r receive antennas and L radio ports each connected to N_t transmit antennas, assuming that $N_r \geq LN_t$. The input-output model for this D-MIMO system is

$$\mathbf{y} = \sqrt{\gamma}\mathbf{H}\boldsymbol{\Xi}^{1/2}\mathbf{x} + \mathbf{n} \tag{1}$$

where $\mathbf{x} \in \mathbb{C}^{LN_t \times 1}$ and $\mathbf{y} \in \mathbb{C}^{N_r \times 1}$ are the transmitted and received signal vectors, respectively, while $\mathbf{n} \sim \mathcal{CN}(\mathbf{0}, N_0\mathbf{I}_{N_r})$ is the complex AWGN term, where N_0 is the noise power. The average SNR is defined as γ. The large-scale fading effects are represented by the diagonal matrix $\mathbf{\Xi} \in \mathbb{R}^{LN_t \times LN_t}$ whose structure is $\mathbf{\Xi} = \text{diag}\{\mathbf{I}_{N_t}\xi_i/D_i^{\upsilon}\}$ for $i = 1, \ldots, L$. Note that all N_t antennas in the i-th radio port experience the same large-scale fading. The distance between the receiver and the i-th radio port is denoted by D_i, while υ is the path-loss exponent. The large-scale fading coefficients ξ_i are modeled as independent IG random variables (RVs), $\xi_i \sim \text{IG}(\mu_i, \lambda_i)$, or

$$p(\xi_i) = \sqrt{\frac{\lambda_i}{2\pi}}\xi_i^{-\frac{3}{2}} \exp\left(-\frac{\lambda_i(\xi_i - \mu_i)^2}{2\mu_i^2\xi_i}\right), \quad \xi_i > 0 \tag{2}$$

where $\mu_i > 0, \lambda_i > 0$ are the mean and the scale parameters of the IG distribution, respectively [9].

The entries of the channel matrix $\mathbf{H} \in \mathbb{C}^{N_r \times LN_t}$ are assumed to be independent and identically distributed (i.i.d.) Rayleigh RVs, i.e., $h_{st} \sim \mathcal{CN}(0, 1)$, where $s = 1, \ldots, N_r$ and $t = 1, \ldots, LN_t$. We now invoke that a squared Rayleigh RV follows the Gamma distribution with scale parameter 1 and also that the sum of n i.i.d. Gamma RVs with common scale parameter θ and shape parameters $\{k_i\}_{i=1}^n$ is also Gamma distributed with parameters $\left(\sum_{i=1}^n k_i, \theta\right)$ [10]. As such, the sum of N_r i.i.d. Gamma RVs with scale parameter 1 is distributed as $\varphi_i \sim \text{Gamma}(N_r, 1)$, or

$$p(\varphi_i) = \frac{\varphi_i^{N_r-1}}{\Gamma(N_r)} \exp(-\varphi_i), \quad \varphi_i \geq 0. \tag{3}$$

III. Performance analysis of D-MIMO systems

In this section, we present a detailed performance analysis of D-MIMO systems with optimal and linear MMSE receivers in RIG fading channels.

A. Optimal receivers

We assume that the receiver has perfect channel state information (CSI) while the transmitter has nor statistical neither instantaneous CSI and as such performs uniform power allocation across all the data streams. Then, the MIMO ergodic capacity reads as

$$\mathcal{C}_{\text{erg}} = \mathcal{E}\left[\log_2\left(\det\left(\mathbf{I}_{LN_t} + \frac{\gamma}{LN_t}\mathbf{\Xi}\mathbf{H}^H\mathbf{H}\right)\right)\right] \tag{4}$$

where the expectation is taken over all channel realizations of $\mathbf{H}$, $\mathbf{\Xi}$ and the channel is assumed to be ergodic.

1) Exact analysis: We now derive new ergodic capacity upper and lower bounds for optimal receivers. Capitalizing on the results of [2], we first derive an upper capacity bound.

Proposition 1: For D-MIMO systems with optimal receivers in RIG fading channels, the ergodic capacity in (4) is upper bounded by $\mathcal{C}_{\text{UB}}$, with

$$\mathcal{C}_{\text{UB}} = \frac{\gamma}{2\sqrt{\pi}\ln 2\, L\, \Gamma(N_r)} \sum_{i=1}^{L} \frac{1}{D_i^{\upsilon}} \exp\left(\frac{\lambda_i}{\mu_i}\right) \sum_{j=1}^{N} w_j V_i(x_j) \tag{5}$$

where $V_i(t) = t^{-\frac{1}{2}} \exp\left(-\frac{\lambda_i^2}{4\mu_i^2 t}\right) G_{3,2}^{1,3}\left(\frac{\gamma_i \mu_i t}{LN_t\lambda_i D_i^{\upsilon}}\Big|_{0,-1}^{-N_r,0,0}\right)$, $\{x_j\}_{j=1}^N$ are the zeros of the N-th order Laguerre polynomial, $\{w_j\}_{j=1}^N$ are the weight factors tabulated in [11, Table 25.9], and $G_{p,q}^{m,n} = \left[x\big|_{a_1,\ldots,a_p}^{b_1,\ldots,b_q}\right]$ denotes the Meijer's-G function [8, Eq. (9.301)].

Proof: Using [2, Eq. (64)], we can rewrite the ergodic capacity in (4) as

$$\mathcal{C}_{\text{erg}} \leq \mathcal{C}_{\text{UB}} = \frac{N_t}{\ln 2} \sum_{i=1}^{L} \underbrace{\mathcal{E}\left[\ln\left(1 + \frac{\gamma}{LN_t}\frac{\xi_i\varphi_i}{D_i^{\upsilon}}\right)\right]}_{I_1}. \tag{6}$$

To evaluate I_1 we first express $\ln(1 + ax)$ in terms of a Meijer's-G function using [12, Eq. (8.4.6.5)]. Then, combining (3) with [8, Eq. (7.813.1)] gives

$$I_1 = \frac{1}{\Gamma(N_r)} \int_0^{\infty} G_{3,2}^{1,3}\left(\frac{\gamma_i\xi_i}{LN_tD_i^{\upsilon}}\Big|_{1,0}^{1-N_r,1,1}\right) p(\xi_i)\, d\xi_i. \tag{7}$$

Substituting (2) into (7), applying a change of variables, $t_i = (2\xi_i\mu_i^2/\lambda_i)$, and thereafter using [8, Eq. (9.31.5)], we end up with the following expression

$$I_1 = \frac{\gamma \exp\left(\frac{\lambda_i}{\mu_i}\right)}{2\sqrt{\pi}LN_tD_i^{\upsilon}\Gamma(N_r)} \int_0^{\infty} \exp(-t_i)\; V_i(t_i)\; dt_i \tag{8}$$

where $V_i(t_i)$ is defined in (5). The above integral can be efficiently evaluated by Gauss-Laguerre quadratic integration [11, Eq. (25.4.45)]. Thus, we can conclude the proof. ■

In the above proof, Gauss-Laguerre quadratic integration has been used to approximate the integral expression. While (5) can be used to compute the upper bound for D-MIMO systems in RIG fading channels, the computation of Gauss-Laguerre quadratic integration can still be time consuming, especially at low SNRs (e.g., $\gamma < -15$ dB). More importantly, the above upper bound, though in analytical form, provides limited physical insights. It is thus of interest to consider the high-SNR regime for further analyzing the upper bound.

Corollary 1: At high-SNRs ($\gamma \to \infty$), the ergodic capacity upper bound $\mathcal{C}_{\text{UB}}$ simplifies to

$$\mathcal{C}_{\text{UB}}^{\infty} = LN_t \log_2\left(\frac{\gamma}{LN_t}\right) + \frac{LN_t}{\ln 2}\psi(N_r) + N_t \sum_{i=1}^{L}\Bigg(\log_2(\mu_i) - \upsilon\log_2(D_i) + \frac{1}{\ln 2}\exp\left(\frac{2\lambda_i}{\mu_i}\right)\texttt{Ei}\left(\frac{-2\lambda_i}{\mu_i}\right)\Bigg). \tag{9}$$

Proof: The proof is trivial and therefore omitted. ■

Clearly, the high-SNR upper bound in (9) effectively decouples the effects of small-scale and large-scale fading on the ergodic capacity. Now, we give a new ergodic capacity lower bound via the following proposition:

Proposition 2: For D-MIMO systems with optimal receivers in RIG fading channels, the ergodic capacity in (4)

is lower bounded by $\mathcal{C}_{\mathrm{LB}}$, with

$$\mathcal{C}_{\mathrm{LB}} = LN_t \log_2\Bigg(1 + \frac{\gamma}{LN_t}\exp\Bigg(\frac{1}{L}\sum_{i=1}^{L}\Bigg(\ln\mu_i - \upsilon\ln D_i + \exp\Big(\frac{2\lambda_i}{\mu_i}\Big)\,\mathtt{Ei}\Big(\frac{-2\lambda_i}{\mu_i}\Big)\Bigg) + \frac{1}{LN_t}\sum_{k=0}^{LN_t-1}\psi(N_r-k)\Bigg)\Bigg). \quad (10)$$

Proof: The proof relies on the application of Minkowski's inequality to (4), as proposed in [13, Th. 1]. Exploiting the fact that $\ln(1+\alpha\exp(x))$ is convex in x for $\alpha>0$, and thereafter applying Jensen's inequality, we can obtain the following lower bound

$$\mathcal{C}_{\mathrm{LB}} = LN_t \log_2\Bigg(1+\frac{\gamma}{LN_t}\exp\Bigg(\frac{1}{LN_t}\underbrace{\mathcal{E}\Big[\ln\big(\det\left(\boldsymbol{\Xi}\mathbf{H}^H\mathbf{H}\right)\big)\Big]}_{I_2}\Bigg)\Bigg).$$

Recalling the identity $\det(\mathbf{AB}) = \det(\mathbf{A})\det(\mathbf{B})$, we can express the above expectation term as follows:

$$I_2 = \mathcal{E}\Big[\ln(\det(\boldsymbol{\Xi}))\Big] + \mathcal{E}\Big[\ln\left(\det\left(\mathbf{H}^H\mathbf{H}\right)\right)\Big]. \quad (11)$$

Since $\boldsymbol{\Xi}$ is diagonal, the first term in (11) can be given as

$$\mathcal{E}\Big[\ln(\det(\boldsymbol{\Xi}))\Big] \overset{(50)}{=} -N_t\upsilon\sum_{i=1}^{L}\ln D_i + N_t\sum_{i=1}^{L}\left(\ln\mu_i + \exp\left(\frac{2\lambda_i}{\mu_i}\right)\mathtt{Ei}\left(\frac{-2\lambda_i}{\mu_i}\right)\right). \quad (12)$$

Since $\mathbf{H}$ is Rayleigh distributed, the term $\mathbf{H}^H\mathbf{H}$ follows a central Wishart distribution (zero-mean) [14]. Using [14, Eq. (A.8.1)], the last term in (11) can be easily evaluated. Thus, we can conclude the proof. ∎

Note that, in the high-SNR regime, the lower bound becomes by definition exact and equal to the ergodic capacity [13].

2) Low-SNR analysis: We now examine the ergodic capacity in the power-limited (or low-SNR) regime. The low-SNR performance of MIMO systems is typically analyzed via the normalized receive energy per bit (E_b^r/N_0) rather than via the per-symbol SNR [15]. This capacity representation is given by

$$\mathcal{C}_{\mathrm{erg}}\left(\frac{E_b}{N_0}\right) \approx \mathcal{S}_0\log_2\left(\frac{\frac{E_b}{N_0}}{\frac{E_b}{N_{0\,\mathtt{min}}}}\right) \quad (13)$$

$$\frac{E_b}{N_{0\,\mathtt{min}}} = \frac{1}{\dot{\mathcal{C}}_{\mathrm{erg}}(0)} \quad \text{and} \quad \mathcal{S}_0 = -2\ln 2\frac{\left(\dot{\mathcal{C}}_{\mathrm{erg}}(0)\right)^2}{\ddot{\mathcal{C}}_{\mathrm{erg}}(0)} \quad (14)$$

where $E_b/N_{0_{\mathtt{min}}}$ and $\mathcal{S}_0$ are the *minimum normalized energy per information bit required to convey any positive rate reliably* and the *wideband slope*, respectively, while $\dot{\mathcal{C}}_{\mathrm{erg}}(0)$ and $\ddot{\mathcal{C}}_{\mathrm{erg}}(0)$ denote the first- and second-order derivatives of the ergodic capacity in (4) w.r.t. the SNR, respectively [15].

Proposition 3: For D-MIMO systems with optimal receivers in RIG fading channels, the minimum energy per information bit and the wideband slope are

$$\frac{E_b}{N_{0\,\mathtt{min}}}^{\mathtt{opt}} = \frac{L\ln 2}{N_r}\left(\sum_{i=1}^{L}\mu_i D_i^{-\upsilon}\right)^{-1} \quad (15)$$

$$\mathcal{S}_0^{\mathtt{opt}} = \frac{2}{\frac{1}{N_r}+\frac{1}{N_t}\left(\frac{\sum_{i=1}^{L}\left(\mu_i^2+\frac{\mu_i^3}{\lambda_i}\right)D_i^{-2\upsilon}}{\left(\sum_{i=1}^{L}\mu_i D_i^{-\upsilon}\right)^2}\right)}. \quad (16)$$

Proof: First, we recall that

$$\frac{d}{dx}\ln\left(\det\left(\mathbf{I}+x\mathbf{A}\right)\right)\big|_{x=0} = \mathrm{tr}(\mathbf{A}). \quad (17)$$

Now, we set $\gamma\to 0$ in (6) and evaluate $\dot{\mathcal{C}}_{\mathrm{erg}}$ as

$$\dot{\mathcal{C}}_{\mathrm{erg}}(0) = \mathcal{E}\Big[\mathrm{tr}\left(\mathbf{Z}^H\mathbf{Z}\right)\Big] = \frac{N_t}{LN_t\ln 2}\sum_{i=1}^{L}\int_0^\infty\int_0^\infty\frac{\xi_i\varphi_i}{D_i^\upsilon}\,p(\varphi_i)\,p(\xi_i)\,d\varphi_i\,d\xi_i \quad (18)$$

where $\mathbf{Z} = \mathbf{H}\boldsymbol{\Xi}^{1/2}$ and $\xi_i\varphi_i/D_i^\upsilon$ are the real, non-negative diagonal elements of $\mathbf{Z}^H\mathbf{Z}$. Substituting (2) and (3) into (18), thereafter using [8, Eq. (3.381.4)] and the first moment of a IG RV ($\mathcal{E}[\xi_i]=\mu_i$), we get

$$\dot{\mathcal{C}}_{\mathrm{erg}}(0) = \frac{N_r}{L\ln 2}\sum_{i=1}^{L}\mu_i D_i^{-\upsilon}. \quad (19)$$

For the wideband slope $\mathcal{S}_0^{\mathtt{opt}}$, we invoke a classical result from random matrix theory on correlated Rayleigh MIMO channels [16, Eq. (19)]. We assume no correlation at the receiver (i.e., $\boldsymbol{\Theta}_R = \mathbf{I}_{N_r}$ and $\boldsymbol{\Theta}_T = \boldsymbol{\Xi}$) and we can obtain the dispersion of random matrix $\boldsymbol{\Xi}$ [16, Eq. (8)] using (51) and (52). Thus, we can conclude the proof. ∎

Note that $E_b/N_{0_{\mathtt{min}}}^{\mathtt{opt}}$ in (15) is independent of N_t, which agrees with the results of [15] and [16], while a higher N_r improves the low-SNR capacity in (13) by reducing $E_b/N_{0_{\mathtt{min}}}^{\mathtt{opt}}$. On the other hand, the presence of the large-scale fading mean parameter μ_i increases $E_b/N_{0_{\mathtt{min}}}^{\mathtt{opt}}$, especially in severe fading conditions (i.e., small values of μ_i). Note that the wideband slope in (16) is by definition always greater than one.

We can now validate the above theoretical expressions via a set of Monte-Carlo simulations. We generate 10,000 random realizations of the small- and large-scale fading matrices, $\mathbf{H}$ and $\boldsymbol{\Xi}$, respectively. In Fig. 1, the simulated ergodic capacity of (4) is compared with the analytical low-SNR approximation in (13). We change only the large-scale fading mean parameter μ_i and keep all other fading parameters constant. We can clearly observe that the low-SNR capacity increases, whereas the wideband slope decreases when μ_i gets larger. On the other hand, the analytical approximation becomes tighter for smaller values of μ_i.

3) High-SNR analysis: We now examine the ergodic capacity in the high-SNR ($\gamma\to\infty$) regime. To get better insights into the high-SNR capacity performance, we can invoke the following affine capacity expansion, which was originally

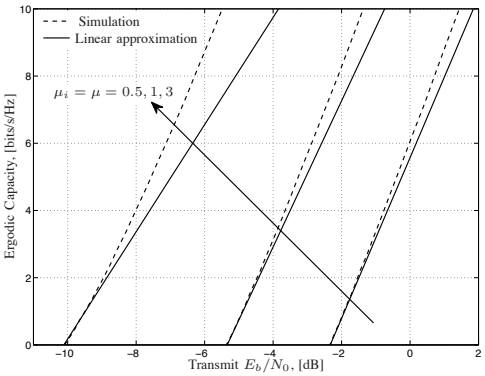

Fig. 1. Simulated ergodic capacity and low-SNR approximation against the transmit E_b/N_0 for different values of the large-scale fading mean $\mu_i = \mu$ parameter ($N_r = 12$, $N_t = 2$, $L = 3$, $\lambda_i = \lambda = 3$, $D_i = D = 1500$m $(\forall i = 1, \ldots, L)$, and $\upsilon = 4$).

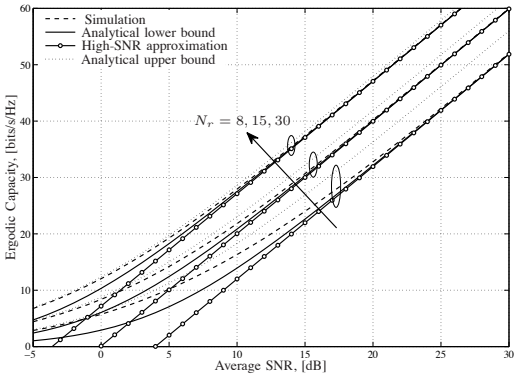

Fig. 2. Simulated ergodic capacity, analytical high-SNR approximation, analytical upper and lower bounds against the average SNR ($N_t = 2$, $L = 3$, $\mu_i = [4, 2, 3]$, $\lambda_i = [3, 5, 7]$, $D_i = [1000\text{m}, 1500\text{m}, 2000\text{m}]$, where $i = 1, \ldots, L$, and $\upsilon = 4$).

applied in the context of multiple access systems with random spreading [17] and thereafter in the analysis of MIMO systems [18]:

$$\mathcal{C}_{\text{erg}} = \mathcal{S}_\infty \left(\log_2(\gamma) - \mathcal{L}_\infty\right) + o(1) \tag{20}$$

where $\mathcal{S}_\infty$ is the so-called *high-SNR slope* in bits/s/Hz per 3-dB units, while $\mathcal{L}_\infty$ is the zero-th order term or *high-SNR power offset*, in 3-dB units [17], [18].

Proposition 4: For D-MIMO systems with optimal receivers in RIG fading channels, the high-SNR parameters are

$$\mathcal{S}_\infty^{\mathtt{opt}} = LN_t \tag{21}$$

$$\mathcal{L}_\infty^{\mathtt{opt}} = \log_2(LN_t) - \frac{1}{L}\sum_{i=1}^{L}\Bigg(\log_2(\mu_i) - \upsilon\log_2(D_i) + \frac{1}{\ln 2}\exp\!\left(\frac{2\lambda_i}{\mu_i}\right)\mathtt{Ei}\left(\frac{-2\lambda_i}{\mu_i}\right)\Bigg) - \frac{1}{LN_t\ln 2}\sum_{k=0}^{LN_t-1}\psi(N_r-k). \tag{22}$$

Proof: For MIMO systems with optimal receivers, the slope and the offset are obtained by [19, Eq. (16), (17)]

$$\mathcal{S}_\infty^{\mathtt{opt}} = \min(N_r, LN_t) \tag{23}$$

$$\mathcal{L}_\infty^{\mathtt{opt}} = \log_2(LN_t) - \frac{1}{LN_t\ln 2}\mathcal{E}\Big[\ln\left(\det\left(\boldsymbol{\Xi}\mathbf{H}^H\mathbf{H}\right)\right)\Big]. \tag{24}$$

Combining (11) with (24) gives (22) after simplifications. ■

From (22), we can infer that the small- and large-scale fading terms are effectively decoupled in the high-SNR regime. Furthermore, larger values of D_i, reduce the ergodic capacity due to the increased path-loss attenuation. Note that the high-SNR slope in (21) verifies that the high-SNR ergodic capacity increases linearly with the minimum number of antennas, which is in line with [13] and [14].

In Fig. 2, the simulated ergodic capacity is compared with the analytical high-SNR approximation (20), the analytical upper and lower bounds from (5) and (10), respectively. Both the upper and lower bounds become tighter when the number of receive antennas, N_r, increases. Also, we can easily observe that the high-SNR approximations become exact even at moderate SNR values. In the low-SNR regime, the lower bound converges asymptotically to the empirical value of ergodic capacity. These observations are consistent with the results of [3], [13], and [20].

4) Large-system analysis: We now examine the ergodic capacity lower bound in the large-system regime.

Corollary 2: When the number of receive antennas grows large (i.e., $N_r \to \infty$), while N_t, L are kept fixed, the ergodic capacity lower bound becomes

$$\mathcal{C}_{\text{LB}} = LN_t\log_2\left(1 + \frac{\gamma N_r}{LN_t}\exp\left(\frac{1}{L}\sum_{i=1}^{L}\left(\ln\mu_i - \upsilon\ln D_i + \exp\left(\frac{2\lambda_i}{\mu_i}\right)\mathtt{Ei}\left(\frac{-2\lambda_i}{\mu_i}\right)\right)\right)\right). \tag{25}$$

Proof: First, we recall that [11, Eq. (6.3.18)]

$$\psi(x) \approx \ln x, \text{ if } x \to \infty. \tag{26}$$

Substituting (26) into (10) gives (25) after appropriate simplifications. ■

From the large-system result in (25), we can clearly conclude that the small-scale fading effects are asymptotically averaged out and only the large-scale fading effects remains, when the number of receive antennas grows very large, which agrees with the results of [21]. Note also that the capacity increases logarithmically with the number of receive antennas.

Next, we analyze an important case when both LN_t and N_r grow large. More specifically, when $LN_t \to \infty$ we need to analyze the two cases based on $N_t \to \infty$ (L fixed) and $L \to \infty$ (N_t fixed) separately. Also, we assume $\beta = \frac{N_r}{LN_t} > 1$ and based on this fixed and finite ratio, we examine the ergodic capacity lower bound in the following two cases:

(i) L: Fixed *and* $N_t \to \infty, N_r \to \infty$: In this case, the ergodic capacity lower bound (10) is given by

$$\frac{\mathcal{C}_{\rm LB}}{N_t} \overset{N_t,N_r\to\infty}{=} L\log_2\left(1+\frac{\gamma\beta^\beta}{\exp(1)(\beta-1)^{(\beta-1)}}\right.$$
$$\left.\times\exp\left(\frac{1}{L}\sum_{i=1}^{L}\ln\mu_i - \upsilon\ln D_i + \exp\left(\frac{2\lambda_i}{\mu_i}\right)\texttt{Ei}\left(\frac{-2\lambda_i}{\mu_i}\right)\right)\right). \quad (27)$$

Proof: Using (26), we express the last sum term in (10) as follows:

$$\frac{1}{LN_t}\sum_{k=0}^{LN_t-1}\psi(N_r-k) \approx \ln N_r + \frac{1}{LN_t}\sum_{k=0}^{LN_t-1}\ln\left(1-\frac{k}{N_r}\right) \quad (28)$$
$$\approx \ln N_r + \frac{1}{LN_t}\int_0^{LN_t}\ln\left(1-\frac{k}{N_r}\right)dk \quad (29)$$
$$= \ln N_r + (\beta-1)\ln\left(\frac{\beta}{\beta-1}\right) - 1 \quad (30)$$

where in (29), we expressed the sum term in (28) as an integral function and then, we used the following integral identity [25] to obtain (30)

$$\int_0^M \ln\left(1-\frac{x}{N}\right)dx = (N-M)\ln\left(\frac{N}{N-M}\right) - M, \text{ if } N>M.$$

Substituting (30) into (10) gives (27) after simplifications. ■

From (27), we can infer that the capacity increases linearly with the number of transmit antennas for any $\beta > 1$.

(ii) N_t: Fixed *and* $L \to \infty, N_r \to \infty$: In this case, we assume that all radio ports are uniformly distributed in a circle of radius R_0, centered by the base station and all radio ports experience to have the same fading effects. As such, we can set $\mu_i = \mu, \lambda_i = \lambda$ fixed values and D_i varying for all L ports, where $i = 1, \ldots, L$. The corresponding probability distribution of the distance between the radio ports and base station is given by [22, Eq. (7)]

$$p_D(x) = \frac{2x}{R_0^2}, \quad 0 \le x \le R_0. \quad (31)$$

Next, we rearrange the large-system lower bound in (27) as

$$\mathcal{C}_{\rm LB} = LN_t\log_2\left(1+a\exp\left(\frac{1}{L}\sum_{i=1}^{L}\ln D_i^{-\upsilon}\right)\right) \quad (32)$$

where $a \triangleq \gamma\mu\beta^\beta(\beta-1)^{(1-\beta)}\exp\left(\exp\left(\frac{2\lambda}{\mu}\right)\texttt{Ei}\left(\frac{-2\lambda}{\mu}\right)-1\right)$. When $L \to \infty$, the argument in the exponential term is nothing but an ensemble average w.r.t. D_i (distribution of distances). As such, we can express (32) as

$$\frac{\mathcal{C}_{\rm LB}}{L} \overset{L,N_r\to\infty}{=} N_t\log_2\left(1+a\exp\left(\mathcal{E}_{D_i}\left[\ln D_i^{-\upsilon}\right]\right)\right). \quad (33)$$

We now recall L'Hospital's rule to get

$$\lim_{x\to 0^+} x\ln(x) = \lim_{x\to 0^+}\frac{\ln(x)}{1/x} = \lim_{x\to 0^+}\frac{1/x}{-1/x^2} = 0. \quad (34)$$

Combining [8, Eq. (2.723.1)] with (34), we can easily obtain the following expression.

$$\mathcal{E}_{D_i}\left[\ln D_i^{-\upsilon}\right] = -\upsilon\ln R_0 + \frac{\upsilon}{2}. \quad (35)$$

Substituting (35) into (33) gives

$$\frac{\mathcal{C}_{\rm LB}}{L} \overset{L,N_r\to\infty}{=} N_t\log_2\left(1+aR_0^{-\upsilon}\exp\left(\frac{\upsilon}{2}\right)\right). \quad (36)$$

At high-SNRs, we can further approximate (36) as

$$\frac{\mathcal{C}_{\rm LB}^{\infty}}{L} \overset{L,N_r\to\infty}{=} N_t\log_2(a) - \upsilon N_t\log_2(R_0) + \frac{\upsilon N_t}{2\ln 2}. \quad (37)$$

From (37), we can clearly infer that a large cell radius R_0 decreases the ergodic capacity logarithmically.

B. MMSE receivers

We can now pursue a similar sum rate analysis for the case of MMSE receivers. Assuming independent decoding at the receiver, the achievable sum rate is expressed as [19]

$$\mathcal{R}^{\texttt{mmse}} = LN_t\,\mathcal{E}\left[\log_2\left(\det\left(\mathbf{I}_{LN_t}+\frac{\gamma}{LN_t}\boldsymbol{\Xi}\mathbf{H}^H\mathbf{H}\right)\right)\right]$$
$$-\sum_{i=1}^{LN_t}\mathcal{E}\left[\log_2\left(\det\left(\mathbf{I}_{LN_t-1}+\frac{\gamma}{LN_t}\boldsymbol{\Xi}_{ii}\mathbf{H}_i^H\mathbf{H}_i\right)\right)\right]. \quad (38)$$

Since an exact SNR analysis in tedious, we elaborate on the low- and high-SNR regimes. We begin with the former:

1) Low-SNR analysis: We now examine the sum rate performance of D-MIMO MMSE receivers in the power-limited regime.

Proposition 5: For D-MIMO systems with MMSE receivers in RIG fading channels, the minimum energy per information bit is given by

$$\frac{E_b}{N_0}^{\texttt{mmse}}_{\texttt{min}} = \frac{\ln 2}{N_r\left(N_t\sum_{i=1}^{L}\frac{\mu_i}{D_i^{\upsilon}} - \frac{1}{LN_t}\sum_{i=1}^{LN_t}\sum_{\substack{j=1\\ j\neq i}}^{LN_t}\frac{\mu_j}{D_j^{\upsilon}}\right)} \quad (39)$$

while the wideband slope is given by (40) shown at the bottom of this page.

Proof: For proving (39), we need to take the first derivative of (38) w.r.t. $\gamma \to 0$. Using (17), we can easily express the first derivative as

$$\dot{\mathcal{R}}^{\texttt{mmse}}(0) = \frac{LN_t}{\ln 2}\,\mathcal{E}\left[\frac{1}{LN_t}\text{tr}\left(\boldsymbol{\Xi}\mathbf{H}^H\mathbf{H}\right)\right]$$
$$-\frac{1}{\ln 2}\sum_{i=1}^{LN_t}\mathcal{E}\left[\frac{1}{LN_t}\text{tr}\left(\boldsymbol{\Xi}_{ii}\mathbf{H}_i^H\mathbf{H}_i\right)\right]. \quad (41)$$

$$\mathcal{S}_0^{\texttt{mmse}} = \frac{2LN_t}{\frac{2LN_t-1}{N_r} + L^2N_t\frac{\sum_{i=1}^{L}\left(\mu_i^2+\frac{\mu_i^3}{\lambda_i}\right)D_i^{-2\upsilon}}{\left(\sum_{i=1}^{L}\mu_iD_i^{-\upsilon}\right)^2} - \frac{(LN_t-1)^2}{LN_t}\sum_{i=1}^{LN_t}\left(\frac{\sum_{\substack{j=1\\ j\neq i}}^{LN_t}\left(\mu_j^2+\frac{\mu_j^3}{\lambda_j}\right)D_j^{-2\upsilon}}{\left(\sum_{\substack{j=1\\ j\neq i}}^{LN_t}\mu_jD_j^{-\upsilon}\right)^2}\right)}. \quad (40)$$

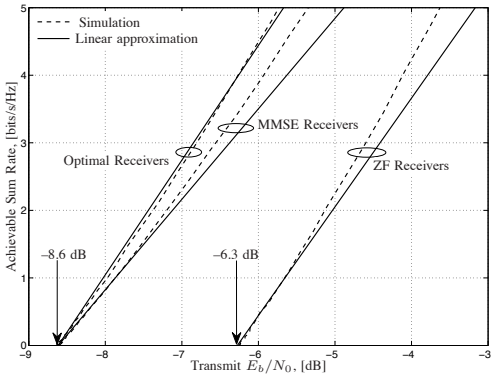

Fig. 3. Low-SNR simulated sum rate (optimal, ZF, and MMSE) and analytical linear approximations against the transmit E_b/N_0 ($N_r = 12$, $N_t = 2$, $L = 3$, $\mu_i = \mu = 1$, $\lambda_i = \lambda = 10$ ($\forall i = 1, \ldots, L$), $D_i = [1000\text{m}, 1500\text{m}, 2000\text{m}]$, and $\upsilon = 4$).

Now, we split (41) as $\dot{\mathcal{R}}^{\mathtt{mmse}}(0) = \dot{\mathcal{R}}_1^{\mathtt{mmse}} - \dot{\mathcal{R}}_2^{\mathtt{mmse}}$. We have already evaluated $\dot{\mathcal{R}}_1^{\mathtt{mmse}}$ in (19) and hence, we evaluate $\dot{\mathcal{R}}_2^{\mathtt{mmse}}$ as

$$\dot{\mathcal{R}}_2^{\mathtt{mmse}} = \frac{1}{LN_t \ln 2} \sum_{i=1}^{LN_t} \mathcal{E}\left[\sum_{\substack{j=1 \\ j\neq i}}^{LN_t} \frac{\xi_j}{D_j^{\upsilon}} \varphi_j \right]. \tag{42}$$

The expectation is the same as in (18). Therefore, we have that

$$\dot{\mathcal{R}}^{\mathtt{mmse}}(0) = \frac{N_r N_t}{\ln 2} \sum_{i=1}^{L} \frac{\mu_i}{D_i^{\upsilon}} - \frac{N_r}{LN_t \ln 2} \sum_{i=1}^{LN_t} \sum_{\substack{j=1 \\ j\neq i}}^{LN_t} \frac{\mu_j}{D_j^{\upsilon}}. \tag{43}$$

To evaluate the wideband slope in (40), we invoke a classical result from random matrix theory on correlated Rayleigh MIMO channels [19, Eq. (75)]. We assume no correlation at the receiver (i.e., $\mathbf{\Theta}_R = \mathbf{I}_{N_r}$ and $\mathbf{\Theta}_T = \mathbf{\Xi}$). The dispersion of random matrix $\mathbf{\Xi}_{ii}$ denoted by $\zeta(\mathbf{\Xi}_{ii})$, is given by

$$\zeta(\mathbf{\Xi}_{ii}) = \frac{(LN_t - 1) \sum_{\substack{j=1 \\ j\neq i}}^{LN_t} \left(\mu_j^2 + \frac{\mu_j^3}{\lambda_j} \right) D_j^{-2\upsilon}}{\left(\sum_{\substack{j=1 \\ j\neq i}}^{LN_t} \mu_j D_j^{-\upsilon} \right)^2}. \tag{44}$$

Combining (51) and (52) with [16, Eq. (8)] gives (44). Substituting all the above results into [19, Eq. (75)] and appropriate simplifications give (40). ■

In Fig. 3, we compare the performance of optimal, linear zero-forcing (ZF)[1] and MMSE receivers in the low-SNR regime. The simulated low-SNR ergodic capacity/sum rates and the analytical linear approximations are plotted against the transmit E_b/N_0. The figure illustrates the big performance gap between optimal and ZF receivers which is due to the high number of total transmit antennas ($LN_t = 6$), that corresponds to the number of interfering data streams. On the other hand, we can easily conclude that the MMSE receivers are optimal in terms of $E_b/N_{0\mathtt{min}}$. MMSE receivers sub-optimality is only reflected via a reduced wideband slope. More importantly, all the analytical linear approximations are sufficiently tight for a wide range of SNR values.

[1]The results for the case of ZF receivers have been omitted due to space constraints.

2) High-SNR analysis: In this case, we examine the sum rate performance of MMSE receivers in the high-SNR regime. We recall that, at high-SNRs, both ZF and MMSE receivers behave equivalently in terms of sum rate [23]. We have already introduced the high-SNR parameters in Section-III-A and hence, we can directly give the following proposition.

Proposition 6: For D-MIMO systems with MMSE receivers in RIG fading channels, the high-SNR parameters are

$$\mathcal{S}_{\infty}^{\mathtt{mmse}} = LN_t \tag{45}$$

$$\begin{aligned}\mathcal{L}_{\infty}^{\mathtt{mmse}} &= \log_2(LN_t) - N_t \sum_{i=1}^{L} \Bigg(\log_2(\mu_i) - \upsilon \log_2(D_i) \\ &+ \frac{1}{\ln 2} \exp\left(\frac{2\lambda_i}{\mu_i}\right) \mathtt{Ei}\left(\frac{-2\lambda_i}{\mu_i}\right) \Bigg) - \frac{1}{\ln 2} \psi(N_r - LN_t + 1) \\ &+ \frac{1}{LN_t} \sum_{i=1}^{LN_t} \sum_{\substack{j=1 \\ j\neq i}}^{LN_t} \Bigg(\log_2(\mu_j) - \upsilon \log_2(D_j) \\ &+ \frac{1}{\ln 2} \exp\left(\frac{2\lambda_j}{\mu_j}\right) \mathtt{Ei}\left(\frac{-2\lambda_j}{\mu_j}\right) \Bigg).\end{aligned} \tag{46}$$

Proof: For MIMO systems with MMSE receivers, the slope and offset parameters are obtained by [19, Eq. (19), (20)] as follows:

$$\mathcal{S}_{\infty}^{\mathtt{mmse}} = \min(N_r, LN_t) \tag{47}$$

$$\begin{aligned}\mathcal{L}_{\infty}^{\mathtt{mmse}} &= \log_2(LN_t) - \mathcal{E}\left[\log_2\left(\det\left(\mathbf{\Xi} \mathbf{H}^H \mathbf{H} \right) \right) \right] \\ &+ \frac{1}{LN_t} \frac{1}{\ln 2} \sum_{i=1}^{LN_t} \mathcal{E}\left[\ln(\det(\mathbf{\Xi}_{ii})) \right] \\ &+ \frac{1}{LN_t} \frac{1}{\ln 2} \sum_{i=1}^{LN_t} \mathcal{E}\left[\ln\left(\det\left(\mathbf{H}_i^H \mathbf{H}_i \right) \right) \right].\end{aligned} \tag{48}$$

Since $\mathbf{\Xi}_{ii}$ is diagonal, we can directly apply (12) to get

$$\begin{aligned}\sum_{i=1}^{LN_t} \mathcal{E}\left[\ln(\det(\mathbf{\Xi}_{ii})) \right] &= \sum_{i=1}^{LN_t} \sum_{\substack{j=1 \\ j\neq i}}^{LN_t} \Bigg(\log_2(\mu_j) - \upsilon \log_2(D_j) \\ &+ \frac{1}{\ln 2} \exp\left(\frac{2\lambda_j}{\mu_j}\right) \mathtt{Ei}\left(\frac{-2\lambda_j}{\mu_j}\right) \Bigg).\end{aligned} \tag{49}$$

Since $\mathbf{H}_i$ is Rayleigh distributed, the term $\mathbf{H}_i^H \mathbf{H}_i$ also follows the central Wishart distribution (zero-mean) [14]. Using [14, Eq. (A.8.1)], the last expectation term in (48) can be easily evaluated. Then, substituting (11), (49) into (48), and appropriate simplifications give (46). ■

Similar to optimal receivers, the small- and large-scale fading terms are decoupled in the high-SNR regime, while (45) verifies that the high-SNR sum rate increases linearly with the minimum number of antennas. As anticipated, higher Tx-Rx distances reduce the sum rate due to the increased path-loss attenuation.

IV. Conclusion

In this paper, we have presented an analytical framework to investigate the performance of D-MIMO systems with optimal and linear MMSE receivers operating over RIG fading channels. More specifically, the implications of small- and large-scale fading effects were analyzed in detail. The main motivation for our performance analysis has been the poor accuracy of the gamma distribution to approximate the log-normal distribution, when the variance of the latter is large. As such, the RIG distribution can serve as an efficient approximation to the classical Rayleigh/log-normal model. At the same time, the mathematical analysis becomes more challenging.

We derived new closed-form upper and lower capacity bounds for this class of channels, which apply for any arbitrary number of antennas and remain sufficiently tight across the entire SNR range. In the high-SNR regime, we explicitly demonstrated that the lower bound becomes exact and in the low-SNR regime, we derived new analytical expressions for the minimum energy per information bit to reliably convey any positive rate and the wideband slope.

Appendix

Lemma 1: For IG distributed RV, $\xi_i \sim \mathrm{IG}(\mu_i, \lambda_i)$, the first log-moment is given by

$$\mathcal{E}\Big[\ln \xi_i\Big] = \ln \mu_i + \exp\left(\frac{2\lambda_i}{\mu_i}\right) \mathtt{Ei}\left(\frac{-2\lambda_i}{\mu_i}\right) \tag{50}$$

where $i = 1, \ldots, L$. The following key results will be particularly useful to obtain the dispersion of large-scale fading random matrix $\boldsymbol{\Xi}$.

$$\mathcal{E}\Big[\mathrm{tr}(\boldsymbol{\Xi})\Big] = N_t \sum_{i=1}^{L} \mathcal{E}\big[\xi_i\big] D_i^{-\upsilon} = N_t \sum_{i=1}^{L} \mu_i D_i^{-\upsilon} \tag{51}$$

$$\mathcal{E}\Big[\mathrm{tr}(\boldsymbol{\Xi}^2)\Big] = N_t \sum_{i=1}^{L} \frac{\mathcal{E}\big[{\xi_i}^2\big]}{D_i^{2\upsilon}} = N_t \sum_{i=1}^{L} \left(\mu_i^2 + \frac{\mu_i^3}{\lambda_i}\right) D_i^{-2\upsilon}. \tag{52}$$

Proof: Using (2) and the integral identity [24, Eq. (2.6.22.8)], we can easily obtain (50) after basic simplifications. We now recall that for IG distributed RVs, the first two moments about zero are $\mathcal{E}[\xi_i] = \mu_i$ and $\mathcal{E}[\xi_i^2] = \mu_i^2 + \frac{\mu_i^3}{\lambda_i}$, respectively [9]. Using these two moments, we can directly obtain (51) and (52), respectively. ∎

Acknowledgments

The work of M. Matthaiou has been supported in part by the Swedish Governmental Agency for Innovation Systems (VINNOVA) within the VINN Excellence Center Chase. The work of C. Zhong has been supported by the Fundamental Research Funds for Central Universities (2012QNA5011) and the Zhejiang Provincial Natural Science Foundation of China (No. LQ12F01006).

References

[1] H. Zhang and H. Dai, "On the capacity of distributed MIMO systems," in *Proc. Conf. Inform. Sciences and Systems (CISS)*, Princeton University, Princeton, NJ, Mar. 2004.

[2] C. Zhong, K.-K. Wong, and S. Jin, "Capacity bounds for MIMO Nakagami-m fading channels," *IEEE Trans. Signal Process.*, vol. 57, no. 9, pp. 3613–3623, Sep. 2009.

[3] M. Matthaiou, N. D. Chatzidiamantis, G. K. Karagiannidis, and J. A. Nossek, "On the capacity of generalized-K fading MIMO channels," *IEEE Trans. Signal Process.*, vol. 58, no. 11, pp. 5939–5944, Nov. 2010.

[4] Karmeshu and R. Agrawal, "On efficacy of Rayleigh-Inverse Gaussian distribution over K-distribution for wireless fading channels," *Wireless Commun. Mob. Comput.*, vol. 7, no. 1, pp. 1–7, Jan. 2007.

[5] N. D. Chatzidiamantis, H. G. Sandalidis, G. K. Karagiannidis, and M. Matthaiou, "Inverse Gaussian modeling of turbulence-induced fading in free-space optical systems," *J. Lightw. Technol.*, vol. 29, no. 10, pp. 1590–1596, May 2011.

[6] A. Laourine, M.-S. Alouini, S. Affes, and A. Stéphenne, "On the performance analysis of composite multipath/shadowing channels using the $\mathcal{G}$-distribution," *IEEE Trans. Commun.*, vol. 57, no. 4, pp. 1162–1170, Apr. 2009.

[7] C. Zhong, M. Matthaiou, G. K. Karagiannidis, A. Huang, and Z. Zhang, "Capacity bounds for AF dual-hop relaying in $\mathcal{G}$ fading channels," *IEEE Trans. Veh. Technol.*, vol. 61, no. 4, pp. 1730–1740, May 2012.

[8] I. S. Gradshteyn and I. M. Ryzhik, *Table of Integrals, Series, and Products*, 7th ed., San Diego, CA: Academic, 2007.

[9] R. S. Chhikara and J. L. Folks, *The Inverse Gaussian Distribution: Theory, Methodology, and Applications*, New York: Marcel Dekker, 1989.

[10] M. Evans, N. Hastings, and B. Peacock, *Statistical Distributions*, 3rd ed., New York: Wiley, 2000.

[11] M. Abramowitz and I. A. Stegun, *Handbook of Mathematical Functions with Formulas, Graphs, and Mathematical Tables*, 9th ed., New York: Dover, 1970.

[12] A. P. Prudnikov, Y. A. Brychkov, and O. I. Marichev, *Integrals and Series, Vol. 3: More Special Functions*, New York: Gordon & Breach, 1990.

[13] Ö. Oyman, R. Nabar, H. Bölcskei, and A. Paulraj, "Characterizing the statistical properties of mutual information in MIMO channels," *IEEE Trans. Signal Process.*, vol. 51, no. 11, pp. 2782–2795, Nov. 2003.

[14] A. Grant, "Rayleigh fading multi-antenna channels," *EURASIP J. Appl. Signal Process.*, vol. 2002, no. 3, pp. 316–329, Mar. 2002.

[15] S. Verdú, "Spectral efficiency in the wideband regime," *IEEE Trans. Inf. Theory*, vol. 48, no. 6, pp. 1319–1343, Jun. 2001.

[16] A. Lozano, A. M. Tulino, and S. Verdú, "Multiple-antenna capacity in the low-power regime," *IEEE Trans. Inf. Theory*, vol. 49, no. 10, pp. 2527–2544, Oct. 2003.

[17] S. Shamai (Shitz) and S. Verdú, "The impact of frequency-flat fading on the spectral efficiency of CDMA," *IEEE Trans. Inf. Theory*, vol. 47, no. 4, pp. 1302–1327, May 2001.

[18] A. Lozano, A. M. Tulino, and S. Verdú, "High-SNR power offset in multiantenna communications," *IEEE Trans. Inf. Theory*, vol. 51, no. 12, pp. 4134–4151, Dec. 2005.

[19] M. R. McKay, I. B. Collings, and A. M. Tulino, "Achievable sum rate of MIMO MMSE receivers: A general analytic framework," *IEEE Trans. Inf. Theory*, vol. 56, no. 1, pp. 396–410, Jan. 2010.

[20] M. Matthaiou, N. D. Chatzidiamantis, and G. K. Karagiannidis, "A new lower bound on the ergodic capacity of distributed MIMO systems," *IEEE Signal Process. Lett.*, vol. 18, no. 4, pp. 227–230, Apr. 2011.

[21] F. Rusek, *et al.*, "Scaling up MIMO: Opportunities and challenges with very large arrays," *in press IEEE Signal Process. Mag.*, 2012.

[22] C. T. Lau and C. Leung, "Capture models for mobile packet radio networks," *IEEE Trans. Commun.*, vol. 40, no. 5, pp. 917–925, May 1992.

[23] A. Paulraj, R. Nabar, and D. A. Gore, *Introduction to Space-Time Wireless Communications*, Cambridge University Press, May 2003.

[24] A. P. Prudnikov, Y. A. Brychkov, and O. I. Marichev, *Integrals and Series, Vol. 1: Elementary Functions*, New York: Gordon & Breach, 1986.

[25] Wolfram, The Wolfram|Alpha Site [Online]. Available: http://www.wolframalpha.com/

References

[1] I. S. Gradshteyn and I. M. Ryzhik, *Table of Integrals, Series, and Products*, 7th ed., San Diego, CA: Academic, 2007.

[2] A. Goldsmith, *Wireless Communications*, Cambridge University Press, 2005.

[3] D. Tse and P. Viswanath, *Fundamentals of Wireless Communication*, Cambridge University Press, 2005.

[4] T. S. Rappaport, *Wireless Communications - Principles and Practice*, 2nd ed., Prentice Hall, 2001.

[5] G. J. Foschini, "Layered space-time architecture for wireless communications in a fading environment when using multiple antennas," *Bell Labs Tech. J.*, vol. 1, no. 2, pp. 41–59, Aug. 1996.

[6] I. E. Telatar, "Capacity of multi-antenna Gaussian channels," *Europ. Trans. Telecommun.*, vol. 10, no. 6, pp. 585–595, Nov./Dec. 1999.

[7] L. Zheng and D. N. C. Tse, "Diversity and multiplexing: A fundamental tradeoff in multiple-antenna channels," *IEEE Trans. Inf. Theory*, vol. 49, no. 5, pp. 1073–1096, May 2003.

[8] W. Weichselberger, *Spatial structure of multiple antenna radio channels: A signal processing viewpoint*, Ph.D. dissertation, Technical University of Vienna, Dec. 2003.

[9] E. Dahlman, S. Parkvall, J. Sköld, and P. Beming, *3G Evolution HSPA and LTE for Mobile Broadband*, 2nd ed., Academic Press, 2008.

[10] H. Zhang and H. Dai, "On the capacity of distributed MIMO systems," in *Proc. Conf. Inform. Sciences Systems (CISS)*, Princeton University, Princeton, NJ, Mar. 2004.

[11] C. Zhong, K.-K. Wong, and S. Jin, "Capacity bounds for MIMO Nakagami-m fading channels," *IEEE Trans. Signal Process.*, vol. 57, no. 9, pp. 3613–3623, Sep. 2009.

[12] M. Matthaiou, N. D. Chatzidiamantis, G. K. Karagiannidis, and J. A. Nossek, "On the capacity of generalized-K fading MIMO channels," *IEEE Trans. Signal Process.*, vol. 58, no. 11, pp. 5939–5944, Nov. 2010.

[13] M. Matthaiou, N. D. Chatzidiamantis, and G. K. Karagiannidis, "A new lower bound on the ergodic capacity of distributed MIMO systems," *IEEE Signal Process. Lett.*, vol. 18, no. 4, pp. 227–230, Apr. 2011.

[14] D. A. Gore, R. W. Heath, Jr., and A. Paulraj, "Transmit selection in spatial multiplexing systems," *IEEE Commun. Lett.*, vol. 6, no. 11, pp. 491–493, Nov. 2002.

[15] A. Paulraj, R. Nabar, and D. A. Gore, *Introduction to Space-Time Wireless Communications*, Cambridge University Press, 2003.

[16] M. R. McKay, I. B. Collings, and A. M. Tulino, "Achievable sum rate of MIMO MMSE receivers: A general analytic framework," *IEEE Trans. Inf. Theory*, vol. 56, no. 1, pp. 396–410, Jan. 2010.

[17] M. C. Gursoy, "MIMO wireless communications under statistical queueing constraints," *IEEE Trans. Inf. Theory*, vol. 57, no. 9, pp. 5897–5917, Sep. 2011.

[18] Karmeshu and R. Agrawal, "On efficacy of Rayleigh-Inverse Gaussian distribution over K-distribution for wireless fading channels," *Wireless Commun. Mob. Comput.*, vol. 7, no. 1, pp. 1–7, Jan. 2007.

[19] V. Erceg, L. J. Greenstein, S. Y. Tjandra, S. R. Parkoff, A. Gupta, B. Kulic, A. A. Julius, and R. Bianchi, "An empirically based path loss model for wireless channels in suburban environments," *IEEE J. Select. Areas Commun.*, vol. 17, no. 7, pp. 1205–1211, July 1999.

[20] S. S. Ghassemzadeh, L. J. Greenstein, A. Kavcic, T. Sveinsson, V. Tarokh, "UWB indoor path loss model for residential and commercial buildings," in *Proc. IEEE Veh. Technol. Conf. (VTC)*, Oct. 2003, pp. 3115–3119.

[21] M. K. Simon and M.-S. Alouini, *Digital Communication over Fading Channels*, 2nd ed., Wiley-IEEE Press, 2005.

[22] K. Krishnamoorthy, *Handbook of Statistical Distributions with Applications*, Chapman & Hall/CRC Press, 2006.

[23] M. Nakagami, "The m-distribution - A general formula of intensity distribution of rapid fading," *Statistical Methods in Radio Wave Propagation*, Oxford, U.K.: Pergamon Press, 1960, pp. 3–36.

[24] J. Aitchison and J. A. C. Brown, *The Lognormal Distribution*, Cambridge University Press, 1963.

[25] U. Charash, *A Study of Multipath Reception with Unknown Delays*, Ph.D. dissertation, Univ. California, Berkeley, Jan. 1974.

[26] I.M. Kostić, "Analytical approach to performance analysis for channel subject to shadowing and fading," in *IEE Proc. Commun.*, vol. 152, no. 6, pp. 821–827, Dec. 2005.

[27] A. Abdi and M. Kaveh, "On the utility of the gamma PDF in modeling shadow fading (slow fading)," in *Proc. IEEE Veh. Technol. Conf. (VTC)*, Houston, TX, May 1999, pp. 2308–2312.

[28] A. Abdi, H. Allen Barger, and M. Kaveh, "A simple alternative to the lognormal model of shadow fading in terrestrial and satellite channels," in *Proc. IEEE Veh. Technol. Conf. (VTC)*, Atlantic City, NJ, Oct. 2001, pp. 2058–2062.

[29] N. L. Johnson, S. Kotz, and N. Balakrishnan, *Continuous Univariate Distributions*, vol. 1, 2nd ed., John Wiley & Sons Inc., 1994.

[30] M. Evans, N. Hastings, and B. Peacock, *Statistical Distributions*, 3rd ed., New York: Wiley, 2000.

[31] A. H. Marcus, "Power-sum distributions: An easier approach using the Wald distribution," *J. of American Statistical Assoc.*, vol. 71, no. 353, pp. 237–238, 1976.

[32] E. W. Montroll and M. F. Shlesinger, "Maximum entropy formalism, fractals, scaling phenomena and 1/f noise: A tale of tails," *J. of Statistical Physics*, vol. 32, no. 2, pp. 209–230, 1983.

[33] R. S. Chhikara and J. L. Folks, *The Inverse Gaussian Distribution: Theory, Methodology, and Applications*, New York: Marcel Dekker, 1989.

[34] M. C. K. Tweedie, "Inverse statistical variates," *Nature*, vol. 155, no. 3937, pp. 453, 1945.

[35] M. C. K. Tweedie, "Functions of a statistical variate with given means, with special reference to Laplacian distributions," in *Proc. of the Cambridge Philosph. Soc.*, vol. 43, no. 1, pp. 41–49, 1947.

[36] M. C. K. Tweedie, "Statistical properties of inverse Gaussian distributions I," *Ann. Math. Statist.*, vol. 28, no. 2, pp. 362–377, 1957.

[37] M. C. K. Tweedie, "Statistical properties of inverse Gaussian distributions II," *Ann. Math. Statist.*, vol. 28, no. 3, pp. 696–705, 1957.

[38] A. Wald, *Sequential Analysis*, New York: Wiley, 1947.

[39] Karmeshu and R. Agrawal, "Rayleigh-inverse Gaussian distribution for fading-shadowing in wireless communication channels," *Lett. Communicated to Trans. IEICE.*

[40] K. R. Baker, "On the WMC density as an inverse Gaussian probability density," *IEEE Trans. Commun.*, vol. 44, no. 1, pp. 15–17, Jan. 1996.

[41] N. D. Chatzidiamantis, H. G. Sandalidis, G. K. Karagiannidis, and M. Matthaiou, "Inverse Gaussian modeling of turbulence-induced fading in free-space optical systems," *J. Lightw. Technol.*, vol. 29, no. 10, pp. 1590–1596, May 2011.

[42] N. D. Chatzidiamantis, H. G. Sandalidis, G. K. Karagiannidis, and S. A. Kotsopoulos, "On the Inverse-Gaussian Shadowing," in *Proc. IEEE Int. Conf. Commun. Info. Tech. (ICCIT)*, May 2011, pp. 142–146.

[43] R. S. Chhikara and J. L. Folks, "The inverse Gaussian distribution and as a lifetime model," *Technometrics*, vol. 19, no. 4, pp. 461–468, Nov. 1977.

[44] B. Seshardi, *The Inverse Gaussian Distribution*, Clarendon Press-Oxford, 1993.

[45] G. L. Stüber, *Principles of Mobile Communications*, Norwell, MA: Kluwer Academic Publishers, 1996.

[46] H. Suzuki, "A statistical model for urban multipath propagation," *IEEE Trans. Commun.*, vol. COM-25, pp. 673–680, July 1977.

[47] F. Hansen and F. I. Meno, "Mobile fading–Rayleigh and lognormal superimposed," *IEEE Trans. Veh. Technol.*, vol. VT-26, pp. 332–335, Nov. 1977.

[48] M. J. Ho and G. L. Stüber, "Co-channel interference of microcellular systems on shadowed Nakagami fading channels," in *Proc. IEEE Veh. Technol. Conf. (VTC)*, Secaucus, NJ, May 1993, pp. 568–571.

[49] E. Lutz, D. Cygan, M. Dippold, F. Dolainsky, and W. Papke, "The land mobile satellite communication channel–recording, statistics, and channel model," *IEEE Trans. Veh. Technol.*, vol. VT-40, pp. 375–386, May 1991.

[50] A. Abdi, W. C. Lau, M.-S. Alouini, and M. Kaveh, "A new simple model for land-mobile satellite channels: First- and second-order statistics," *IEEE Trans. Wireless Commun.*, vol. 2, no. 3, pp. 519–528, May 2003.

[51] A. Abdi and M. Kaveh, "K distribution: An appropriate substitute for Rayleigh-lognormal distribution in fading-shadowing wireless channels," *IEE Electron. Lett.*, vol. 34, pp. 851–852, Apr. 1998.

[52] G. Parry and P. N. Pusey, "K distribution in atmospheric propagation of laser light," *J. Opt. Soc. Am.*, vol. 69, pp. 796–798, 1979.

[53] K. D. Ward, "Application of the K distribution to radar clutter–a review," in *Proc. IEICE Int. Symp. Noise and Clutter Rejection in Radars and Imaging Sensors*, Kyoto, Japan, 1989, pp. 15–20.

[54] A. C. Frery, H.-J. Müller, C. C. F. Yanasse, and S. J. S. Sant'Anna, "A model for extremely heterogeneous clutter," *IEEE Trans. Geosci. Remote Sens.*, vol. 35, no. 3, pp. 648–659, May 1997.

[55] A. Laourine, M.-S. Alouini, S. Affes, and A. Stéphenne, "On the performance analysis of composite multipath/shadowing channels using the $\mathcal{G}$-distribution," *IEEE Trans. Commun.*, vol. 57, no. 4, pp. 1162–1170, Apr. 2009.

[56] C. Zhong, M. Matthaiou, G. K. Karagiannidis, A. Huang, and Z. Zhang, "Capacity bounds for AF dual-hop relaying in $\mathcal{G}$ fading channels," *IEEE Trans. Veh. Technol.*, vol. 61, no. 4, pp. 1730–1740, May 2012.

[57] M. Abramowitz and I. A. Stegun, *Handbook of Mathematical Functions with Formulas, Graphs, and Mathematical Tables*, 9th ed., New York: Dover, 1970.

[58] A. P. Prudnikov, Y. A. Brychkov, and O. I. Marichev, *Integrals and Series, Vol. 3: More Special Functions*, New York: Gordon & Breach, 1990.

[59] Ö. Oyman, R. Nabar, H. Bölcskei, and A. Paulraj, "Characterizing the statistical properties of mutual information in MIMO channels," *IEEE Trans. Signal Process.*, vol. 51, no. 11, pp. 2782–2795, Nov. 2003.

[60] A. Grant, "Rayleigh fading multi-antenna channels," *EURASIP J. Appl. Signal Process.*, vol. 2002, no. 3, pp. 316–329, Mar. 2002.

[61] S. Verdú, "Spectral efficiency in the wideband regime," *IEEE Trans. Inf. Theory*, vol. 48, no. 6, pp. 1319–1343, Jun. 2001.

[62] A. Lozano, A. M. Tulino, and S. Verdú, "Multiple-antenna capacity in the low-power regime," *IEEE Trans. Inf. Theory*, vol. 49, no. 10, pp. 2527–2544, Oct. 2003.

[63] J. R. Michael, W. R. Schucany, and R. W. Haas, "Generating random variates using transformations with multiple roots," *The American Statistician*, vol. 30, no. 2, pp. 88–90, May 1976.

[64] S. Shamai (Shitz) and S. Verdú, "The impact of frequency-flat fading on the spectral efficiency of CDMA," *IEEE Trans. Inf. Theory*, vol. 47, no. 4, pp. 1302–1327, May 2001.

[65] A. Lozano, A. M. Tulino, and S. Verdú, "High-SNR power offset in multiantenna communications," *IEEE Trans. Inf. Theory*, vol. 51, no. 12, pp. 4134–4151, Dec. 2005.

[66] H. Shin and J. H. Lee, "Capacity of multi-antenna fading channels: Spatial fading correlation, double scattering, and keyhole," *IEEE Trans. Inf. Theory*, vol. 49, no. 10, pp. 2636–2647, Oct. 2003.

[67] M. R. McKay and I. B. Collings, "General capacity bounds for spatially correlated Rician MIMO channels," *IEEE Trans. Inf. Theory*, vol. 51, no. 9, pp. 3121–3145, Sept. 2005.

[68] F. Rusek, D. Persson, B. K. Lau, E. G. Larsson, T. L. Marzetta, O. Edfors, and F. Tufvesson, "Scaling up MIMO: Opportunities and challenges with very large arrays," *in press IEEE Signal Process. Mag.*, 2012.

[69] A. W. Marshall and I. Olkin, *Inequalities: Theory of Majorization and Its Applications*, New York: Academic Press, 1979.

[70] Wolfram, The Wolfram|Alpha Site [Online]. Available: http://www.wolframalpha.com/

[71] C. T. Lau and C. Leung, "Capture models for mobile packet radio networks," *IEEE Trans. Commun.*, vol. 40, no. 5, pp. 917–925, May 1992.

[72] M. Matthaiou, C. Zhong, and T. Ratnarajah, "Novel generic bounds on the sum rate of MIMO ZF receivers," *IEEE Trans. Signal Process.*, vol. 59, no. 9, pp. 4341–4353, Sept. 2011.

[73] R. H. Y. Louie, M. R. McKay, and I. B. Collings, "Maximum sum-rate of MIMO multiuser scheduling with linear receivers," *IEEE Trans. Commun.*, vol. 57, no. 11, pp. 3500–3510, Nov. 2009.

[74] C. Zhong, T. Ratnarajah, K.-K. Wong, and M.-S. Alouini, "Effective capacity of correlated MISO channels," in *Proc. IEEE Int. Conf. Commun. (ICC)*, Kyoto, Japan, Jun. 2011.

[75] R. Blum, J. Winters, and N. R. Sollenberger, "On the capacity of cellular systems with MIMO," *IEEE Commun. Lett.*, vol. 6, no. 6, pp. 242–244, Jun. 2002.

[76] R. Blum, "MIMO capacity with interference," *IEEE J. Select. Areas Commun.*, vol. 21, no. 5, pp. 793–801, Jun. 2003.

[77] M. Chiani, M. Z. Win, and H. Shin, "Capacity of MIMO systems in the presence of interference," in *Proc. IEEE Global Telecommun. Conf. (GLOBECOM)*, San Francisco, CA, Nov. 2006.

[78] S. Jin, M. R. McKay, C. Zhong, and K.-K. Wong, "Ergodic capacity analysis of amplify and forward MIMO dual-hop systems," *IEEE Trans. Inf. Theory*, vol. 56, no. 5, pp. 2204–2224, May 2010.

[79] A. P. Prudnikov, Y. A. Brychkov, and O. I. Marichev, *Integrals and Series, Vol. 1: Elementary Functions*, New York: Gordon & Breach, 1986.

[80] D. P. Palomar and Y. Jiang, "MIMO transceiver design via majorization theory," *Found. Trends Commun. Inf. Theory*, vol. 3, no. 4–5, pp. 331–551, Now Publishers Inc. Hanover, MA, Nov. 2006.

[81] E. Jorswieck and H. Boche, "Majorization and matrix-monotone functions in wireless communications," *Found. Trends Commun. Inf. Theory*, vol. 3, no. 6, pp. 553–701, Now Publishers Inc. Hanover, MA, Jun. 2007.